MODELING AND CONTROL OF SI AND SI-HCCI HYBRID COMBUSTION ENGINES

By

Xiaojian Yang

A DISSERTATION

Submitted to
Michigan State University
in partial fulfillment of the requirements
for the degree of

DOCTOR OF PHILOSOPHY

Mechanical Engineering

2011

ABSTRACT

MODELING AND CONTROL OF SI AND SI-HCCI HYBRID COMBUSTION ENGINES

By

Xiaojian Yang

As a special combustion mode of internal combustion (IC) engines, homogeneous charge compression ignition (HCCI) combustion has the potential to meet the increasingly stringent emissions regulations with improved fuel economy. In order to take advantage of this combustion mode, the traditional spark ignition (SI) engine needs to operate in both SI and HCCI modes, and the combustion mode transition between the SI and HCCI combustions is inevitable. It is fairly challenging to operate the engine in the two distinct combustion modes, and it is even more difficult to have smooth combustion mode transition between the two modes due to the distinct engine operational parameters over the two combustion modes and the cycle-to-cycle residual gas dynamics. In this research, the modeling and control of the combustion mode transition problem were studied for a multi-cylinder engine with dual-stage valve lift and electrical variable valve timing (VVT) systems.

In order to describe engine continuous time and event-based dynamics a mixed time-based and crank-based engine model was developed. The continuous dynamics of engine air-handling system and crankshaft were modeled by traditional time-based mean value models; and the engine combustion process was modeled as a function of crank angle (crank-based) using the two-zone combustion modeling approach. The developed combustion model is capable of

simulating the SI, HCCI, and SI-HCCI hybrid combustion modes. This unique modeling approach made it possible for the engine model to be simulated in real-time in a dSPACE based hardware-in-the-loop (HIL) system, due to its low computational throughput. The developed engine model was calibrated and validated using the simulation results from the corresponding one-dimensional GT-Power engine model in the dSPACE based HIL engine simulation environment.

Through HIL simulations using the developed engine model, a multistep SI to HCCI combustion mode transition strategy was incrementally developed. It takes several engine cycles (typically five) to complete the combustion mode transition. During the combustion mode transition, a model based linear quadratic (LQ) engine MAP (intake manifold absolute pressure) tracking controller was used to maintain the air-to-fuel ratio in the desired range by regulating the engine throttle; the DI (direct injection) fuel quantity of individual cylinder was controlled via iterative learning control (ILC); and spark ignitions were maintained to enable the SI-HCCI hybrid combustions; The other engine parameters, such as the intake/exhaust valve timing and lift, external EGR (exhaust gas recirculation) valve opening were controlled in an open loop. The entire control strategy was validated in the developed HIL simulation environment. The simulation results demonstrated the effectiveness of the proposed control strategy under both constant and transient engine operating conditions. It can be concluded that smooth combustion mode transition is achievable for IC engines using dual-stage valve lift and electrical VVT systems as the valve actuation systems.

Copyright by
Xiaojian Yang
2011

TO MY PARENTS AND FAMILY

ACKNOWLEDGMENTS

This dissertation would not have come into existence without the generous support and encouragement of many people. There are no words sufficient to express my gratitude to them.

First and foremost, I would like to express my profound gratitude to my advisor, Dr. Guoming Zhu, for his continued support and guidance for my research work, and generous help with my life during the past four years. His comprehensive knowledge of automotive control theory and application inspired me and led me into this interesting area, and I learned a lot. Dr. Guoming Zhu also encouraged me to read and write many technical papers, and improved my reading and writing skills at the same time. These skills are very important to me, not only for my Ph.D. study, but also for my future career.

I would also like to acknowledge my committee members: Dr. Clark Radcliffe, Dr. Harold Schock, and Dr. Hassan Khalil, for their helpful discussions and insightful comments during my dissertation work, as well as for the knowledge they shared with me in their lectures that were essential for me to make progress throughout my Ph.D. program. Having this committee for my dissertation was a great privilege.

Further thanks are extended to past and current graduate students and other lab personnel who helped me considerably with many aspects of my research work: Xuefei Chen, Andrew Huisjen, Taotao Jin, Gary Keeney, Mittal Mayank, Stephen Pace, Xing Rao, Zhen Ren, Cody Squibb, Tom Stuecken, Yuxin Zhang.

Lastly, I am overly grateful for my parents and my wife, for their never-ending love and encouragement. I want to dedicate this dissertation to them. I also want to dedicate this dissertation to my precious daughter, Yuning Yang, and wish her a splendid future.

LIST OF CONTENTS

LIST OF TABLES

LIST OF FIGURES

NOTATIONS

Symbol	Description	Unit
$\Delta\theta$	Predicted burn duration	*deg*
η_{comp}	Thermal efficiency of compressor	
η_{HCCI}	Combustion efficiency in HCCI combustion mode	
η_{IN}	Volumetric efficiency of the intake process	
η_{SI}	Combustion efficiency in SI combustion mode	
η_{turb}	Thermal efficiency of turbine	
θ	Current crank position	*deg* ACTDC
θ_{ST}	Spark timing in degree after combustion TDC	*deg* ACTDC
θ_{INTM}	Intake valve timing at peak lift	*deg* AGTDC
θ_{EXTM}	Exhaust valve timing at peak lift	*deg* BGTDC
κ	Heat capacity ratio	
λ	Normalized air-to-fuel ratio	
Π_{lift}	Peak lift of intake/exhaust valve	*mm*
ϕ_{TPS}	Engine throttle position	%
ϕ_{acc}	Acceleration pedal position	%
ϕ_{EGR}	External EGR valve opening	%

A_c	Instant cylinder inner surface area	m^2
A_v	Cross area of valve flow	m^2
b_{ETC}	Damping ratio of throttle plate	
c_{ETC}	Torque constant of throttle drive motor	$N.m/A$
C_d	Valve discharge coefficient	
C_p	Specific heat for constant pressure	$kJ/kg \cdot K$
C_v	Specific heat for constant volume	$kJ/kg \cdot K$
e	Specific internal energy	kJ/kg
F_{DI}	Direct injection (DI) fuel pulse duration	(*ms*/cycle)
F_{FB}, F_{FF}	Feedback/feedforward portions of F_{DI}	(*ms*/cycle)
F_{ILC}	ILC portion of DI pulse duration	(*ms*/cycle)
h	Specific enthalpy	kJ/kg
H_{LHV}	Lower heating value	kJ/kg
i	Indexes of ILC iteration	
I_{ETC}	Actuator current of electric throttle control (ETC) system	A
J_e	Rotational inertia of the engine crankshaft	$Kg.m^2$
J_{turbo}	Rotational inertia of the turbocharger shaft	$Kg.m^2$
k	Index of sampling time for time based control logic	

k_{ETC}	Spring constant of throttle plate	
m_{comp}	Gas mass flow rate through compressor	*g/s*
m_{in}	Inlet gas mass flow rate	*g/s*
m_{out}	Outlet gas mass flow rate	*g/s*
m_{turb}	Gas mass flow rate through turbine	*g/s*
m_v	Mass flow rate across the valve	*g/s*
M	Mass of gas mixture	*g*
M_B	Mass of burned zone gas mixture in SI combustion	*g*
M_f	Fuel mass of each cylinder per engine cycle	*g*
M_r	Mass of residual gas	*g*
M_t	Total mass of in-cylinder charge	*g*
M_U	Mass of unburned zone gas mixture in SI combustion	*g*
N_e	Engine speed	*rpm*
P	Instant in-cylinder gas pressure	*bar*
P_{amb}	Ambient pressure	*bar*
P_{down}	Valve downstream pressure	*bar*
P_{EM}	Gas pressure at exhaust manifold	*bar*
P_{IM}	Gas pressure at intake manifold	*bar*

P_m	Gas pressure at manifolds, or connecting pipes	*bar*
P_{up}	Valve upstream pressure	*bar*
Q	Heat transfer to combustion chamber surface	*kJ/deg*
r	Radius of throttle plate	*m*
R	Gas constant	*kJ/kg·K*
T	Instant in-cylinder gas temperature	*K*
T_{amb}	Ambient temperature	*K*
T_B	Gas temperature of burned zone in SI combustion	*K*
T_U	Gas temperature of unburned zone in SI combustion	*K*
T_m	Gas temperature at manifolds, or connecting pipes	*K*
T_e	Engine brake torque	*N.m*
T_l	Engine load torque	*N.m*
V	Instant cylinder volume	m^3
V_B	Volume of burned zone gas mixture in SI combustion	m^3
V_d	Engine displacement	m^3
V_m	Volume of intake manifold	m^3
V_U	Volume of unburned zone gas mixture in SI combustion	m^3
w	The average in-cylinder gas velocity	*m/s*
x	Mass fraction burned	

x_{EGR}	EGR gas fraction in engine intake manifold	
MAP	Intake manifold absolute pressure	*bar*
IMEP	Indicated mean effective pressure	*bar*
$IMEP_{ref}$	IMEP learning reference used in ILC	*bar*
ACTDC	After combustion TDC	
BGTDC	Before gas exchange TDC	
DI	Direct injection	
EGR	Exhaust gas recirculation	
EMP	Exhaust manifold pressure	
EVC	Exhaust valve closing	
EVO	Exhaust valve opening	
HCCI	Homogeneous charge compression ignition	
HIL	Hardware in the loop	
HP	High pressure	
IC	Internal combustion	
ILC	Iterative learning control	
IVC	Intake valve closing	
IVO	Intake valve opening	
LP	Low pressure	
MBT	Minimal advance for the best torque	
MFB	Mass fraction burned	
MFR	Mass flow rate	

PFI	Port fuel injection
PID	Proportional, integral, and derivative
SI	Spark ignition
SOHCCI	Start of HCCI combustion
TDC	Top dead center
VVA	Variable valve actuation
VVT	Variable valve timing
WOT	Wide open throttle

CHAPTER 1

INTRODUCTION

1.1 New Technologies and Challenges

The imminent energy crisis and the increasingly stringent emission and fuel economy regulations of automobiles are key factors to promote the research and development of many new engine technologies in the past decade that increase internal combustion (IC) engine system complexity significantly. Among these technologies engine downsizing using single or dual-stage turbocharger and homogeneous charge compression ignition (HCCI) combustion are two promising ones.

1.1.1 Engine downsizing

Downsized engine has higher power density (small displacement), leading to improved fuel economy ([1] and [2]). Turbocharger is widely used in downsized IC engines, but it leads to slow engine response due to turbo lag [3], which reduces the competitiveness of turbocharged vehicles in the market. Smaller turbocharger reduces turbo lag, but at the same time, it limits the engine boost pressure at high engine speed. Dual-stage turbocharger system has been proposed recently in [4], [5], and [6] due to its potential of covering wide range of engine operational conditions with reduced turbo lag. However the control of a dual-stage turbocharged engine is fairly complicated. The dynamics of two turbochargers staged in series interact with each other, which is different from the dual turbocharger engine with two turbochargers connected in parallel. Furthermore, the turbo system and combustion chamber are connected in a closed loop. The product of the combustion process, exhaust gas, is the energy input to the turbo system; the compressor utilizes the turbo output mechanical energy to generate pressurized intake charge; the intake gas pressure, or in other words, the boost pressure, is directly associated with the combustion efficiency. High boost pressure leads to high combustion efficiency and engine power density [7], but it could also lead to heavy engine knock [8]. Some technologies are introduced to suppress the engine knock, such as high dilution combustion using external EGR (exhaust gas recirculation) gas [8], dual fueling technology [9], and closed-loop combustion control using in-cylinder ionization signal ([10] and [11]) or pressure signal ([12] and [13]). These technologies greatly increase the engine control system complexity, and make it necessary to develop model based control strategies.

1.1.2 HCCI combustion

HCCI combustion is another promising technology [14]. The flameless nature of the HCCI combustion and its capability of high dilution operation lead to low combustion temperature. As a result, the formation of NOx (nitrogen oxides) can be significantly reduced [15]. Furthermore, HCCI combustion is capable of un-throttled operation that greatly reduces engine pumping loss and improves fuel economy ([16] and [17]).

On the other hand, HCCI combustion has its own limitations. As illustrated in Figure 1.1, it is limited at high engine load due to the audible knock ([18] and [19]); and at low load due to misfire caused by the lack of sufficient thermal energy to trigger the auto-ignition of the gas-fuel mixture during the compression stroke ([20] and [21]). In fact, HCCI can be regarded as a type of engine operating mode rather than a type of engine [22]. In order to take advantage of the HCCI combustion mode in an IC engine, other combustion mode, such as spark ignited (SI) combustion, is required at high load, at high speed [23], at ultra-low load (such as idle), and at certain operating conditions, such as at cold start [24].

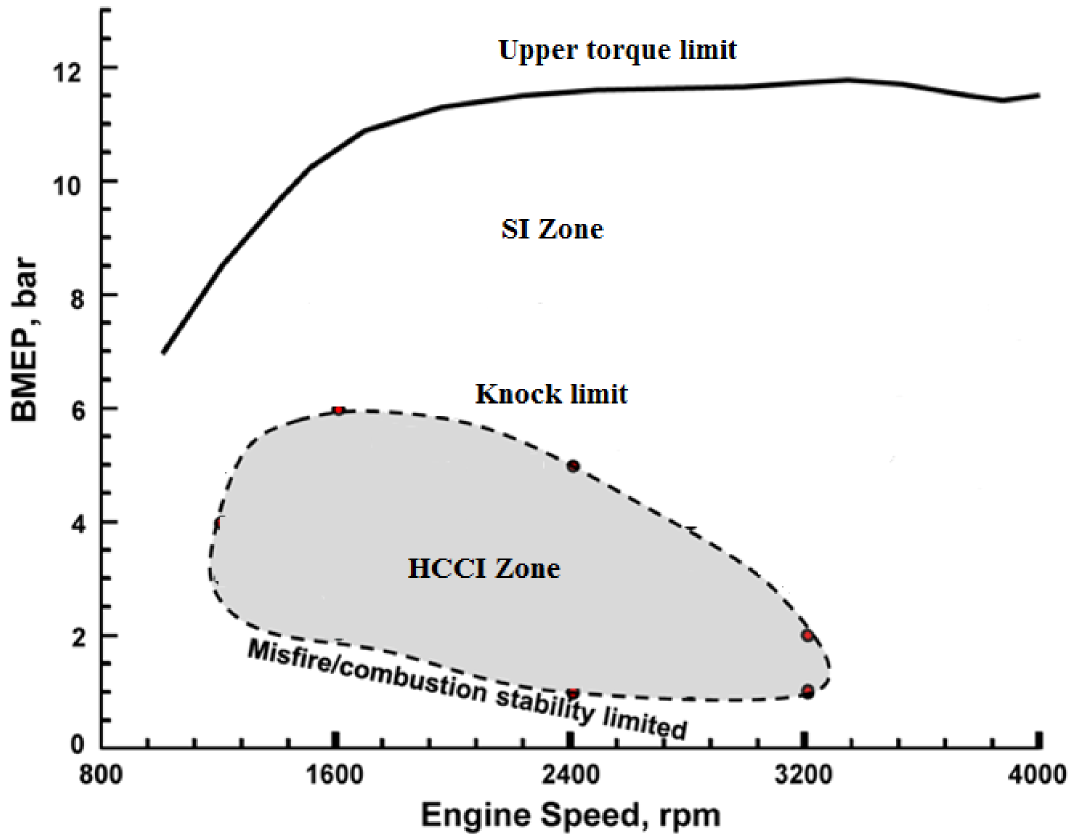

Figure 1.1: HCCI combustion operation range

It is fairly challenging to operate the engine in two distinct combustion modes, and it is even more difficult to have smooth combustion mode transition between the SI and HCCI combustions, because the favorable thermodynamic conditions for one mode are always adverse to the other [25]. For example, high intake charge temperature is required in the HCCI mode to initiate the combustion, while in the SI mode it leads to reduced volumetric efficiency and increased knock tendency [26]. For this reason, engine control parameters, such as intake and exhaust valve timings and lifts, throttle position, and EGR (exhaust gas recirculation) valve opening, are regulated at different level between these two combustion modes. During the combustion mode transition, these engine parameters need to be changed rapidly. However, the physical actuator limitations on response time prevent them from completing their transitions within the required duration, specifically, within one engine cycle [27]. The multi-cylinder operation makes it even more difficult [28]. Accordingly the combustion performance during the transition cannot be maintained unless proper control strategy is applied.

1.2 Related Work

In order to tackle the challenges and implementing these new technologies to IC engines, more attentions have been paid to the researches for advanced control strategies, such as model based control. In this dissertation, control oriented models are presented for the dual-stage turbocharged engine and the HCCI capable SI engine. Furthermore, the model based control strategies were studied for the combustion mode transition control of the HCCI capable SI engine.

1.2.1 HCCI capable engine control

To realize the HCCI combustion in production IC engines, it has two challenges regarding the engine controls. One is the control of the HCCI combustion process, where the challenge is mainly due to the cycle-to-cycle residual gas dynamics; the other is the combustion mode transition control, which is a major concentration of this dissertation.

The control of the HCCI combustion process has been widely studied for different engine configurations in past decades. Among these studies, the combustion timing control is of the greatest interest, due to the lack of direct combustion trigger in the HCCI combustions. In [29], stable HCCI combustion timing was achieved at different engine speeds by regulating the engine VVT (variable valve timing) through a PID (proportional, integral, and derivative) control with gain scheduling. Shaver ([30], [32], and [32]) realized stable combustion timing and work output performances via closed-loop residual gas quantity control, for an HCCI capable engine equipped with a camless VVA (variable valve actuation) system. Ravi developed a model based combined feedback, feedforward and integral control strategy to track desired load-phasing trajectories of the HCCI combustions ([33] and [34]), where the pilot fueling during recompression phase of the HCCI combustions is used as the control knob. Robust HCCI combustions were also achieved for transient operating conditions through control strategies as described in [35], [36], and [37]. These advanced control strategies make the HCCI combustion feasible in practical IC engines, but they bring challenges to the combustion mode transition at the same time, which is inevitable for production engines with the HCCI combustion mode [38].

In order to implement the HCCI combustion technology in production engines, in recent years, the combustion mode transition control has become an interesting topic in the HCCI engine research. In [39] and [40], smooth mode transitions between the SI and HCCI combustions were realized for a single cylinder engine equipped with the camless VVA system. However, the camless VVA system itself is still not feasible for mass production due to its high cost and package issues. In [41], smooth combustion mode transition was realized for a single cylinder GDI engine equipped with VVT system. In [42], a VVT system with dual-stage lifts was used on a multi-cylinder engine for studying the mode transition. Experimental results showed the potential of achieving smooth mode transition by controlling the throttle opening timing and the DI (direct injection) fuel quantity. However, satisfactory engine performance during the mode transition was not accomplished due to the lack of control strategies.

The SI-HCCI hybrid combustion mode as described in [43] and [44] can be observed during the mode transition between the SI and HCCI combustions. It was discovered in [25] that the control of the SI-HCCI hybrid combustion mode is the key to achieve smooth combustion mode transition for engines equipped with the VVT system. Accordingly, this dissertation mainly focuses on the modeling and control development of the hybrid combustion mode.

1.2.2 SI-HCCI hybrid combustion mode

The SI-HCCI hybrid combustion starts in SI combustion mode with a relatively low heat release rate; and once the thermodynamic and chemical conditions of the unburned gas satisfy the start of the HCCI (SOHCCI) combustion criteria, the combustion continues in the HCCI combustion mode, which is illustrated by the dashed curves of mass fraction burned (MFB) shown in Figure 1.2. During an ideal SI to HCCI combustion transition process, the percentage of SI combustion (ST to SOHCCI, see Figure 1.2) decreases gradually while the HCCI combustion percentage (SOHCCI to end of combustion or MFB = 1) increases gradually [45]. For the HCCI to SI combustion transition, the process is reversed. This hybrid combustion mode transition process allows using conventional cam phase system since the required cam phase will change gradually.

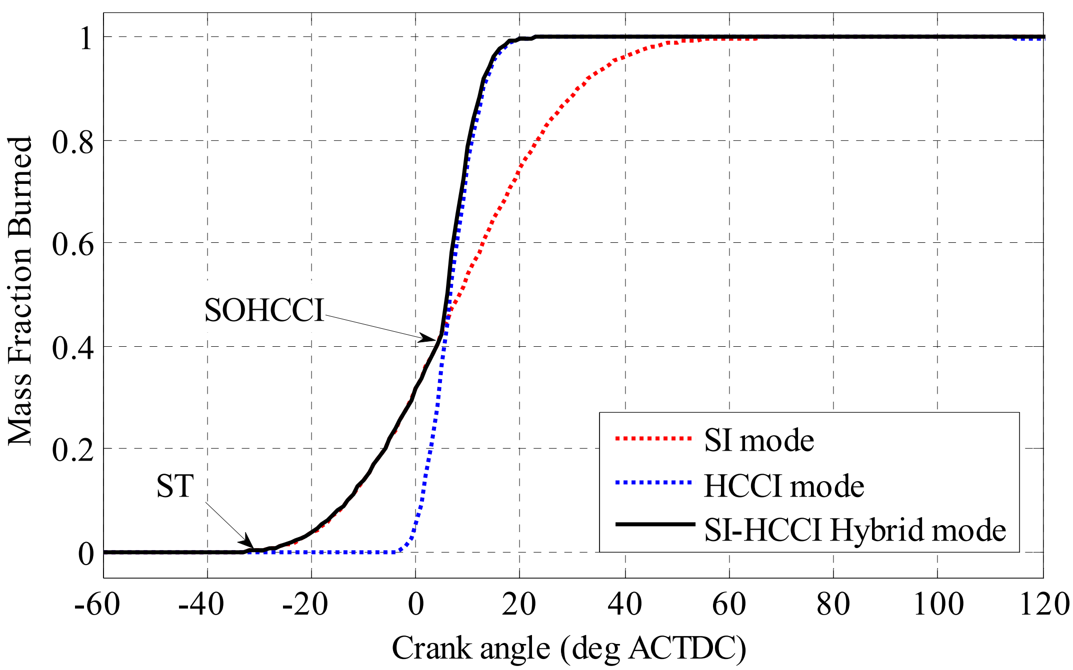

Figure 1.2: MFB in SI-HCCI hybrid combustion mode transition process

"For interpretation of the references to color in this and all other figures, the reader is referred to the electronic version of this dissertation."

During the combustion mode transition, the engine thermodynamic conditions are between the SI and HCCI modes. The typical control strategies of both SI and HCCI combustion modes cannot be applied under the transitional conditions, due to the lack of control variables [25]. However, the SI-HCCI hybrid combustion mode is feasible under the transitional conditions. Implementing the hybrid combustion mode during the combustion mode transition, the engine performances such as the IMEP (indicated mean effective pressure) can be controlled by the spark ignition, fuel quantity, and intake/exhaust valve timings. The multistep mode transition control strategy developed in this dissertation is based on the SI-HCCI hybrid combustion mode.

1.2.3 Related control methods

The SI-HCCI hybrid combustion mode control is studied in this dissertation for the first time, to achieve smooth SI to HCCI combustion mode transition, for an HCCI capable SI engine equipped with dual-stage turbocharger system. For the control development, three control methods were utilized. They are linear quadratic (LQ) tracking control, iterative learning control (ILC), and PI (proportional and integral) control.

LQ tracking control minimizes a quadratic tracking error over a given time period based upon the LQ optimal control theory, where a nonzero reference signal is given, see [46], [47], and [48]. In this dissertation, this method is used to make the engine MAP (intake manifold absolute pressure) track the desired reference during the combustion mode transition. As a result, the air-to-fuel ratio of each engine cylinder can be maintained within the desired range, which makes the engine IMEP (indicated mean effective pressure) controllable through regulating DI (direct injection) fuel quantity.

ILC is a feedforward control method [49] with numerous applications, such as in [50] and [51]. In this dissertation, to eliminate the significant cylinder-to-cylinder and cycle-to-cycle variations of the engine IMEP during the mode transition, ILC was applied to the DI fuel quantity of individual cylinder. The motivation of using this method is mainly due to the repetitive nature of the combustion mode transition process.

PI control is a popular feedback control method. In this dissertation, it is combined with the ILC to smooth the combustion mode transition process under transient engine load conditions.

The control methods discussed above are well known in theory, but to apply them to the specific application a validation approach is required and the HIL engine simulation is adopted.

1.2.4 HIL engine simulation

The HIL simulation is a powerful tool used in the development and validation of a complex real-time embedded control system, such as an engine control system. Utilizing the appropriate engine model, an HIL simulator, such as the dSPACE engine simulation system, is capable of providing various engine output signals based upon the control signals provided by the engine controller at different engine operational conditions [46]. Development of an engine control system using the HIL simulation environment could reduce cost and shorten development cycle. Therefore, HIL simulations are widely used in the automotive industry for power-train system research and development [53]. To take the advantage of the HIL simulation, a control oriented engine model is required.

In order to provide high resolution engine signals, the HIL simulator always runs with a very short time step. Accordingly the model needs to be updated within a given short period. For example, if the in-cylinder pressure signal is updated every crank degree, the combustion model calculation needs to be completed every crank degree, which is corresponding to 56 microseconds when engine speed is 3000 rpm. The requirement of real-time simulation limits the complexity of the control oriented engine model.

1.2.5 Engine modeling

For control strategy development, zero dimensional mean value engine models are widely used, see [54] through [58], due to their simplicity and low simulation throughput. For the engine air handling system or crankshaft dynamics, mean value models are accurate enough since the piston reciprocating movement has less impact on these subsystems than on the combustion process. Therefore, the mean value modeling approach is also used for these subsystems in this dissertation. The disadvantage of the mean value engine modeling is that it does not provide detailed information about engine combustion process, such as in-cylinder gas pressure, temperature, and ionization signals, which have been widely used for closed-loop combustion control ([59], [60] and [61]). The in-cylinder pressure rise ($dP/d\theta$) is a key indicator for detecting engine knocks [62].

In order to explore the details about the engine combustion process, multi-zone, three dimensional CFD (computational fluid dynamics) models with detailed chemical kinetics are presented in [63], [64] and [65], and they are able to precisely describe the thermodynamic, fluid-flow, heat transfer, and pollutant formation phenomena of the HCCI combustion. Similar combustion models have also been implemented into commercial codes such as GT-Power [66] and Wave. However, these models with high fidelity cannot be directly used for control strategy development since they are too complicated to be used for real-time simulations, but they can be used as reference models for developing simplified (or control oriented) combustion models for control purpose.

For real-time HIL simulations, it is necessary to develop a type of combustion model with its complexity inter-between the time based mean value models and the CFD models. This motivates the combustion modeling work presented in this dissertation. The 0D (zero dimensional) crank based combustion model is selected for this dissertation. Table 1.1 compares the capability of this modeling method with the other two.

Table 1.1: Features for different combustion model

	0D time based combustion model	0D crank based combustion model	1D & 3D CFD combustion model
Implementation tool	Matlab/Simulink	Matlab/Simulink and HIL simulator	GT-Power, Wave and Fluent
Time cost per cycle	Micro seconds	Real-time	Minutes to hours
One-zone	Yes	Yes	Yes
Two-zone	No	Yes	Yes
Multi-zone	No	No	Yes
Chemical concentration	No	No	Yes
Gas-fuel mixing model	No	No	Yes
In-cylinder flow dynamics	No	No	Yes
IMEP	Yes	Yes	Yes
In-cylinder pressure	No	Yes	Yes
In-cylinder temperature	No	Yes	Yes
Ionization signal	No	Yes	No

1.3 Dissertation Contributions

This research begun with modeling the dual-stage turbocharged SI engine. A mixed time-based and crank-based modeling method was used. The engine air-handling system was modeled in a time-based mean-value approach, and SI combustion process was modeled as functions of engine crank angle. The same modeling approach was then applied to model the HCCI capable SI engine. The developed combustion model is capable of simulating the SI, the

HCCI and the SI-HCCI hybrid combustion modes. Both engine models were calibrated and validated by the corresponding GT-Power models. Afterwards the engine models were implemented and validated in the dSPACE based HIL simulation environment.

The HCCI capable SI engine control was studied in the developed HIL simulation environment. A multistep control strategy was developed to achieve smooth combustion mode transition between the SI and HCCI combustion modes. The HIL simulation results demonstrated the effectiveness of the developed control strategy under both constant and transient engine operating conditions.

The dissertation has the following major contributions:

- The mixed time-based and crank-based engine models were developed for a dual-stage turbocharged SI engine and an HCCI capable SI engine. They are capable of real-time simulation with accuracy comparable to the relatively high fidelity GT-Power model.
- The SI-HCCI hybrid combustion process was modeled for the first time using a mixed two-zone and one-zone combustion models. The SI and HCCI combustions are special cases in the SI-HCCI hybrid combustion model.
- Smooth SI to HCCI combustion mode transition was demonstrated using multistep control strategy, where the SI-HCCI hybrid combustion mode was implemented to relax the charge temperature requirement, LQ optimal tracking control was used to regulate the charge air-to-fuel ratio at desired range so that the engine IMEP can be regulated through DI fuel quantity control, and the IMEP of each engine cylinder was regulated through iterative learning control of the DI fuel quantity of the corresponding cylinder.

1.4 Dissertation Outline

The material presented in this dissertation is organized into six chapters. In Chapter 2, the dual-stage turbocharged SI engine model is developed using the mixed time-based and crank-based method; the model is also validated with the corresponding GT-Power model. In Chapter 3, the SI-HCCI hybrid combustion mode is defined and the corresponding model is presented along with the gas exchange process model; the model validation results are also discussed. In Chapter 4, the implementation of the developed model into the real-time HIL simulation environment is depicted with the proposed numerical approach; the HIL simulation results are presented to introduce the control study for the following chapter. In Chapter 5, the challenges of the SI to HCCI combustion mode transition are analyzed and the multistep combustion mode transition control strategy is presented with HIL validations. In Chapter 6, conclusions and future work are drawn.

CHAPTER 2

DUAL-STAGE TURBOCHARGED SI ENGINE MODELING USING MIXED MEAN VALUE AND CRANK BASED METHOD

2.1 Introduction

Downsized engine using dual-stage turbocharger has been discussed in the previous chapter for its high power density and ability to cover wide range of engine operational conditions [6]. However dual-stage turbocharger may lead to extreme engine operational conditions. For instance, the engine load could reach 30 bar IMEP (indicated mean effective pressure) with 3 bar MAP (intake manifold absolute pressure), which could result in heavy engine knock that can't be ignored. Using the external cooled EGR gas to reduce combustion temperature and the rate of in-cylinder pressure rise is introduced in [11]. VVT technique is also recommended to adjust the effective compression ratio at high load to suppress the engine knock. Flex fuel, such as ethanol, is also an effective way to reduce engine knock ([67] and [68]).

These technologies require sophisticated engine control strategies, such as model-based control, to operate the engine at its most efficient conditions, which requires a control oriented engine model for the control strategy development and validation. This control oriented model has to be accurate enough to include detailed engine dynamics, and capable of being simulated in real-time at the same time. A mixed mean value and crank based engine model is proposed and developed in this chapter. The engine model contains both time based engine dynamics, such as crankshaft dynamics, and crank based engine combustion process.

This chapter is organized as follows. In Section 2.2 the engine configuration and its GT-Power model are discussed. In Section 2.3 the time based mean value models of the engine air handling system are presented. Section 2.4 provides the governing equations of combustion process as a function of the crank angle. Model validation is accomplished in Section 2.5.

2.2 Engine Configuration and GT-Power Model

Figure 2.1 shows the downsized three-cylinder engine with cooled EGR and dual-stage turbocharger. The HP (high pressure) turbocharger, connected to the engine intake and exhaust manifolds, is smaller than that of the LP (low pressure) turbocharger. Accordingly, the HP compressor has a smaller capacity of air mass flow rate than the LP one. A bypass valve is connected to the HP compressor, and it is used to match the air mass flow rate of both compressors. Each stage of turbine is equipped with solenoid controlled continuously adjustable waste-gate. An intake cooler is connected between the HP compressor and intake manifold. Unlike traditional engines, this engine utilizes intake throttles located close to the three intake runners between the intake manifold and intake ports to improve transient responses. The engine also features dual intake and exhaust valves with independent variable valve timing (VVT) control. Both cam phasing actuators are adjustable in the range of ±20 crank degrees. The EGR cooler and controllable EGR valve in Figure 2.1 composes the external EGR system of the engine. Cooled EGR gas can be re-circulated through the external EGR system back to cylinder, and acts as inertia gas to cool down the combustion temperature. The engine is also equipped with dual fuel injection systems: port fuel injection (PFI) and direct injection (DI), and can be operated with any blend of ethanol and gasoline.

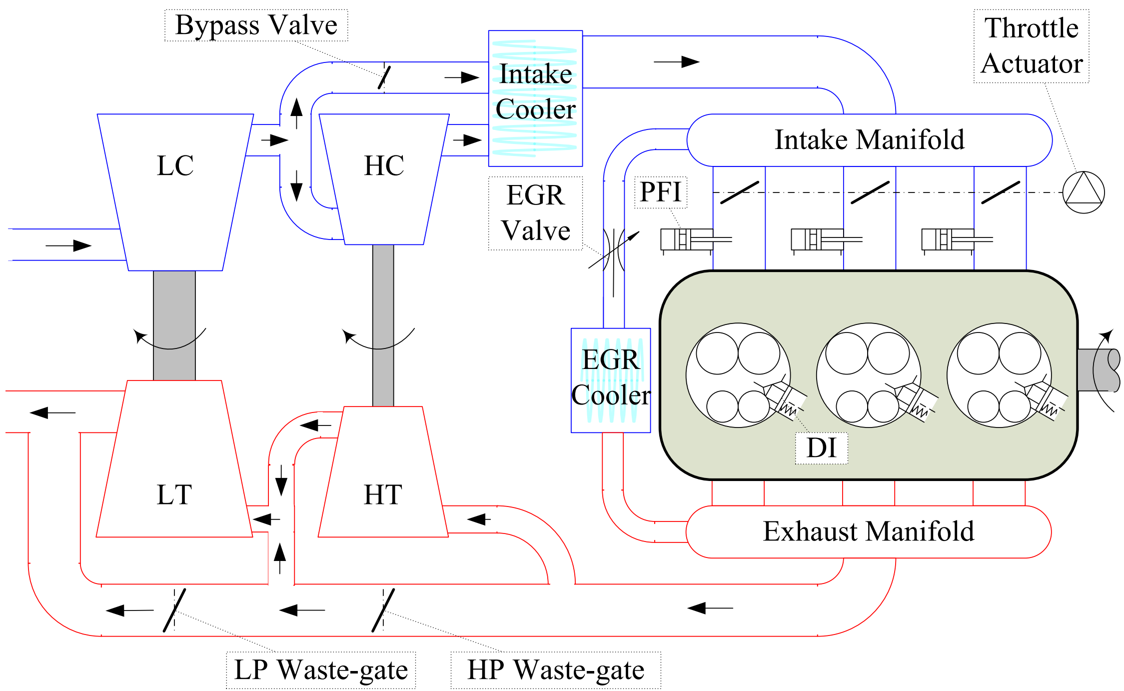

Figure 2.1: Dual-stage turbocharged SI engine configuration

Table 2.1: Dual-stage turbocharged SI engine specification

Engine parameter	**Model value**
Bore/stroke/con-rod length	83mm/73.9mm/123mm
Compression ratio	13.5:1
Intake valve/exhaust valve diameter	31.4mm/22.5mm
Throttle diameter	3×48mm
Intake manifold/exhaust manifold volume	2.0L/0.57L
Inertia of HP-stage turbocharger shaft	3.807E-6kg.m^2
Inertia of LP-stage turbocharger shaft	2.7E-5kg.m^2

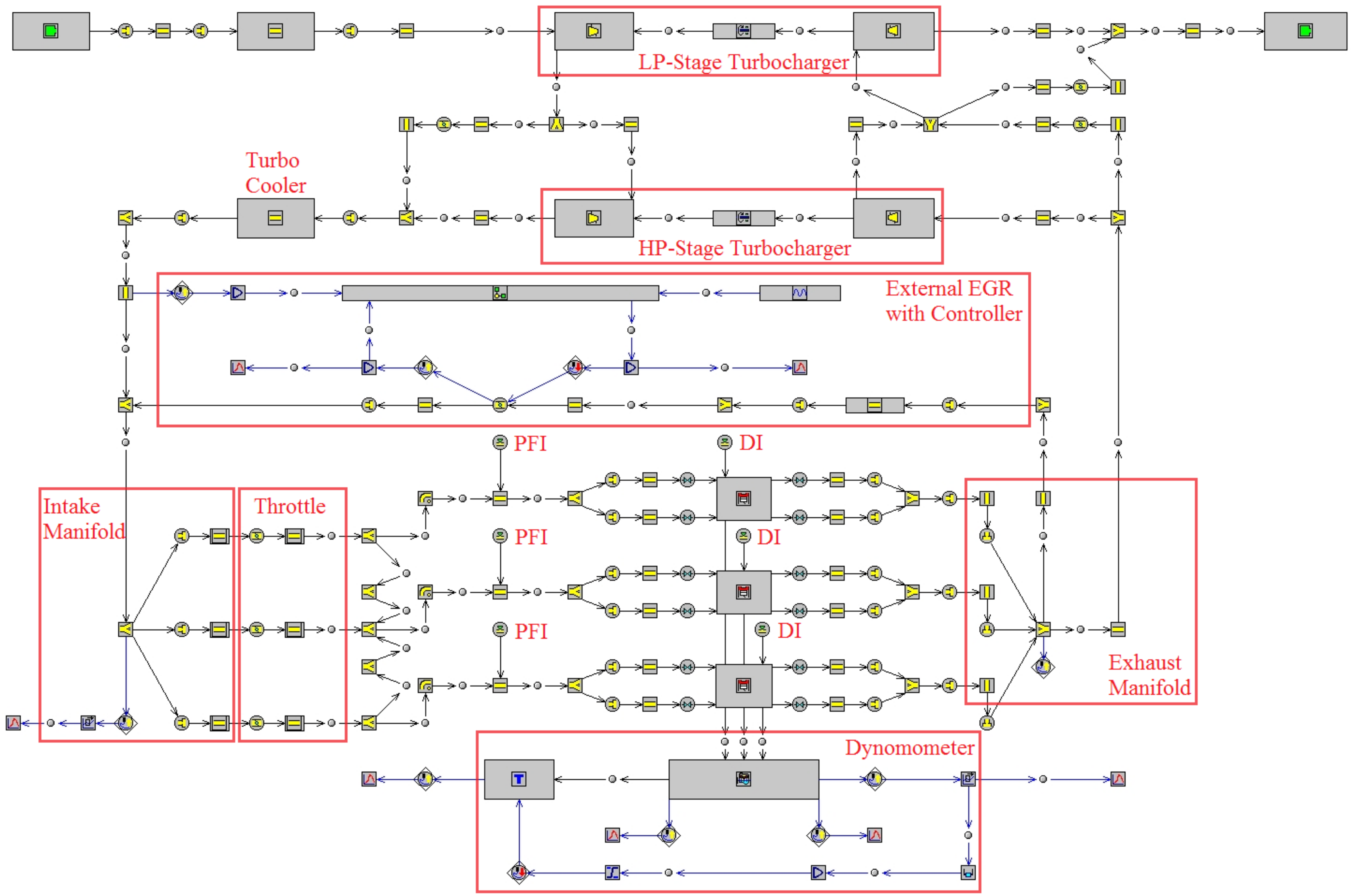

Figure 2.2: GT-Power engine model diagram

The key engine geometry dimensions are listed in Table 2.1. The actual engine is still under development. Accordingly a GT-Power engine model was developed corresponding to the engine configuration shown in Figure 2.1 as the baseline for the engine control system development in the early stage of the research.

GT-Power is commercial software for vehicle powertrain system modeling and simulation. It is widely used in the automotive industry. It features an object-based code design, which allows user to build an engine part by part, module after module. As shown Figure 2.2, the layout of the GT-Power engine model is consistent with the engine configuration in Figure 2.1. The parameters of each engine component can be specified individually by editing the property dialogue box of the corresponding block. Most of the key parameters were given by the engine manufacturer, such as the intake and exhaust valve lifts.

The GT-Power model is mainly based on one-dimensional fluid dynamics, representing the flow and heat transfer in the piping and other flow components of an engine system [66]. It takes relatively long time (sometimes, in hours) for the model solution to converge and provides the steady state performance of the engine. This makes it impossible to use the GT-Power model for real-time engine simulation. Furthermore, GT-Power is capable of providing accurate steady state simulation results but relatively weak in transient simulations. Therefore, GT-Power modeling tools are usually used to estimate steady state engine performance.

To meet the requirements of the real-time HIL simulation, a control oriented engine model was developed in Matlab/Simulink with “C” S-functions to be implemented into dSPACE or Opal-RT based HIL simulators. The GT-Power model introduced in this section was used to calibrate and validate the engine model developed in the remaining chapter.

2.3 Mean Value Models for Engine Air Handling System

This section describes mathematical subsystem models for those engine subsystems whose averaged dynamic behaviors are required for control purpose, even though they are functions of engine reciprocating phenomenon. All parameters and variables used in these models are functions of time *t*.

2.3.1 Valve model

The valve model, described below, is used for the intake throttle, the HP and LP waste-gate, and EGR valve since these actuators share same physical characteristic. Assuming that the spatial effects of the connecting pipes before and after these valves are neglected and their thermodynamic characteristics are isentropic expansion [69], the governing equation of the valve model is

$$m_v = C_d A_v \frac{P_{up}}{\sqrt{RT_{up}}} \psi\left(\frac{P_{down}}{P_{up}}\right) \tag{2.1}$$

where

$$\psi(x) = \begin{cases} \sqrt{2x(1-x)}, & \text{if} \quad 1/2 < x < 1 \\ 1/\sqrt{2}, & \text{if} \quad x < 1/2 \end{cases} \tag{2.2}$$

C_d is the valve discharge coefficient; A_v is the valve open area; P_{up} and T_{up} are the valve upstream pressure and temperature; P_{down} is the valve downstream pressure; and m_v is the mass flow rate across the valve. Note that both C_d and A_v are functions of the valve opening angle θ_v.

2.3.2 Manifold filling dynamic model

This model is mainly used for the intake and exhaust manifolds, inter-compressor and inter-turbine pipes. The receiving behavior is assumed to be an adiabatic process in these manifolds [69]. Their thermodynamic states are uniform over the entire manifold volume and the manifold temperature is averaged over one engine cycle for this mean value model. Then the governing equation for the manifold filling dynamics is

$$\frac{dP_m}{dt} = \frac{RT_m}{V_m}\left(m_{in} - m_{out}\right) \tag{2.3}$$

where P_m is the manifold pressure; T_m is the manifold temperature; V_m represents the manifold volume; m_{in} and m_{out} are the inlet and outlet air mass flow rates, respectively.

2.3.3 Crankshaft dynamic model

Based upon Newton theory, assuming a rigid crankshaft, it can be derived as

$$\frac{dN_e}{dt} = \frac{60}{2\pi}\frac{T_e - T_l}{J_e} \tag{2.4}$$

where J_e is the rotational inertia of the engine crankshaft; T_e and T_l are the engine brake torque and load torque, respectively. Note that in future simulations, T_l is generated by an engine dynamometer model controlled by a PID feedback controller to maintain the desired engine speed.

2.3.4 Turbine and compressor models

The turbocharger is modeled using the so-called energy conservative equations based upon its steady state compressor and turbine maps, which can be found in [6] and [70]. Notice that the turbo mass flow rate (MFR) and shaft speed in the turbo mapping equations given below are in the so-called reduced form, to make the turbo maps applicable for all inlet conditions. Without this conversion, it would require different turbo maps for each combination of inlet pressure and temperature [71].

Both turbine and compressor dynamics are described below in equations (2.5) to (2.12), where P_{in} and T_{in} are either turbine or compressor inlet pressure and temperature; P_{out} and T_{out} are either turbine or compressor outlet pressure and temperature; N_{turbo} is the turbocharger shaft speed in rpm; and η denotes thermal efficiency.

1) Turbine mapping: Turbine maps (f_{turb} and f'_{turb}) in equations (2.5) and (2.6) are used to calculate the reduced MFR m_{turb} and thermal efficiency η_{turb} based on pressure ratio across the turbine and the reduced turbo shaft speed. The actual MFR can be calculated from the reduced MFR m_{turb} by

$$m_{turb} = f_{turb}\left(\frac{P_{in}}{P_{out}}, \frac{N_{turbo}}{\sqrt{T_{in}}}\right)\frac{P_{in}}{\sqrt{T_{in}}} \tag{2.5}$$

and

$$\eta_{turb} = f'_{turb}\left(\frac{P_{in}}{P_{out}}, \frac{N_{turbo}}{\sqrt{T_{in}}}\right) \tag{2.6}$$

2) Compressor mapping: Compressor maps (f_{comp} and f'_{comp}) in equations (2.7) and (2.8) are used to calculate the compressor pressure ratio and thermal efficiency η_{comp} based on reduced MFR m_{comp} and reduced turbo shaft speed by

$$\frac{P_{out}}{P_{in}} = f_{comp}\left(\frac{m_{comp}\sqrt{T_{in}}}{P_{in}}, \frac{N_{turbo}}{\sqrt{T_{in}}}\right) \tag{2.7}$$

and

$$\eta_{comp} = f'_{comp}\left(\frac{m_{comp}\sqrt{T_{in}}}{P_{in}}, \frac{N_{turbo}}{\sqrt{T_{in}}}\right) \tag{2.8}$$

3) Temperature calculation: The outlet temperature of the turbine or compressor can be calculated based upon:

$$\frac{T_{out}}{T_{in}} = \left(\frac{P_{out}}{P_{in}}\right)^{(\kappa-1)/\kappa} \tag{2.9}$$

Notice that equation (2.9) assumes isentropic gas expansion and compressing process for either turbine or compressor. However, the actual physical process is not isentropic, leading to more enthalpy remaining in the gas due to thermal efficiency, which makes the actual outlet temperature higher than that given by equation (2.9), but the difference is relatively small. Simulation results presented in Figure 2.5 show an acceptable correlation between GT-Power results and the temperature calculated using equation (2.9). Therefore, this assumption is acceptable.

4) Turbine power calculation: The power generated by turbine, denoted as E_{turb}, is calculated by

$$E_{turb} = m_{turb} C_p \eta_{turb} T_{in} \left[1 - \left(\frac{P_{out}}{P_{in}}\right)^{\frac{\kappa-1}{\kappa}}\right] \tag{2.10}$$

5) Compressor power calculation: The power required to drive compressor, denoted as E_{comp}, is calculated by

$$E_{comp} = m_{comp} C_p \frac{1}{\eta_{comp}} T_{in} \left[\left(\frac{P_{out}}{P_{in}}\right)^{\frac{\kappa-1}{\kappa}} - 1\right] \tag{2.11}$$

6) Power balance on turbocharger shaft: The power balance on the turbocharger shaft is calculated by

$$E_{turb} - E_{comp} = J_{turbo} N_{turbo} \frac{dN_{turbo}}{dt} \tag{2.12}$$

where J_{turbo} is the rotational inertia of the turbocharger shaft.

2.4 Crank Based One-Zone SI Combustion Model

This section presents the mathematic model of the SI combustion model based on the one-zone assumption of the in-cylinder gas-fuel mixture.

2.4.1 Crank based methodology

The purpose of the combustion process modeling is to correlate the trapped in-cylinder gas properties, such as air-to-fuel ratio, trapped EGR gas mass, in-cylinder gas pressure and temperature, to the combustion characteristics such as misfire, knock, burn duration, and IMEP. The developed combustion model will be combined with the mean value air handling system model to construct the entire engine model used for model-based control strategy development and validation of the dual-stage turbocharger engine. Note that the combustion model also needs to meet the real-time HIL simulation requirements.

Some combustion related parameters in the combustion model are updated every crank degree, such as in-cylinder gas pressure and temperature, while the others, such as IMEP and air-to-fuel ratio are updated once every engine cycle at the given crank position. The latter reflects cycle-to-cycle dynamics of the combustion process. Overall they are all discrete functions of engine crank position θ_i, which is different from the mean value model presented in the last section, where the parameters are continuous functions of time t.

There are many motivations of using the crank based modeling approach. The first is due to the fact that most combustion characteristics are usually functions of the crank angle, such as burn duration and peak pressure location; and the second is that the entire combustion process is divided into several combustion phases associated with certain events as a function of crank position. As shown in Figure 2.3, these events are intake valve closing (IVC), spark ignition timing (ST), exhaust valve opening (EVO), exhaust valve closing (EVC), and intake valve opening (IVO). The in-cylinder behaviors (such as pressure, temperature, etc.) are modeled differently during each combustion phase that is defined between two combustion events.

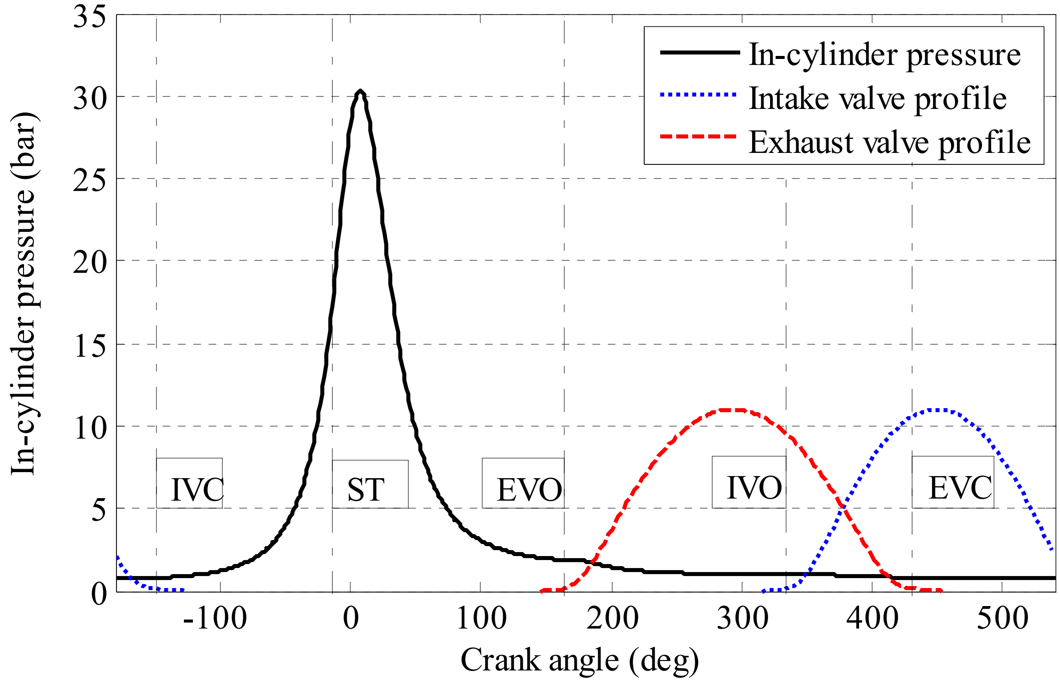

Figure 2.3: SI combustion related events and phases

The crank based modeling approach has its own limitation, too. During the real-time simulation the entire model needs to be executed within the time period associated with the desired update period (for example, one crank degree). This leads to short computational time window at high engine speed. For instant, 3000 rpm of engine speed corresponds to 56 micro seconds for one crank degree, while 6000 rpm corresponds to only 28 micro seconds. If the upper limit of engine speed is set to 6000 rpm, in order to avoid the overrun during the simulation, the computation of the combustion model must be completed within 28 micro seconds. This limits the complexity of the combustion model.

In Figure 2.3, the combustion phase starts from ST and ends with EVO. The gas exchange process from EVO to IVC and compression process from IVC to ST are also important to the combustion process, since the gas-fuel mixture is prepared during these two phases.

2.4.2 Gas exchange process modeling

1) EVO to IVO: After the exhaust valve is opened, the in-cylinder gas isentropically expands in the engine cylinder, exhaust ports and manifold, and this phase is called gas exhaust. Simply assume the in-cylinder pressure in this phase equals the exhaust manifold absolute pressure (EMP) P_{EM}

$$P(\theta_i) = P_{EM} \tag{2.13}$$

where θ_i is the current crank position. The in-cylinder gas temperature is calculated by

$$T(\theta_i) = T(\theta_{EVO}) \cdot \left[\frac{P_{EM}}{P(\theta_{EVO})} \right]^{\frac{\kappa-1}{\kappa}} \tag{2.14}$$

where $T(\theta_{EVO})$ and $P(\theta_{EVO})$ are the temperature and pressure at the crank position of exhaust valve closing, and they are derived from the combustion phase.

2) IVO to EVC: this phase is usually called valve overlap phase. During this phase the intake valve starts to open while exhaust valve is closing. The opening of both valves makes the flow dynamics more complicated and difficult to model. For simplicity, assume the in-cylinder gas pressure equals the mean value of the pressures in exhaust manifold and intake manifold. That is,

$$P(\theta_i) = \frac{P_{EM} + P_{IM}}{2} \tag{2.15}$$

where P_{IM} is the intake manifold absolute pressure. The gas temperature can be calculated same as in the last phase

$$T(\theta_i) = T(\theta_{IVO}) \left[\frac{P_{EM} + P_{IM}}{2P(\theta_{IVO})} \right]^{\frac{\kappa-1}{\kappa}} \tag{2.16}$$

In addition, at EVC the residual gas mass is calculated based on ideal gas law as follows,

$$M_r = \frac{P(\theta_{EVC})V(\theta_{EVC})}{T(\theta_{EVC})R} \tag{2.17}$$

3) EVC to IVC: during this phase fresh air is trapped into engine cylinder. The in-cylinder pressure is mainly influenced by intake manifold pressure but not always equal to it. It can be calculated by:

$$P(\theta_i) = P_{IM}\eta_{IN} \tag{2.18}$$

where η_{IN} is actually the volumetric efficiency of the intake process, and it is a function of engine speed N_e and engine load P_{IM}. In-cylinder gas temperature is calculated by

$$T(\theta_i) = T(\theta_{EVC}) \left[\frac{P_{IM}\eta_{IN}}{P(\theta_{EVC})} \right]^{\frac{\kappa-1}{\kappa}} \tag{2.19}$$

Additionally, the total mass of in-cylinder gas mixture for the compression and combustion phases is calculated at IVC also based on ideal gas law as follows,

$$M_t = \frac{P(\theta_{IVC})V(\theta_{IVC})}{T(\theta_{IVC})R} = \eta_{IN} \frac{P_{IM}V(\theta_{IVC})}{T(\theta_{IVC})R} \tag{2.20}$$

4) IVC to ST: This phase is the compression phase without combustion. The governing equations of this phase are also based on the isentropic law of ideal gas. They are

$$P(\theta_i) = P(\theta_{i-1}) \left[\frac{V(\theta_{i-1})}{V(\theta_i)} \right]^{\kappa} \tag{2.21}$$

and

$$T(\theta_i) = T(\theta_{i-1}) \left[\frac{V(\theta_{i-1})}{V(\theta_i)} \right]^{(\kappa - 1)} \tag{2.22}$$

where $V(\theta_i)$ is the cylinder volume at crank position $V(\theta_i)$ and is calculated by

$$V(\theta_i) = \left[\frac{1}{2} + \frac{1}{r-1} + \frac{L}{S} - \frac{\cos(\theta_i)}{2} - \sqrt{\frac{L^2}{S^2} - \sin^2(\theta_i)} \right] \frac{\pi B^2 S}{4} \tag{2.23}$$

Note that r is compression ratio; L is connecting rod length; S is piston stroke; B is piston bore. The values of these parameters can be found in Table 2.1.

2.4.3 Fueling dynamics and air-to-fuel ratio calculation

As shown in Figure 2.1, the engine is equipped with dual fueling systems: DI and PFI. The vaporization and mixing of DI fuel is complicated and difficult to be modeled in a zero dimension model. The combustion model simply assumes that the total DI fuel of every cycle is completely vaporized and well mixed with the in-cylinder air. On the other hand, the DI fueling has less dynamic influence on engine combustion, since the DI fuel injected in current engine cycle has negligible impact on the combustion of next cycle if combustion is normal. Whereas for the PFI fuel, the vaporization and mixing inside the engine cylinder are nearly complete, but the wall wetting phenomena of the PFI fuel spray on the intake port and the back of the intake valve introduces cycle-to-cycle dynamics and affects the engine transient performance seriously. It must be modeled in the engine model.

The wall wetting phenomena of the PFI fuel injection can be described in such a way that only part of the injected fuel ($\beta \cdot M_{inj}$, $0 < \beta < 1$) enters the cylinder while the rest of the fuel ($(1-\beta) \cdot M_{inj}$) remains on the surface of the intake port and the back of intake valves. Then the total fuel injected into the cylinder consists of the fuel directly injected into the cylinder and the fuel vapor ($\alpha \cdot M_{res}$, $0 < \alpha < 1$) from fuel mass stored from previous injection. Wall wetting phenomenon leads to the most important dynamics in PFI fuel mass calculation, which affects engine transient performance significantly [72]. The governing equation of the wall wetting dynamics is

$$\begin{cases} M_{fuel}[k] = \alpha \cdot M_{res}[k-1] + \beta \cdot M_{inj}[k] \\ M_{res}[k] = (1-\alpha) \cdot M_{res}[k-1] + (1-\beta) \cdot M_{inj}[k] \end{cases} \tag{2.24}$$

where k is the index representing engine cycle number, k indicates current engine cycle and k-1 indicates the last engine cycle; M_{fuel} is the quantity of fuel mass flowed into the cylinder; M_{res} is the quantity of fuel mass left on the port and the back of intake valves; M_{inj} is the amount of fuel injected by the PFI injector for the given engine cycle; coefficients α and β are functions of engine coolant temperature, engine speed and load.

The engine gas exchange behavior introduces dynamics to the air-to-fuel ratio calculation too, since a substantial part of the burned gas remains inside the cylinder, especially at low load. This gas fraction carries the air-to-fuel ratio of the previous engine cycle to the current one. Therefore, the air-to-fuel ratio is model cycle-by-cycle below

$$\lambda[k] = \frac{\lambda_f[k]\left(M_t[k] - M_r[k-1]\right) + \lambda[k-1] \cdot M_r[k-1]}{M_t[k]} \tag{2.25}$$

where λ is the normalized air-to-fuel ratio of gas mixture inside engine cylinder after IVC; λ_f is the normalized air-to-fuel ratio of fresh charge in current cycle, and it is defined as

$$\lambda_f[k] = \frac{M_t[k] - M_r[k-1]}{M_{fuel}[k](1+\sigma)} \tag{2.26}$$

and σ is stoichiometric air-to-fuel ratio of the fuel.

2.4.4 One-zone SI combustion model

In the SI combustion mode, the start of combustion is forced by the spark ignition, which can be controlled at any desired crank position ST. After ST the mass fraction burned of trapped fuel can be represented by the S-shaped Wiebe function [73] as

$$x(\theta_i) = 1 - \exp\left[-a\left(\frac{\theta_i - \theta_{ST}}{\Delta\theta_{SI}} \right)^{m+1} \right] \tag{2.27}$$

where $\Delta\theta_{SI}$ is the predicted burn duration of SI combustion mode (a calibration parameter of engine speed, engine load (MAP) and coolant temperature); and m is the Weibe exponent (m=2 was used in the model). Coefficient a depends on how the burn duration $\Delta\theta_{SI}$ is defined. If $\Delta\theta_{SI}$ is specified as 10% to 90% MFB, a is calculated by

$$a = \left\{ \left[-\ln(1-0.9) \right]^{\frac{1}{m+1}} - \left[-\ln(1-0.1) \right]^{\frac{1}{m+1}} \right\}^{m+1} \tag{2.28}$$

Assuming both burned and unburned gases are evenly mixed in one zone, the SI combustion process is simplified into a heat transfer with volume change process of entire in-cylinder gas. The in-cylinder gas temperature can be calculated by

$$T(\theta_i) = T(\theta_{i-1})\left[\frac{V(\theta_{i-1})}{V(\theta_i)} \right]^{(\kappa-1)} + \frac{\eta_{SI} M_f H_{LHV} \left[x(\theta_i) - x(\theta_{i-1}) \right] - Q(\theta_i)}{M_t C_v} \tag{2.29}$$

where η_{SI} is function of engine speed and engine load, calibrated by matching the calculated IMEP with that given by GT-Power; and Q represents the heat transfer between the in-cylinder gas and cylinder inner surface. Only convection was considered in the model, since for gasoline engine the heat transfer due to radiation is relatively small in comparison with the convective heat transfer [3]. Woschni correlation model ([38] and [74]) is used to calculate the heat transfer term,

$$Q(\theta_i) = A_c h_c \left[T(\theta_{i-1}) - T_w \right] \tag{2.30}$$

where h_c is called Woschni correlation, and it can be written as

$$h_c = cB^{m-1}P^m w^m T^{0.75-1.62m} \big/ N_e \tag{2.31}$$

The coefficients c and exponent m in equation (2.31) can be used to correlate the simulation results to the experimental data, or GT-Power simulation results; c=0.54 and m=0.8 were found to have good correlation for the model in this research.

There are two terms in the right hand of equation (2.29). The first term represents an isentropic compressing or expanding process, while the second term calculates the temperature rise due to the heat transfer during the combustion. Therefore, the complicated thermodynamic process of the combustion is simplified into an isentropic volume change process without heat exchange in one crank degree period and the heat absorption from combusted fuel without volume change in an infinitely small time period. Based on the updated gas temperature from equation (2.29), the gas pressure can be calculated by applying ideal gas law to the in-cylinder gas as follows,

$$P(\theta_i) = P(\theta_{i-1}) \cdot \frac{V(\theta_{i-1})}{V(\theta_i)} \cdot \frac{T(\theta_i)}{T(\theta_{i-1})} \tag{2.32}$$

2.4.5 Engine torque computation

The equations presented in the last sub-sections provide a complete profile of in-cylinder gas pressure of each engine cycle. Based on this pressure profile and the cylinder volume profile, the engine IMEP (indicated mean effective pressure) can be calculated by a simple integration

$$P_{IMEP} = \frac{1}{V_d} \cdot \sum_{i=0}^{i=719} \left\{ P(\theta_i) \cdot \left[V(\theta_i) - V(\theta_{i-1}) \right] \right\} \tag{2.33}$$

where V_d is the cylinder displacement; and

$$V_d = V(\theta_{BDC}) - V(\theta_{TDC}) \tag{2.34}$$

At last engine torque output is calculated by

$$T_e = \frac{60n(P_{IMEP} - P_{FMEP})V_d}{2\pi N_e} \tag{2.35}$$

where P_{FMEP} is the friction mean effective pressure and n is the quantity of engine cylinders.

2.5 Model Validation Using GT-Power Model

The crank based combustion model was assembled with the mean value air handling model to build the entire control oriented engine model. Chapter 4 provides details about how they are assembled and implemented into the HIL simulator. To validate the developed engine model, HIL simulations were performed and results were compared with those from GT-Power model.

Table 2.2 lists some key parameters of the engine setup, and Table 2.3 shows how the dual-stage turbocharger was adjusted for different engine conditions. Both full and half load engine simulations were performed for engine speeds between 1000 and 5000 rpm with a 500 rpm increment. The fuel quantity was controlled in a closed-loop to maintain stoichiometric air-to-fuel ratio for all simulations, and engine spark timing was adjusted to MBT timing [75] for all simulations, too. The same parameter set was used for both GT-Power engine model and the developed engine model in all simulations.

Table 2.2: Engine setting for both full and half load simulation

Actuator Parameter	Setting
Intake valve timing (peak valve lift)	460° ACTDC
Exhaust valve timing (peak valve lift)	260° ACTDC
EGR valve duty	0
Intake throttle opening	Full: 90°; half: 20°
Air-to-fuel ratio	stoichiometric

Table 2.3: Dual-stage turbocharger setting for full/half load simulation

Engine speed (rpm)	HP Waste-gate (°)		LP Waste-gate (°)		Bypass valve (°)	
	Full	Half	Full	Half	Full	Half
1000	0	90	0	90	0	0
1500	1.5	2.7	0	90	0	0
2000	3.5	3.2	0	90	0	0
2500	4.5	3.6	0.5	90	0	0
3000	4	3.8	1.8	90	0	0
3500	90	3.5	3.4	90	90	0
4000	90	90	4.1	15	90	90
4500	90	90	6	18	90	90
5000	90	90	7.8	24	90	90

In Table 2.3 the waste-gates and bypass valve positions of the dual-stage turbocharger were selected to achieve the best engine performances while maintaining the stability of the compressor and turbo systems. For instance, for the full load simulations, the LP compressor always operates within the surge and over speed limits of its compressor map to maintain stable engine operations without damaging itself, as shown Figure 2.4. Note that for this downsized engine, high boost pressure is desired to achieve maximum engine torque output at full load, and as a result, the LP compressor tends to operate at the region close to its surge limit to have the best performance.

Figure 2.5 presents the correlations of the engine torque; IMEP, MAP, and EMP (exhaust manifold pressure). Good correlations were found for most of the simulated conditions over engine speed and load ranges except for a few simulation points that are outside of the ±10% range. One can easily find that the EMP is the worst among the four compared parameters shown in Figure 2.5. This is mainly due to the simplification of turbine dynamics in the real-time HIL simulations. From Table 2.3 one can see that when engine speed is higher than 3500 rpm at full load condition, and 4000 rpm for half load condition, the HP waste-gate and bypass valve are fully opened, and the dual-stage turbocharger system switches to a mode utilizing LP turbine only. To simplify the computation, the HIL Simulink model neglects the pressure drop across the HP turbine when the LP turbine only mode is activated. In the GT-Power model this dynamics is well modeled since in this case there exists a small pressure drop across the HP turbine. In fact, this pressure drop increases as the increment of engine load, leading the HP turbo shaft to rotate, which increases EMP. Therefore, the GT-Power model simulates this small pressure drop in the pure LP mode, providing more accurate results of EMP than those provided by HIL simulations. On the other hand, the small errors of EMP in HIL simulations do not affect engine simulation accuracy significantly in the LP turbine only mode since there is almost no additional boost provided by the HP compressor due to the fully opened bypass valve.

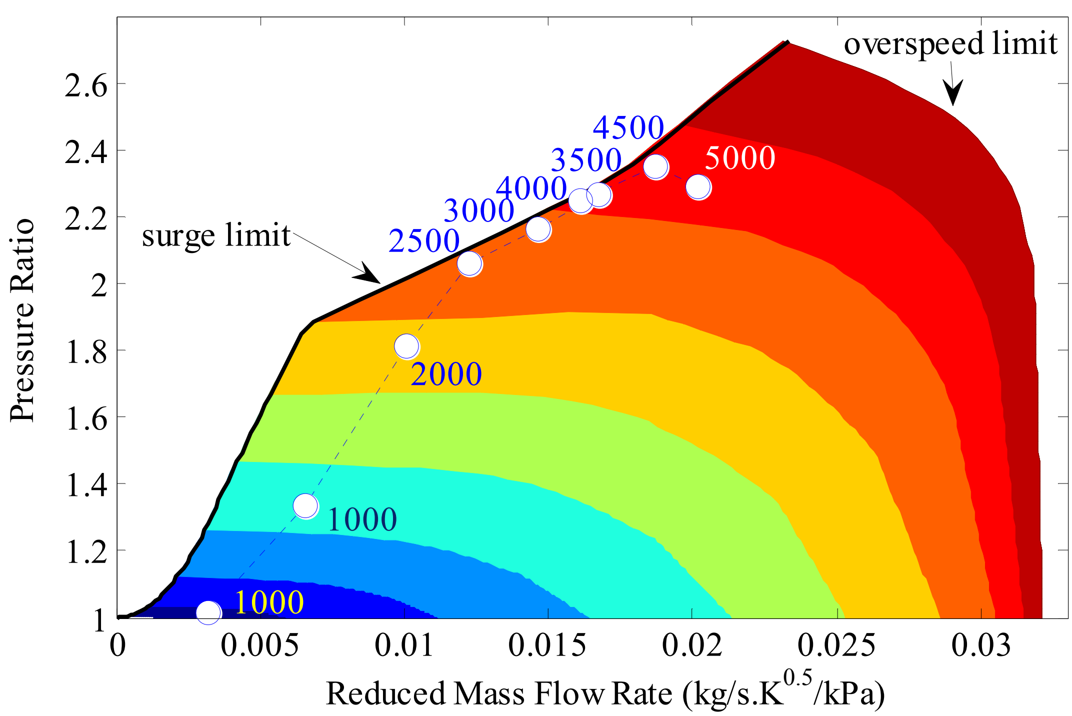

Figure 2.4: Operating status of LP compressor for full load simulation

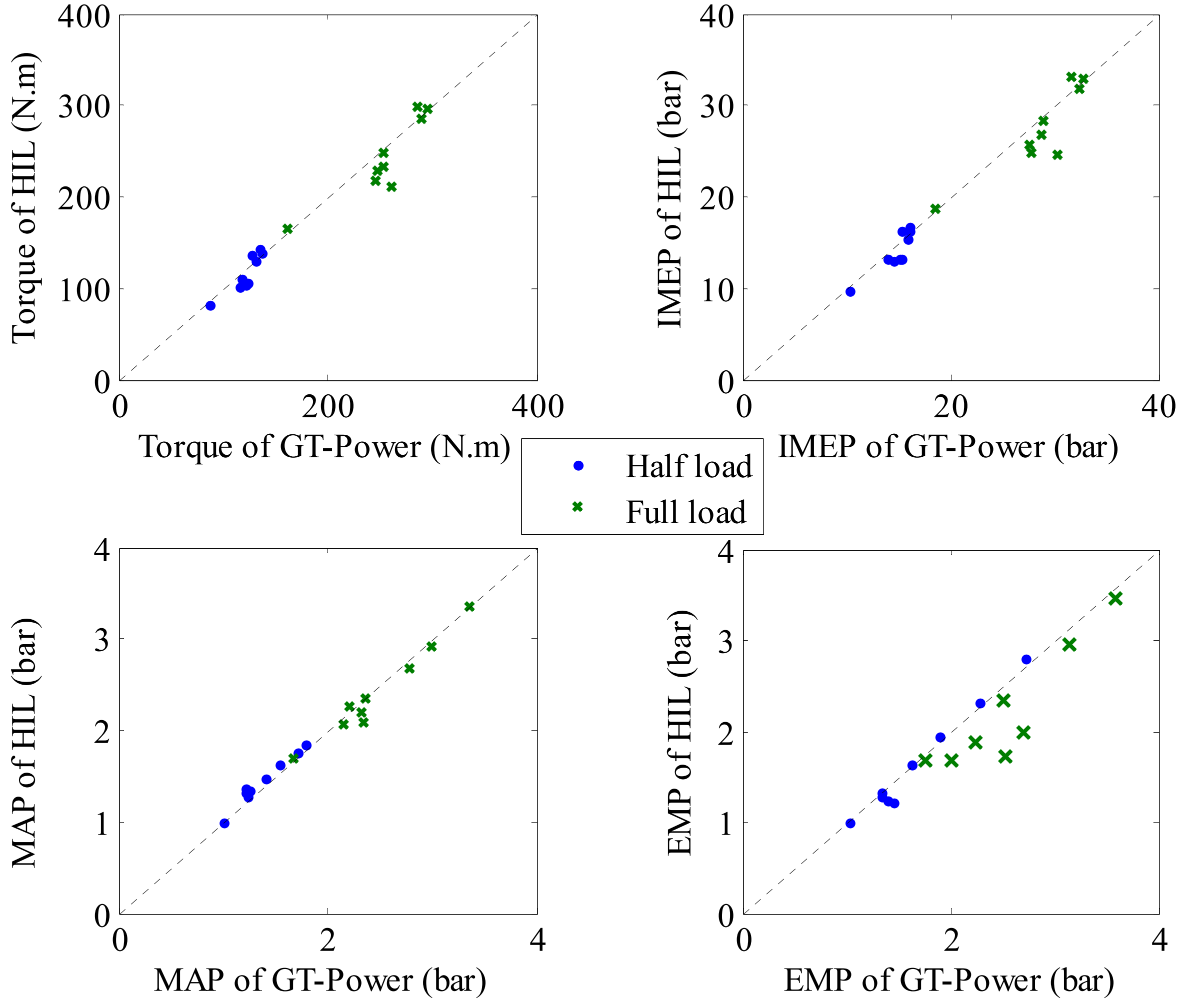

Figure 2.5: Correlation plots of the HIL and GT-Power simulation results

2.6 Conclusions

In this chapter, governing equations for the combustion process and subsystems of a dual-stage turbocharged SI engine are presented with certain assumptions. The steady state HIL (Hardware-In-the-Loop) simulation results are also compared with the corresponding GT-Power simulation results with satisfactory correlations. The following are the three key conclusions.

- Using mean value modeling technique for engine air handling subsystems and crank based modeling method for combustion process is an effective way to model both continuous and discrete engine dynamics.

- One-zone combustion assumption simplifies the SI combustion process modeling. By separating the volume change and the fuel heat release in each crank degree, the in-cylinder gas pressure and temperature can be calculated using two independent equations.
- The developed engine model is capable of real-time simulations with modeling accuracy close to that of the one dimensional GT-Power model.

CHAPTER 3

CONTROL ORIENTED SI-HCCI HYBRID COMBUSTION MODEL FOR AN HCCI CAPABLE INTERNAL COMBUSTION ENGINE

3.1 Introduction

As discussed in chapter 1, the HCCI combustion has potentials to reduce engine out NOx (nitrogen oxides) emissions with the improve fuel economy. However, it has its limitations, too. The HCCI combustion is limited at high engine load due to the audible knock [62] and at low load due to misfire caused by the lack of sufficient thermal energy to trigger the auto-ignition of the gas-fuel mixture late in the compression stroke [76]. In fact, HCCI can be regarded as a type of engine operating mode rather than a type of engine [22]. In order to take advantage of the HCCI combustion mode in an internal combustion engine, the SI combustion mode is still required for those engine operational conditions between the medium load and high load. The HCCI combustion mode can be used for these operational conditions between low load and medium load [77]. Typically, it is between 2.5 bar and 5.5 bar IMEP. For engine load conditions below the low limit, spark ignition is activated again to avoid misfired combustion [78]. Therefore, the HCCI capable engine needs to switch its combustion modes between the SI and HCCI combustions frequently under the practical vehicle operational conditions. However, the combustion mode transition is an open issue that prevents utilizing the HCCI combustion technology. To address this issue, a crank based SI-HCCI hybrid combustion model ([45] and [79]) will be presented in this chapter for the control research of the combustion mode transition.

Using the crank based engine modeling method introduced in the last chapter, a more detailed two-zone SI combustion model was developed and is presented in this chapter. The simulation results of the two-zone SI combustion model demonstrate that there exists an SI-HCCI hybrid combustion mode, which starts with SI combustion and ends with HCCI combustion. During the SI combustion phase, the burned gas applies work to the unburned gas and triggers HCCI combustion of the unburned gas-fuel mixture under certain conditions. Controlling this hybrid combustion process has the potential to have a smooth combustion mode transition, and the HIL simulation results presented in the next chapter demonstrate its feasibility of improving the quality of combustion mode transition. In this chapter, the two-zone SI combustion model is also combined with an one-zone HCCI combustion model with updated gas exchange model to model the SI-HCCI hybrid combustion, where both SI combustion and HCCI combustion are two special operating modes of the SI-HCCI combustion.

This chapter is organized as follows. In Subsection 3.2 the HCCI capable engine is introduced and a GT-Power combustion model is presented as the baseline model for the calibration and validation of the modeling work in this chapter. The SI-HCCI hybrid combustion model architecture is described in Subsection 3.3 to demonstrate the modeled hybrid combustion process and the mode transition between the SI and HCCI combustions. In Subsection 3.4 the gas exchange model is modified based upon the model described in the last chapter. Subsection 3.5 presents the dynamic equations used for the HCCI combustion phase; and Subsection 3.6 describes the two-zone SI combustion model as well as the governing equations under the two-zone assumptions. Some steady state simulation results of the developed model are shown in Subsection 3.7 with comparison to those obtained from the GT-Power simulations.

3.2 Engine Architecture and GT-Power Model

Figure 3.1 shows the engine architecture used for modeling the SI and HCCI combustion modes transition control. It features four cylinders with an external EGR system, dual cam shaft capable of independent timing control of both intake and exhaust valves. The air handling system of this engine is much simpler than the one studied in the last chapter due to the absence of turbocharger system. Intake throttle is installed at intake pipe upstream of the intake manifold. The engine is also equipped with the dual fuel injection system, PFI and DI, to facilitate the combustion study. The major specifications of the engine are given in Table 3.1. According to these parameters one can find that this engine configuration is very close to a typical SI engine, except for the cam and valve systems. Both intake and exhaust cam shafts have two stages of lift profiles, the high and low stages. For both cam shafts, the maximum lift is 9 mm for high stage and 5 mm for the low stage. The engine valve timings can be adjusted independently with a fairly large range of ±40° crank angle for both cam shafts. This cam design enables the engine to operate in the SI combustion mode with high volumetric efficiency, and in the HCCI combustion mode with more internal residual gas and less pumping loss due to the possibility of un-throttled combustion. Compression ratio of 9.8 shown in Table 3.1 might be a little low for the HCCI combustion. In future, higher compression ratio will be adopted to extend the HCCI operation range at light load conditions, such as the idle condition.

The air handling system shown in Figure 3.1 is actually a simplification of the system presented in Figure 2.1. All governing equations of the air handling system are the same as those listed in the last chapter. Therefore, they will not be repeated in this chapter and only the combustion model will be presented in detail.

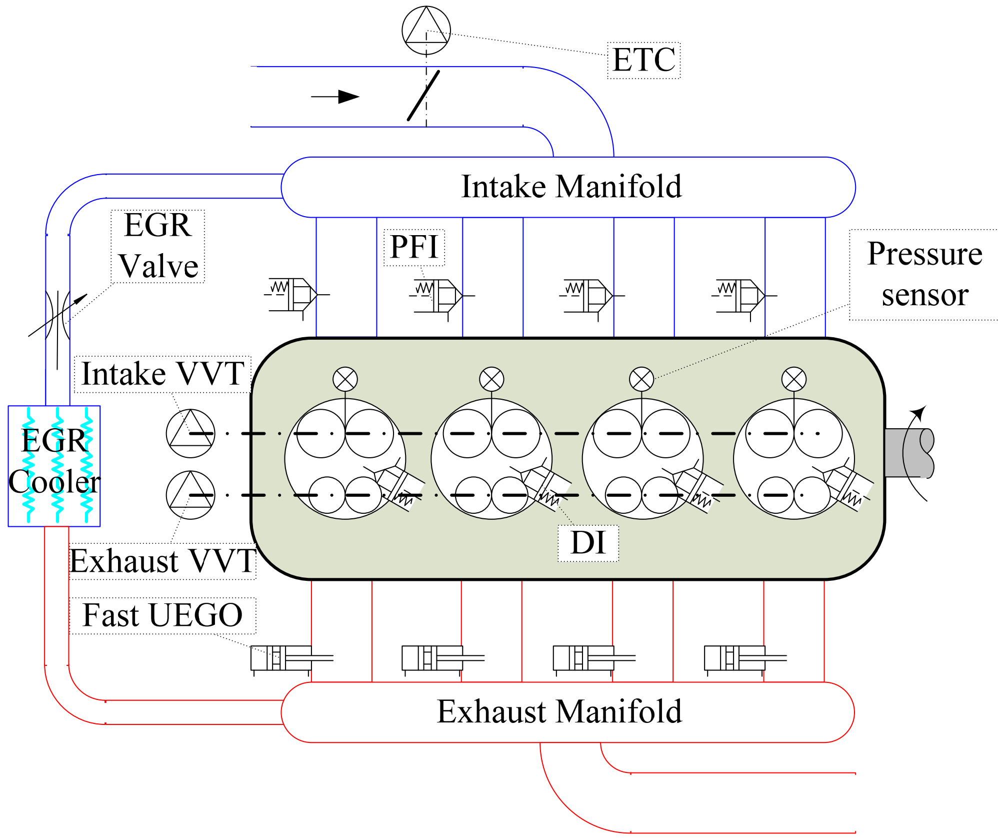

Figure 3.1: HCCI capable engine configuration

Table 3.1: HCCI capable engine specification

Engine parameter	**Model value**
Bore/stroke/con-rod length	86mm/86mm/143.6mm
Compression ratio	9.8:1
Intake/exhaust valve diameters	31.4mm/22.5mm
Intake/exhaust valve lifts of high stage	9mm/9mm
Intake/exhaust valve lifts of low stage	5mm/5mm
Intake/exhaust valve timing range	±40°/±40°
Intake/exhaust valve lifts lash	0.2mm/0.25mm

For the SI-HCCI combustion study, a GT-Power model as shown in Figure 3.2 was also developed, but only for studying the combustion process. It will be used as the baseline model to calibrate the combustion related parameters and validate the combustion performance for the developed model. In order to validate the combustion model without the influence of the engine air handling system, the engine air handling dynamics was not included in the GT-Power combustion model. Furthermore, only one cylinder is modeled, since the combustion process is assumed to be the same for all cylinders with different combustion phase.

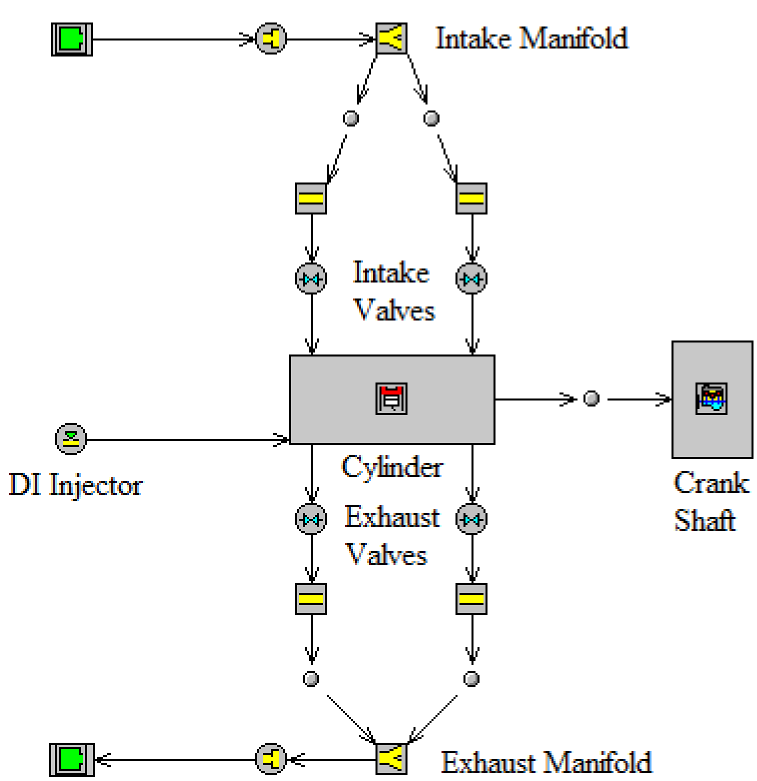

Figure 3.2: GT-Power combustion model

3.3 SI-HCCI Hybrid Combustion Model Architecture

As discussed in Subsection 3.1, three combustion modes have been proposed for the HCCI capable engine. They are SI, HCCI, and SI-HCCI hybrid combustion modes. In the rest of this chapter, a zero dimensional crank based combustion model will be developed to model the three combustion modes.

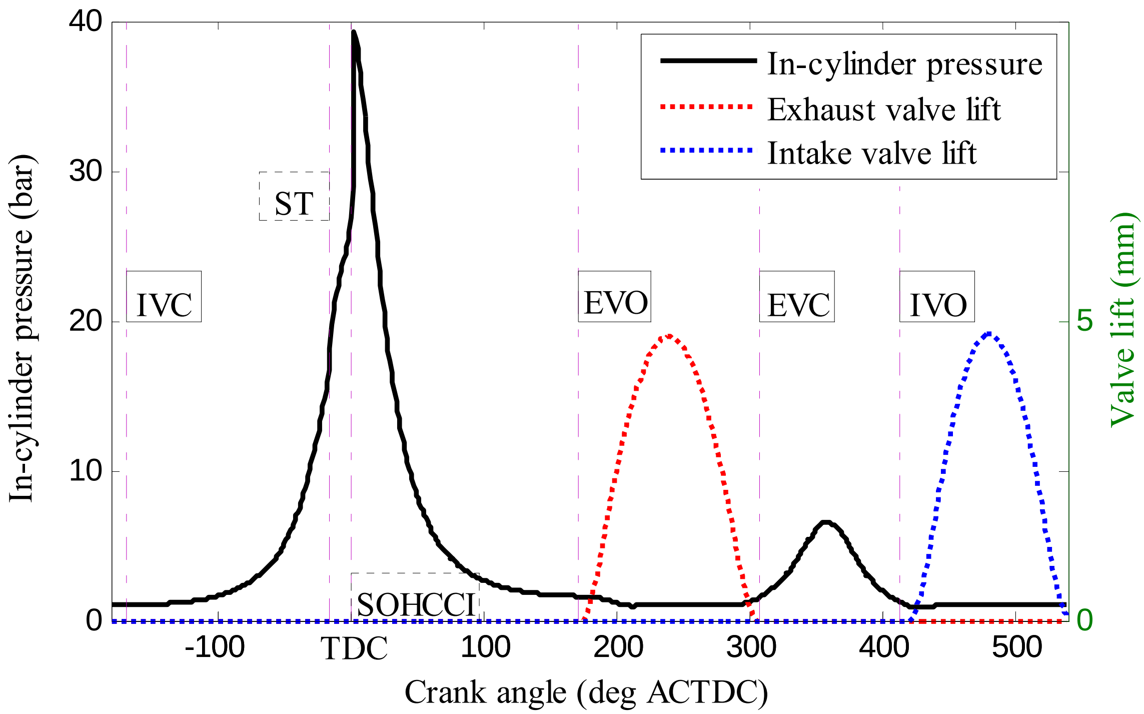

Figure 3.3: SI-HCCI hybrid combustion related events and phases

To understand the characteristic of each combustion mode, the combustion related events and phases of an IC engine are shown in Figure 3.3. Comparing with Figure 2.3, there is one additional event in Figure 3.3. That is the SOHCCI (start of HCCI combustion). Furthermore, both ST and SOHCCI are marked in the boxes with dashed frame to distinguish them from other events, since the occurrences of these two events depend on the combustion mode. The other events exist for any 4-stroke internal combustion engine. Accordingly, the main difference among each combustion mode lies on the phase between IVC and EVO. When the SOHCCI event does not occur in this phase, the engine is operated at the SI combustion mode; and when the SOHCCI event occurs before the SI event, the engine is operated at the HCCI combustion mode; while the SI-HCCI hybrid combustion mode occurs inter-between the HCCI and SI combustion modes. Note that both SI and HCCI combustion modes are special cases of the SI-HCCI hybrid combustion mode. In fact, there is a fourth mode, in which both SI and SOHCCI do not occur in the combustion phase, or SOHCCI happens very late in that phase. The fourth mode is unexpected and needs to be avoided since it means misfire or partial combustion. The diagram in Figure 3.4 illustrates the model architecture and explains how the combustion modes switch between each other. The most important criterion of the mode switch is Arrhenius integration *ARI* ([73], [80], and [81]), which can be represented by

$$ARI = \int_{\theta_{IVC}}^{\theta_i} A x_f^a x_{ox}^b e^{\left(-\frac{E_a}{RT}\right)} d\vartheta \tag{3.1}$$

where x_f and x_{ox} are unburned fuel and oxidizer mass fractions; exponents a and b are the influence factors; multiplier A and Arrhenius activation energy E_a can be obtained by matching the experimentally determined rates of burning. The SOHCCI crank position is defined as the crank angle for 1% fuel burned under HCCI combustion. Accordingly once *ARI* exceeds 1 the combustion model switches to HCCI mode. The Arrhenius integration in equation (3.1) starts at θ_{IVC}, and is reset at θ_{EVO}. During this period the integration is updated every crank degree. The gas temperature T in equation (3.1) is a key parameter that affects the rising speed of *ARI* significantly. If spark ignition never happens, the variable T in equation (3.1) equals to in-cylinder gas temperature; while during the SI combustion phase T equals to unburned gas temperature T_U, which will be calculated by a two-zone SI combustion model presented in this chapter. This is also the main motivation of developing the two-zone SI combustion model, since the one-zone SI combustion model presented in the last chapter does not provide this information.

In Figure 3.4, there are three subroutines in the entire combustion model, the gas exchange model, the one-zone HCCI and two-zone combustion models. In the rest of this chapter, these sub-models will be investigated in great details.

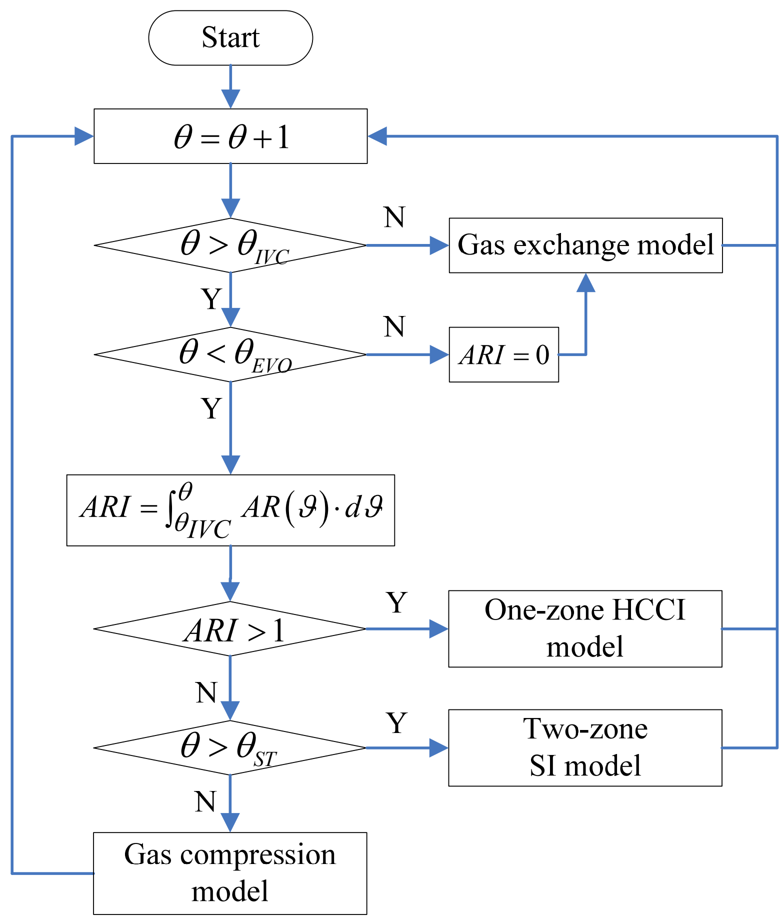

Figure 3.4: SI-HCCI hybrid combustion model diagram

3.4 Revisit the Gas Exchange Process

In HCCI capable engines, the gas exchange process is more complicated than that in SI combustion engines [82], and it affects the combustion timing and duration significantly. Both positive valve overlap (PVO) and negative valve overlap (NVO) might happen in the entire engine operating range depending on the valve control strategy. Figure 3.3 shows the case of NVO, in which IVO comes later than EVC and creates a recompression profile on the in-cylinder pressure signal. Furthermore the low stage lift profiles of both intake and exhaust valves allow the valve timing to shift in a large range. The gas exchange model introduced in last chapter cannot be used here, since it cannot deal with the large range of valve timing. A new gas exchange model is required.

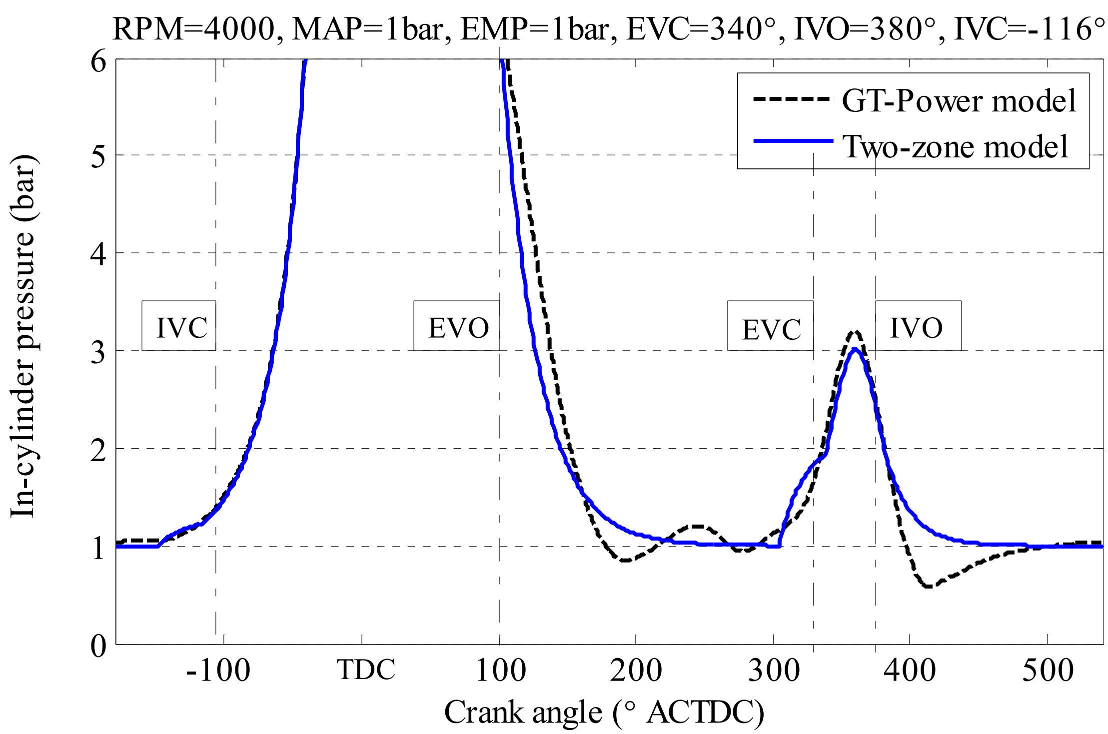

Figure 3.5: In-cylinder pressure trace in gas exchange process

3.4.1 Gas exhaust process

The gas exhaust phase corresponds to the phase from EVO to IVO for PVO and the phase from EVO to EVC for NVO. In this phase, the in-cylinder gas mixture is expanding in the cylinder, exhaust runner and manifold. The in-cylinder pressure drops quickly but not instantaneously down to the level of the exhaust manifold pressure. It normally takes a few crank degrees for the in-cylinder pressure to approach the exhaust manifold pressure. One can find this dynamic delay in Figure 3.5. It is difficult to model this dynamics using simple dynamic equations for real-time simulations. For simplicity, a first order transfer function is used to approximate this dynamic process as

$$P(z) = \frac{1-\tau_{EVO}}{1-\tau_{EVO} \cdot z^{-1}} P_{EM}(z) \tag{3.2}$$

where z is the unit delay operator; τ_{EVO} is the time constant for exhaust valve opening;

The entire gas exhaust process is not an isentropic process because of the heat transfer during the process. However, the entire process is divided into each crank degree, and the process in such small period as a crank degree is also divided into two stages. The first stage is approximated as an isentropic process without heat exchange, and it occupies the duration of one crank degree. Heat exchange happens in the second stage, which occupies an infinitely small time period. Using this method, the computational error is negligible, while the model is as simple as

$$T(\theta_i) = T(\theta_{i-1}) \left[\frac{P(\theta_i)}{P(\theta_{i-1})} \right]^{\frac{\kappa-1}{\kappa}} - \frac{Q(\theta_{i-1})}{M(\theta_{i-1})Cv} \tag{3.3}$$

By investigating the pressure trace provided by the GT-Power model shown in Figure 3.5, one can find that during the late stage of the gas exhaust phase the in-cylinder pressure increases significantly, and it finally reach 1.9 bar at EVC, much bigger than the exhaust manifold pressure (1 bar in this case). There are two causes. One is that the exhaust valve is almost closed during the late stage and restricts gas from leaving the cylinder; and the other is that the EVC timing is before gas exchange TDC in the case. This phenomenon cannot be ignored, since $P(\theta_{EVC})$ is used to calculate residual gas mass M_r, and M_r will affect HCCI combustion timing and duration significantly. This pressure rise dynamics can also be modeled by a first order transfer function

$$P(z) = \frac{1-\tau_{EVC}}{1-\tau_{EVC}\cdot z^{-1}} P_{EM}(z)\eta_{EVC} \tag{3.4}$$

where η_{EVC} is the predicted pressure ratio at EVC, and it is mostly affected by engine speed, EVC timing and exhaust valve lift. A 3D table of the η_{EVC} calibration was derived based upon the GT-Power simulations. As shown in Figure 3.2, this model yield a good match between the pressure traces provided by GT-Power model and the two-zone combustion model, especially at the EVC timing.

Table 3.2: Calibration of η_{EVC} for low stage exhaust valve profile

θ_{EVC} \ RPM	1000	2000	3000	4000	5000
300	1.26	1.4	1.49	1.62	1.72
310	1.31	1.46	1.57	1.72	1.78
320	1.32	1.49	1.63	1.79	1.88
330	1.3	1.49	1.64	1.79	1.9
340	1.25	1.39	1.51	1.68	1.77
350	1.13	1.23	1.31	1.41	1.48
360	1	1.01	1.04	1.04	1.12
370	0.9	0.91	0.83	0.85	0.8
380	0.82	0.77	0.69	0.7	0.63
390	0.75	0.68	0.62	0.61	0.54

Table 3.3: Calibration of η_{EVC} for high stage exhaust valve profile

θ_{EVC} \ RPM	1000	2000	3000	4000	5000
300	1.53	1.74	1.91	2.01	2.28
310	1.57	1.8	2	2.17	2.34
320	1.6	1.88	2.08	2.33	2.4
330	1.57	1.87	2.13	2.45	2.44
340	1.47	1.78	2.03	2.27	2.36
350	1.27	1.47	1.67	1.83	2.05
360	1.03	1.11	1.19	1.29	1.4
370	0.89	0.88	0.86	0.87	0.87
380	0.77	0.73	0.7	0.66	0.66
390	0.68	0.64	0.6	0.55	0.54

3.4.2 Residual gas recompression in NVO

Negative valve overlap (NVO) is often used to regulate the HCCI combustions. There are two main advantages. One is to reform the pilot fuel injected during this phase (between EVC and IVO in Figure 3.3) into short carbon chain molecules (pyrolysis) [83], as a result the active energy E_a in equation (3.1) can be reduced; and the other is to regulate the residual gas temperature. As a result the in-cylinder gas temperature at IVC can be optimized for desired SOHCCI timing. The first effect is difficult to model using governing equations. In [63] and [83], the influence of recompression on E_a is correlated by experimental data. In this chapter, this effect is ignored until experimental data is available. For the second effect, it is modeled as follows.

$$T(\theta_i) = T(\theta_{i-1}) \cdot \left(\frac{V(\theta_{i-1})}{V(\theta_i)} \right)^{(\kappa-1)} - \frac{Q(\theta_{i-1})}{M(\theta_{i-1})Cv} \tag{3.5}$$

and

$$P(\theta_i) = P(\theta_{i-1}) \cdot \left(\frac{V(\theta_{i-1})}{V(\theta_i)} \right)^{\kappa} \tag{3.6}$$

Another important parameter calculated in this phase is the residual gas mass. It is calculated based upon ideal gas law, and updated once per engine cycle at EVC for NVO.

$$M_r = M(\theta_{EVC}) = \frac{P(\theta_{EVC}) \cdot V(\theta_{EVC})}{R \cdot T(\theta_{EVC})} \tag{3.7}$$

3.4.3 Gas exchange behavior in PVO

The gas exchange behavior during the phase from IVO to EVC for the PVO is also very complicated. Since both intake and exhaust valves are partially opened in this phase, residual gas and fresh charge can flow in many ways depending on the pressure ratio across each valve. For simplification, assume gas exchange across exhaust valve is terminated in this phase; part of residual gas can flow to intake port, but finally it flows back into cylinder during the rest of the intake process. Based upon this assumption, the mass of residual gas for PVO case can be calculated by equation (3.8) at IVO instead of EVC for NVO, and gas exchange of this phase is actually a part of the air intake process.

$$M_r = M(\theta_{IVO}) = \frac{P(\theta_{IVO}) \cdot V(\theta_{IVO})}{R \cdot T(\theta_{IVO})} \tag{3.8}$$

This modeling approach may result in slight error for M_r. Fortunately, the PVO only occurs during the SI combustion process, and in this case the influence of residual gas to the entire engine performance is much less than that during the HCCI combustion process which usually involves the NVO strategy. On the other hand, the multiplier η_{EVC} can also be calibrated to match the test data or the high resolution simulation data. For this paper the GT-Power simulation data is used to calibrate the entire combustion model.

3.4.4 Air intake process

The air-intake process starts from IVO and ends at IVC. It is also a process of in-cylinder gases mixing. During this phase the fresh charged air, injected fuel vapor, and residual gas are assumed to be mixed homogeneously, which is the modeling assumption for combustion. At the same time, the in-cylinder pressure drops to the pressure level of intake manifold. A first order transfer function is also used in this model.

$$P(z) = \frac{1-\tau_{IVO}}{1-\tau_{IVO}\cdot z^{-1}} \cdot P_{IM}(z) \tag{3.9}$$

and

$$T(\theta_i) = \frac{M_f \cdot Cv_f \cdot T_f + M_a \cdot Cv_a \cdot T_{IM} + M_r \cdot Cv_r \cdot T_r}{M_f \cdot Cv_f + M_a \cdot Cv_f + M_r \cdot Cv_r} \tag{3.10}$$

where τ_{IVO} is the transition time constant for intake valve opening; M_a is the fresh charge mass (note that it could be the mixture of fresh air and external EGR gas); C_v is specific heat; T_r is the temperature of residual gas, and it can be calculated by the same approach used in equation (3.3).

During the late stage of the air intake phase, the in-cylinder pressure is also increased, see Figure 3.5. This phenomenon is the same as that in exhaust phase. The same approach is used.

$$P(z) = \frac{1-\tau_{IVC}}{1-\tau_{IVC}\cdot z^{-1}} P_{IM}(z)\eta_{IVC} \tag{3.11}$$

where η_{IVC} is the predicted pressure ratio at IVC, and it is function of engine speed, IVC timing and exhaust valve lift. The calibration of η_{EVC} was derived by the GT-Power model. Good match has been illustrated in Figure 3.5 too.

Table 3.4: Calibration of η_{IVC} for low stage intake valve profile

θ_{IVC} \ RPM	1000	2000	3000	4000	5000
460	0.792	0.713	0.646	0.586	0.53
480	0.848	0.784	0.723	0.661	0.597
500	0.908	0.86	0.812	0.743	0.652
520	0.956	0.931	0.901	0.801	0.672
540	0.995	0.986	0.981	0.848	0.699
560	1.016	1.012	1.057	0.911	0.748
580	1.057	1.051	1.145	1.01	0.833
600	1.113	1.13	1.262	1.162	0.975

Table 3.5: Calibration of η_{IVC} for high stage intake valve profile

θ_{IVC} \ RPM	1000	2000	3000	4000	5000
460	0.709	0.621	0.557	0.505	0.46
480	0.783	0.705	0.645	0.594	0.542
500	0.859	0.801	0.75	0.7	0.646
520	0.927	0.892	0.857	0.816	0.768
540	0.986	0.972	0.96	0.938	0.902
560	1.021	1.033	1.042	1.051	1.044
580	1.074	1.094	1.106	1.139	1.175
600	1.155	1.185	1.213	1.244	1.307

3.5 One-zone HCCI Combustion Model

The HCCI combustion is modeled under the one-zone assumption due to its flameless nature. Fuel and air are assumed to be premixed homogeneously throughout the entire cylinder; thermodynamic characteristics such as pressure and temperature are uniformly distributed in the cylinder. Accordingly only the mean value of in-cylinder gas pressure and temperature will be modeled.

Unlike the SI combustion, there is no direct trigger (spark ignition) of the HCCI combustion. The fast heat release process of the HCCI combustion is actually triggered by a very slow chemical reaction of the gas-fuel mixture during the compression phase after IVC. The most common practice in control oriented modeling of the HCCI combustion is to assume the chemical reaction process is governed by single rate Arrhenius equation,

$$AR(\theta_i) = A \cdot x_f^a \cdot x_{ox}^b \cdot e^{\left(-\frac{E_a}{R \cdot T(\theta_i)}\right)} \tag{3.12}$$

where AR is the rate of disappearance of unburned fuel and other parameters have been explained in equation (3.1). As mentioned earlier in this chapter, the integration of the Arrhenius function is used to estimate the SOHCCI timing. The SOHCCI timing is the timing separates the slow chemical reaction with the fast one. During the fast combustion phase the fuel mass fraction burned can also be approximated by the Wiebe function,

$$x(\theta_i) = 1 - \exp\left[-a\left(\frac{\theta_i - \theta_{SOHCCI}}{\Delta\theta_{HCCI}}\right)^{m+1}\right] \tag{3.13}$$

where the burn duration $\Delta\theta_{HCCI}$ is given by

$$\Delta\theta_{HCCI} = k \cdot T(\theta_{SOHCCI})^{-\frac{2}{3}} \cdot T_m^{\frac{1}{3}} \cdot e^{\frac{E_a}{3R \cdot T_m}} \tag{3.14}$$

where k is a scaling constant; E_a is activation energy of the fuel; and T_m is the mean valve of HCCI combustion temperature. It is calculated by

$$T_m = T(\theta_{SOHCCI}) + \frac{\eta_{HCCI} M_f h_{LHV} [1 - x(\theta_{SOHCCI})]}{M_t Cv} \tag{3.15}$$

At last in-cylinder pressure and temperature are calculated by

$$T(\theta_i) = T(\theta_{i-1}) \left(\frac{V(\theta_{i-1})}{V(\theta_i)} \right)^{(\kappa - 1)} + \frac{\eta_{HCCI} M_f h_{LHV} \left[x(\theta_i) - x(\theta_{i-1}) \right] - Q(\theta_i)}{M_t Cv} \tag{3.16}$$

and

$$P(\theta_i) = P(\theta_{i-1}) \frac{V(\theta_{i-1})}{V(\theta_i)} \cdot \frac{T(\theta_i)}{T(\theta_{i-1})} \tag{3.17}$$

where η_{HCCI} is a function of engine speed and fuel mass, it was calibrated by matching the calculated IMEP provided by the GT-Power model.

3.6 Two-zone SI Combustion Model

During the SI combustion the spark ignited flame front divides the in-cylinder gas mixture into two zones, the burned zone and unburned zone, as shown in Figure 3.6. The temperature of the unburned zone is quite different from that of the burned zone as seen in Figure 3.6. However, this difference is ignored in the one-zone SI combustion model discussed in the last chapter, where a mean value of temperature is used for entire in-cylinder gas. This may not lead to large modeling error for the SI combustion, in which the temperature difference does not impact much on the combustion model parameters such as in-cylinder pressure. However, for the SI-HCCI hybrid combustion, the unburned zone temperature is a key parameter for predicting the start of the HCCI combustion. The expansion of the burned zone during the initial SI combustion process applies work to the unburned zone. As a result it makes the unburned zone temperature rise faster, and causes HCCI combustion in the unburned zone. On the other hand, the two-zone SI combustion model is closer to the nature of the SI combustion process. These are the motivations for developing this two-zone combustion model.

3.6.1 Two-zone assumptions

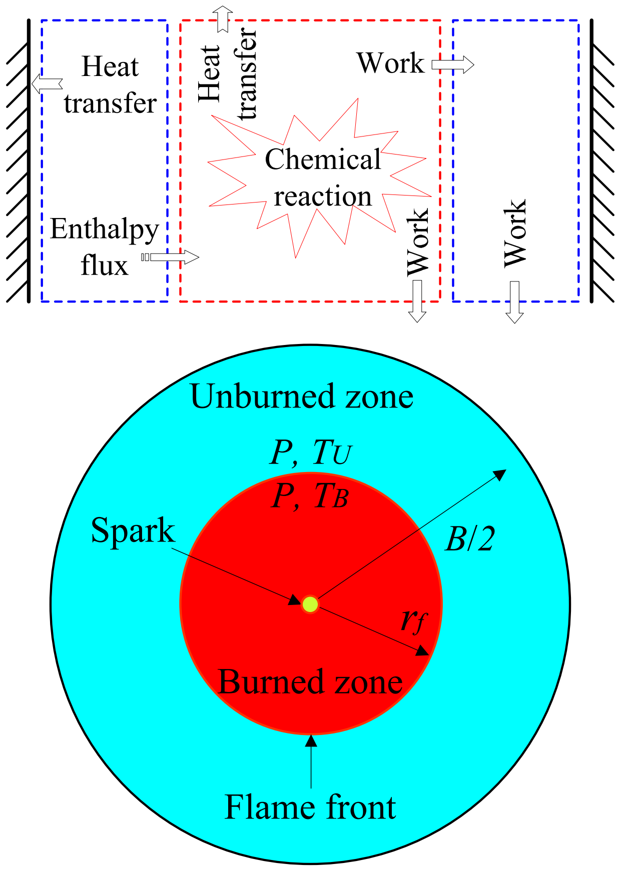

Figure 3.6: Two-zone SI combustion model

For modeling simplicity, some assumptions have been made to the two-zone SI combustion process.

- The fuel, air, and residual gas charges are uniformly premixed at IVC.
- In the two-zone model, the gas mixture pressure is assumed to be evenly distributed throughout both burned and unburned zones.
- During each given crank degree, a portion of gas-fuel mixture is transferred from the

unburned zone to the burned zone. The amount of the gas-fuel mixture is defined by the burn rate of fuel, which is prescribed by the Wiebe function.

- In each step of engine crank degree, the flow of each zone is assumed to be in steady state.
- The total heat transfer between in-cylinder gas mixture and the cylinder inner surface is calculated by equation (2.30) same as that in the one-zone model, except the gas temperature *T* in that equation is replaced by the average temperature of both burned and unburned zones, which is calculated by

$$T = \frac{xCv_B T_B + (1-x)Cv_U T_U}{xCv_B + (1-x)Cv_U} \tag{3.18}$$

- The heat transfer between the burned and unburned zones is neglected.

3.6.2 Governing equations

After spark ignition, the burned zone is created. Both the burned and unburned zones can be regarded as control volumes. Mass, enthalpy, and work exchange between these two control volumes, and also between the control volumes and the surrounding cylinder wall. According to the first law of thermodynamics [84], the energy balance equation of the burned zone is represented by

$$\frac{d(M_B e_B)}{d\theta} + P\frac{dV_B}{d\theta} + xQ = \eta_{SI} H_{LHV} M_f \frac{dx}{d\theta} + \frac{dM_B}{d\theta} h_U \tag{3.19}$$

The subscription *B* and *U* represent the burned and unburned zones, respectively. The energy balance equation of unburned zone is

$$\frac{d(M_U e_U)}{d\theta} + P\frac{dV_U}{d\theta} + (1-x)Q = \frac{dM_U}{d\theta} h_U \tag{3.20}$$

Apply the ideal gas law [84] to the burned zone and get

$$\frac{PV_B}{RT_B} = M_B = xM_t \tag{3.21}$$

Apply the ideal gas law to the unburned zone and get

$$\frac{PV_U}{RT_U} = M_U = (1-x)M_t \tag{3.22}$$

Additionally, the cylinder geometry yields

$$V_B + V_U = V \tag{3.23}$$

3.6.3 Solutions of two-zone model

Equations (3.19) to (3.23) constitute the complete governing equations of the two-zone combustion model. There are five unknowns:

$$\begin{cases} X_1 = V_B(\theta_i) \\ X_2 = V_U(\theta_i) \\ X_3 = T_B(\theta_i) \\ X_4 = T_U(\theta_i) \\ X_5 = P(\theta_i) \end{cases}$$

And they can be computed by solving equations (3.19) to (3.23) using the iterative method as described in equation (4.3) based on the information computed in last crank position $\left[V_B(\theta_{i-1}) \quad V_U(\theta_{i-1}) \quad T_B(\theta_{i-1}) \quad T_U(\theta_{i-1}) \quad P(\theta_{i-1}) \quad x(\theta_{i-1})\right]^T$ and the MFB of current crank position $x(\theta_i)$, which is given by the Wiebe function. The initial conditions are the thermodynamic states at the end of the compression phase, and they are

$$\begin{cases} X_1^0 = 0 \\ X_2^0 = V(\theta_{ST}) \\ X_3^0 = T(\theta_{ST}) \\ X_4^0 = T(\theta_{ST}) \\ X_5^0 = P(\theta_{ST}) \end{cases}$$

Therefore, differential equations (3.19) to (3.23) can be converted to

$$\begin{cases} a_1 X_1 + b_1 X_3 & = & c_1 \\ a_2 X_2 + b_2 X_4 & = & c_2 \\ X_1 X_5 / X_3 & = & c_3 \\ X_2 X_5 / X_4 & = & c_4 \\ X_1 + X_2 & = & c_5 \end{cases} \tag{3.24}$$

where

$$\begin{aligned}
a_1 &= P(\theta_{i-1}) \\
b_1 &= x(\theta_i) M_t Cv \\
a_2 &= P(\theta_{i-1}) \\
b_2 &= [1 - x(\theta_i)] M_t Cv \\
c_1 &= \eta_{SI} H_{LHV} M_f dx(\theta_i) + P(\theta_{i-1}) V_B(\theta_{i-1}) - x(\theta_i) Q(\theta_i) \\
&\quad + M_t x(\theta_{i-1}) Cv T_B(\theta_{i-1}) + M_t dx(\theta_i) Cp T_U(\theta_{i-1}) \\
c_2 &= P(\theta_{i-1}) V_U(\theta_{i-1}) - M_t dx(\theta_i) Cp T_U(\theta_{i-1}) \\
&\quad + M_t [1 - x(\theta_{i-1})] Cv T_U(\theta_{i-1}) - [1 - x(\theta_i)] Q(\theta_i) \\
c_3 &= x(\theta_i) M_t R \\
c_4 &= [1 - x(\theta_i)] M_t R \\
c_5 &= V(\theta_i)
\end{aligned}$$

Equation (3.24) was solved analytically using Matlab symbolic toolbox, and the rational solution was used for numerical solution of the algebraic equations set (3.24) in the HIL simulation. Note that due to the nonlinearity of equations (3.21) and (3.22) the solutions are not unique and they consume large portion of HIL simulator throughput. After implementing the model into the dSPACE HIL simulator for real-time simulations, the two-zone engine model can be simulated at the engine speed up to 5000 rpm without overrun, while the one-zone model can be simulated up to 10000 rpm. Fortunately the possible operating range of the two-zone model (SI-HCCI hybrid mode) is between 1000 and 5000 rpm.

3.7 Model Validation Using GT-Power

Since the GT-Power does not support SI-HCCI hybrid combustion modeling, the hybrid combustion mode cannot be directly validated. In this section only the sub-models are validated with the GT-Power combustion model. The hybrid combustion mode will be validated by the actual engine test data in next stage of the research.

3.7.1 Comparison between two-zone and one-zone model

To validate the developed two-zone SI and one-zone HCCI combustion models, two combustion simulations were conducted using both models. In the SI combustion model used for the simulations, gas exchange model is from this chapter, whereas the combustion model is from the last chapter. The operational conditions for both simulations were selected as following. In the first simulation, engine speed was set to 2000 rpm, and intake manifold absolute pressure (MAP) was set to 1.0 bar as full load condition. In the second simulation engine speed was at 5000 rpm with MAP equals to 0.4 bar to simulate the low load condition. The valve strategies are also different, NVO for the first one (EVC=IVO=360° ACTDC), whereas PVO is used for the second one (EVC=380° ACTDC, IVO=340° ACTDC). Same simulations were also completed by the GT-Power combustion model as the baseline for the comparison. Simulation results are plotted in Figure 3.7 to Figure 3.9. Note that the abbreviation ACTDC represents after TDC, and TDC stands for top dead center of piston movement.

Figure 3.7 shows the in-cylinder pressure and temperature traces. The temperature provided by the two-zone SI combustion model is the average temperature of both burned and unburned zones, and it is given by equation (3.18). From Figure 3.7 one can find that the simulation results of both one-zone and two-zone combustion models have good matches with the GT-Power model results except some small difference of the temperature traces at gas exchange process. The comparisons partially validate both modeling methods.

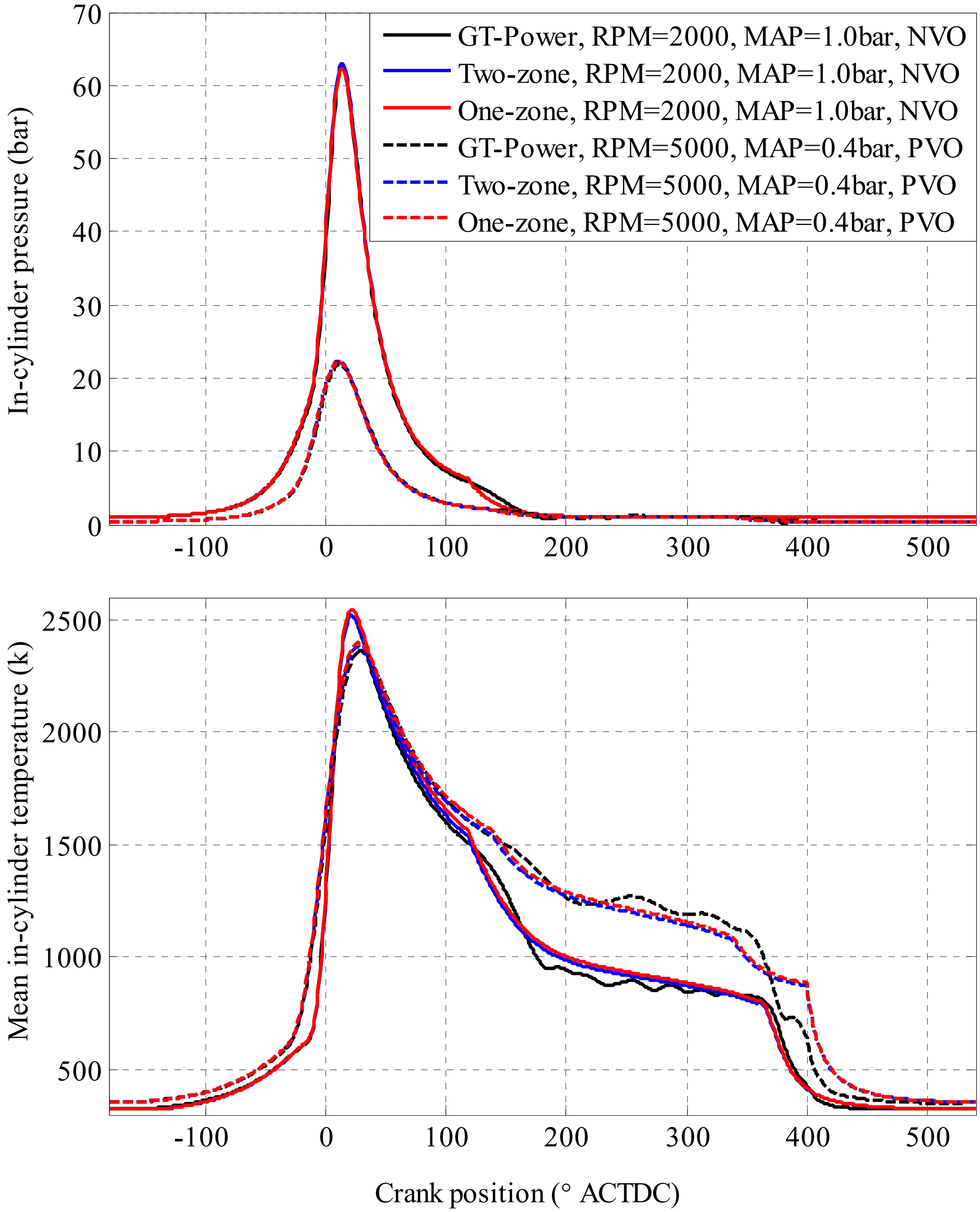

Figure 3.7: In-cylinder gas pressure and temperature traces: correlations between GT-Power model, two-zone SI combustion model and one-zone SI combustion model

The simulation results in Figure 3.7 also show close matches between one-zone and two-zone combustion models. However they are governed by different equations. In the two-zone model five equations were used, whereas in the one-zone model only two equations were used. After investigating all the equations used. It is found that the five equations (3.19) to (3.23) of the two-zone model are derived based on energy conservation and mass conservation of the entire in-cylinder gas; on the other hand, the two equations (2.29) and (2.32) of the one-zone model can also guarantee the energy conservation and mass conservation. So they are based on the same physical principle, but the two-zone model provides more information.

Figure 3.8 and Figure 3.9 demonstrate how the two-zone SI combustion model divided the in-cylinder gas temperature profile into two temperature profiles: the burned zone temperature in Figure 3.8 and unburned zone temperature in Figure 3.9, which one-zone model is not capable to do. Both temperature profiles show good match with the GT-Power simulation results. It further confirms the effectiveness of the two-zone model.

In Figure 3.9 unburned zone temperatures are also compared with the in-cylinder gas temperature simulated without combustion. It shows that before spark ignition (ST=-17° ACTDC in this case), the three temperatures are the same; but after spark ignition, the unburned zone temperature rises faster than the one without SI combustion. This is due to the work applied by the burned zone gas. The Arrhenius integration in equation (3.1) is more sensitive to higher unburned zone temperature, which indicates that the slow chemical reaction before the SOHCCI can be accelerated by the raised temperature. Accordingly if the unburned zone gas temperature can be controlled, the SOHCCI timing of the hybrid combustion model can also be controlled.

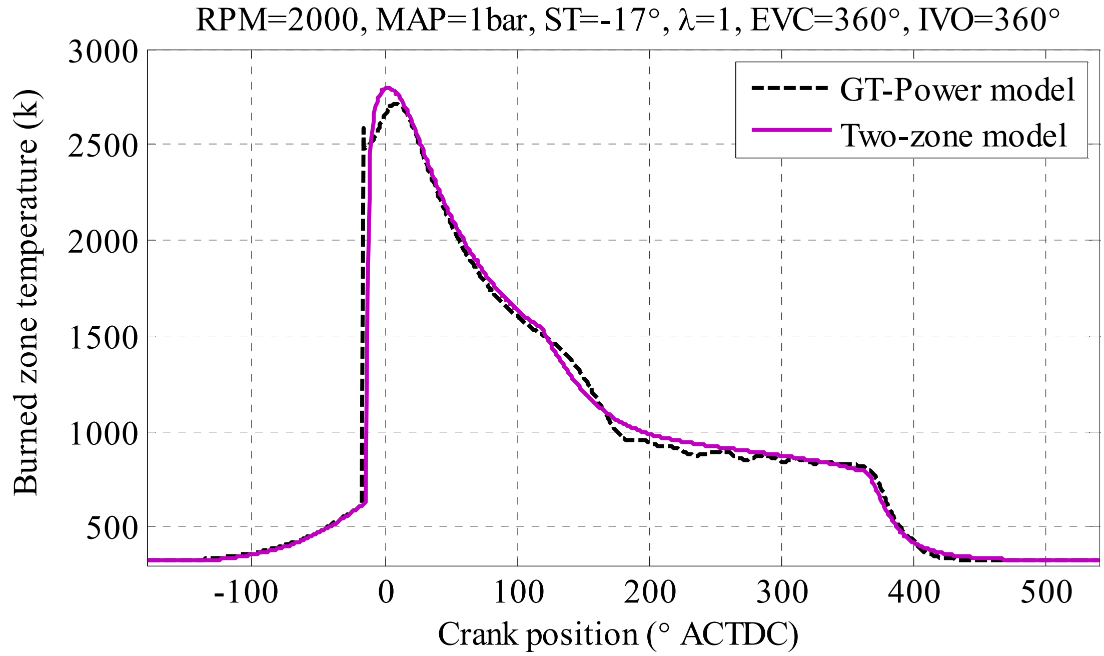

Figure 3.8: Burned zone gas temperature: correlation between GT-Power and two-zone SI combustion models

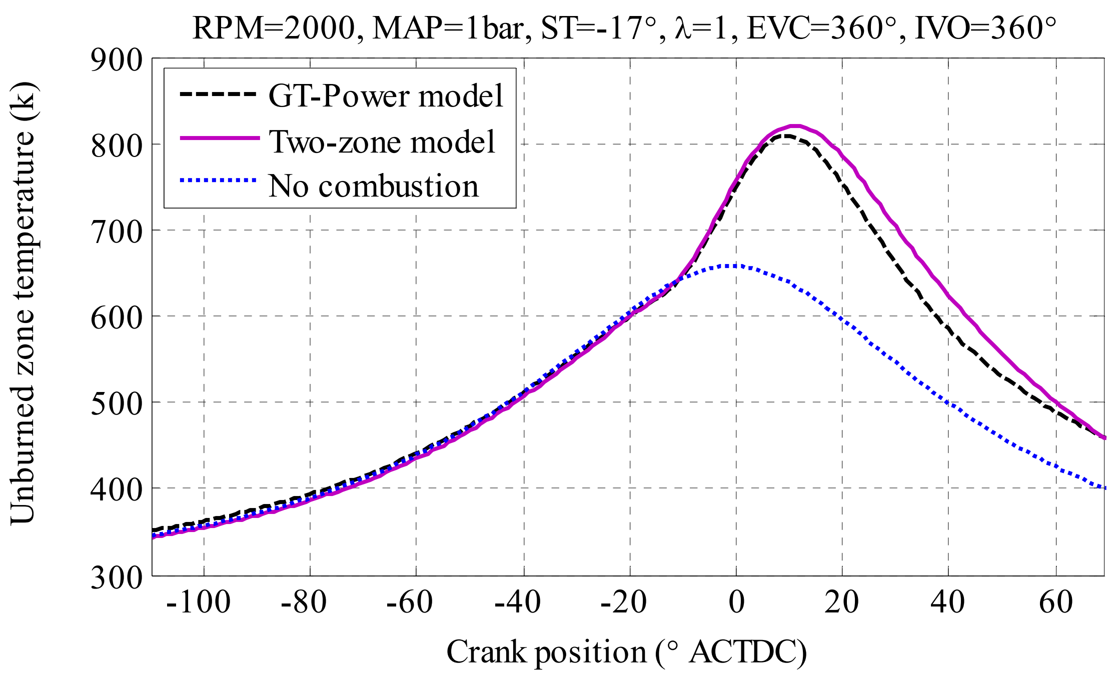

Figure 3.9: In-cylinder gas temperature without combustion; unburned zone gas temperature: correlation between GT-Power and two-zone SI combustion models

3.7.2 Two-zone SI combustion model validation

The two-zone SI combustion model was firstly validated at 3000 rpm of engine speed and in three different engine load conditions: P_{IM} = 0.4, 0.7 and 1.0 bar corresponding to low load, medium load and full load conditions. The combustion durations at the three conditions are different, spark timings were set to MBT (Minimal advance for the Best Torque) for each condition. The valve strategy is PVO. Fairly good correlations of both pressure and temperature can be found in Figure 3.10 and Figure 3.11.

To validate the combustion model in wider engine operating range, more simulations were conducted. In those simulations, engine speed sweeps from 1000 rpm to 5000 rpm with 1000 rpm increment interval; engine load also ranges from low load, medium load to full load conditions. Both PVO and NVO valve strategies were used, for PVO: IVO=340° ACTDC and EVC=380° ACTDC; while for NVO: IVO=380° ACTDC and EVC=340° ACTDC. To simplify the validation, only some key parameters were recorded and plotted in Figure 3.12 and Figure 3.13. Actually these key parameters listed in Figure 3.12 and Figure 3.13 outline the profiles of the pressure, temperatures (burned and unburned).

From Figure 3.12 and Figure 3.13, one can find all pressure related parameters, like IMEP, P_{max} and the crank position of P_{max}, have fairly good correlations with the GT-Power results; whereas for the temperature related parameters, the errors are relatively larger, but still within ±10% of their normal reachable range. One possible reason is that the gas property parameters such as C_v and R used in these two models are different. In the GT-Power model these parameters are functions of not only the gas temperature but also the gas chemical composition. While in the two-zone model chemical composition is not considered due to simplified real-time modeling.

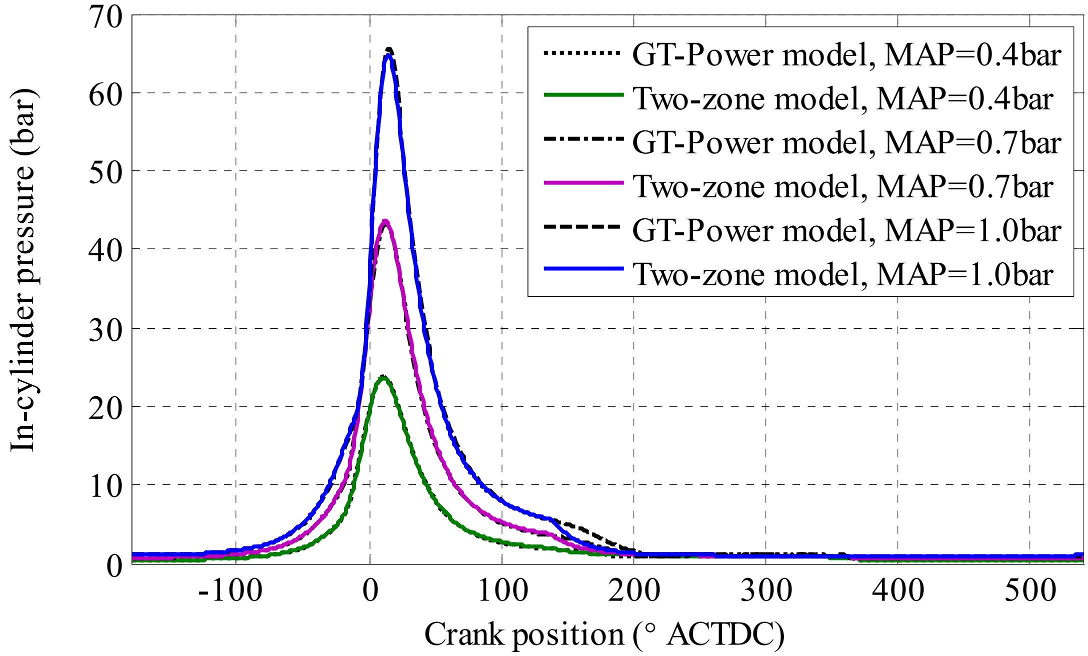

Figure 3.10: In-cylinder pressure traces for different engine load at 3000rpm: correlations between GT-Power and two-zone SI models

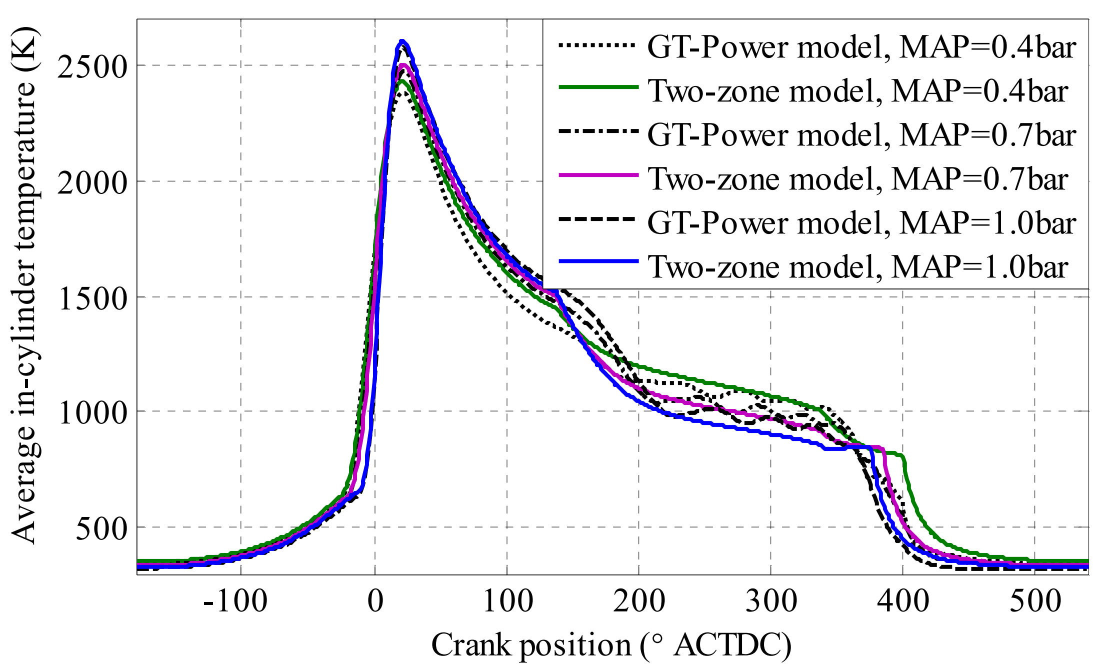

Figure 3.11: In-cylinder temperature traces for different engine load at 3000rpm: correlations between GT-Power and two-zone SI models

Another low correlation parameter is the residual gas M_r. for NVO it is fairly good, but for PVO the correlation becomes worse. As explained in section 3.4, the gas exchange process of PVO is complicated and difficult to be modeled accurately [85]. Fortunately, this only happens to PVO, which is only used for the SI combustion mode. The modeling error of M_r in the SI combustion mode has less impact on the combustion timing and duration than it has in the HCCI mode. Since in the SI mode: combustion timing is controlled by spark ignition input from engine controller, while combustion duration is mainly decided by engine load and speed.

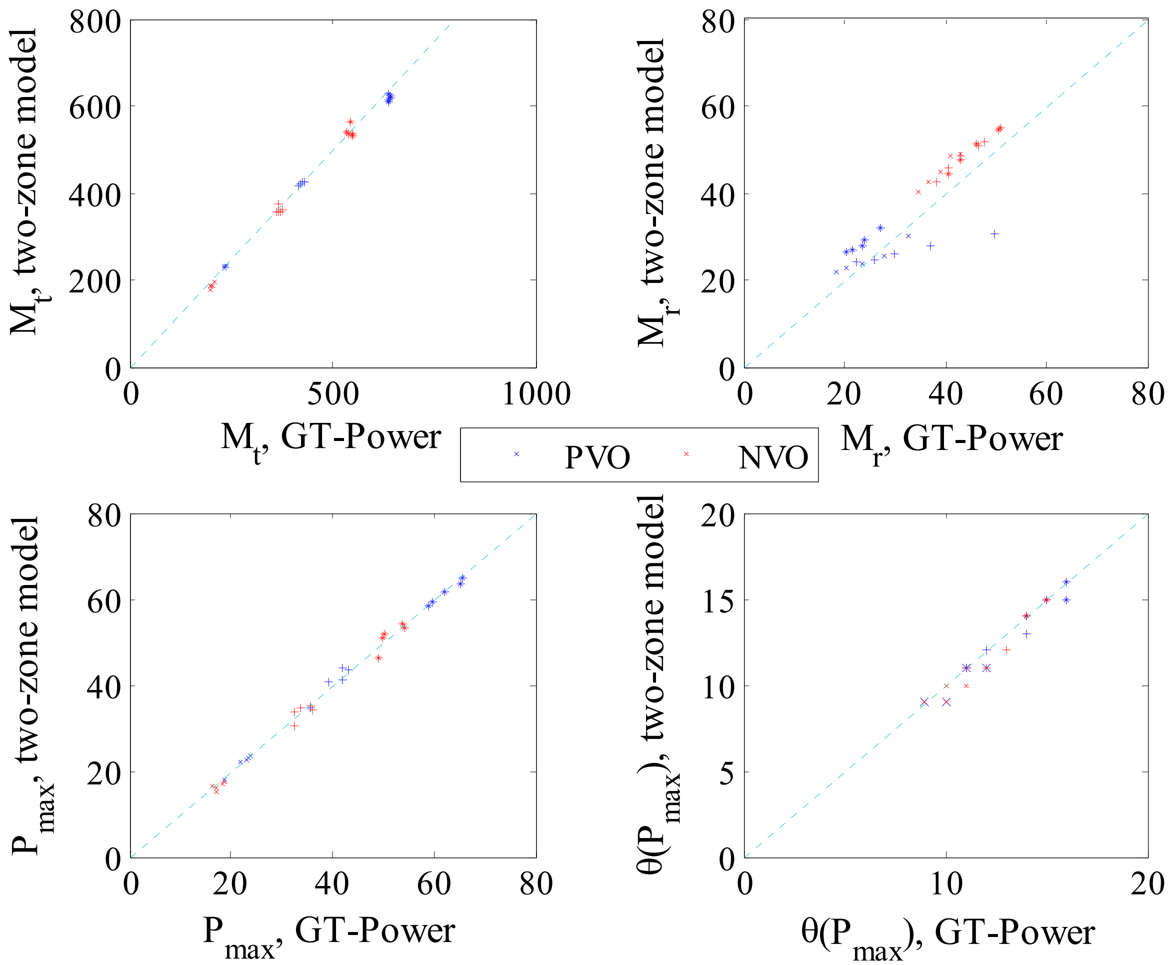

Figure 3.12: Two-zone SI combustion model correlations: total in-cylinder gas mass M_t, residual gas mass M_r, peak in-cylinder pressure P_{max} and crank position of P_{max}

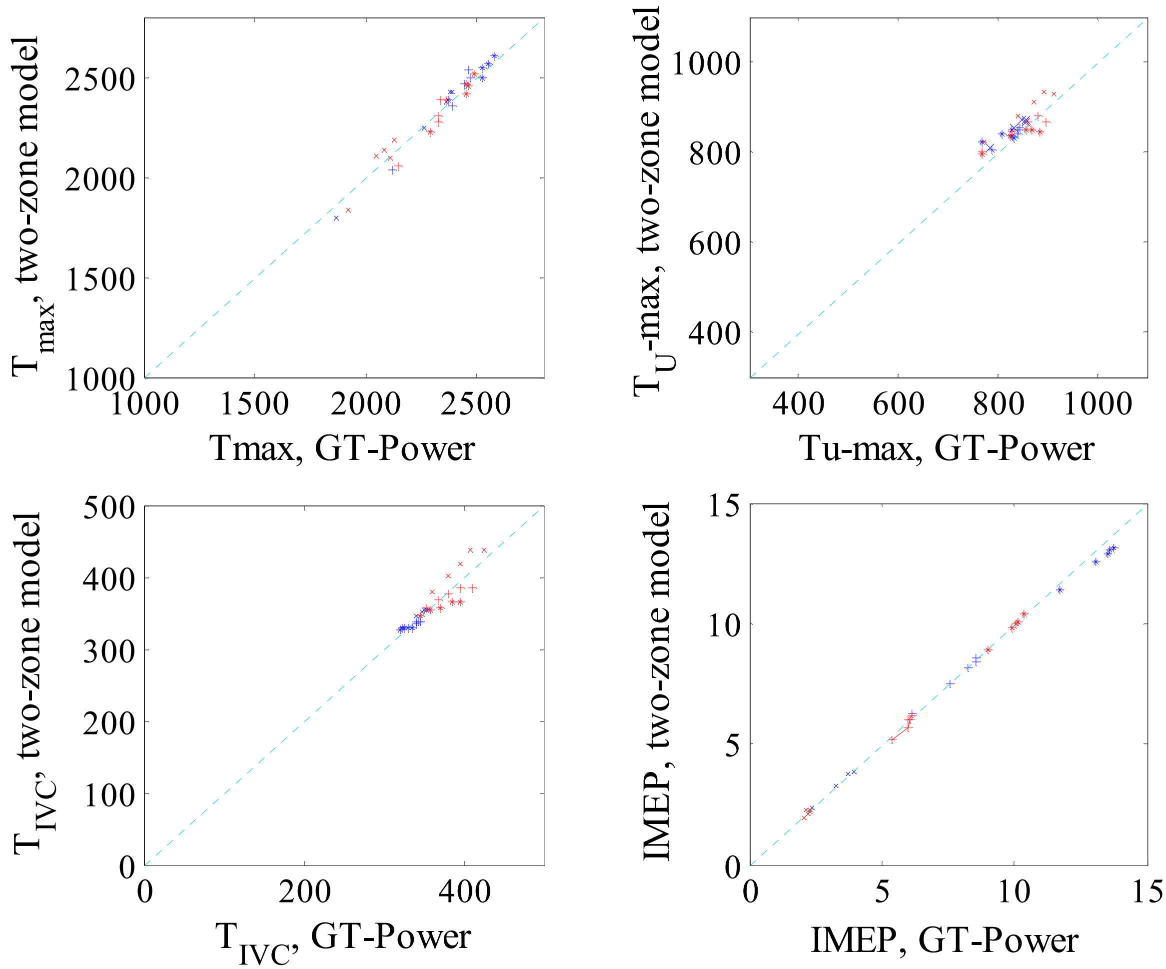

Figure 3.13: Two-zone SI combustion model correlations: peak in-cylinder gas temperature T_{max}, peak unburned zone temperature T_U-max, charge temperature at IVC T_{IVC} and IMEP

Even Figure 3.13 does not show very good correlations on T_{IVC} and T_U-max that are of great interest in the study of the SI-HCCI hybrid combustion, Figure 3.14 and Figure 3.15 demonstrate fairly good consistency when both temperatures vary with the engine speed. Furthermore, in Figure 3.14 and Figure 3.15 strong correlation is also found between T_{IVC} and T_U-max. It indicates that the unburned zone temperature can be regulated by adjusting T_{IVC} through valve timing control.

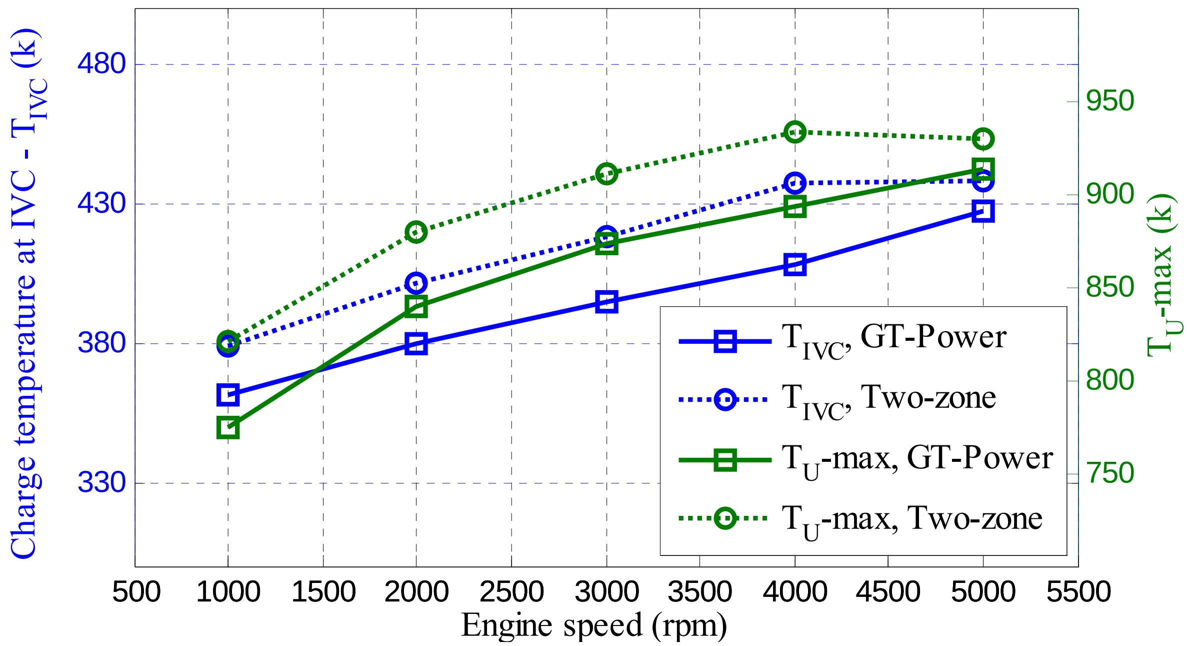

Figure 3.14: Correlations between the peak unburned zone temperature T_U-*max* and in-cylinder gas temperature at IVC T_{IVC} for NVO at different engine speed

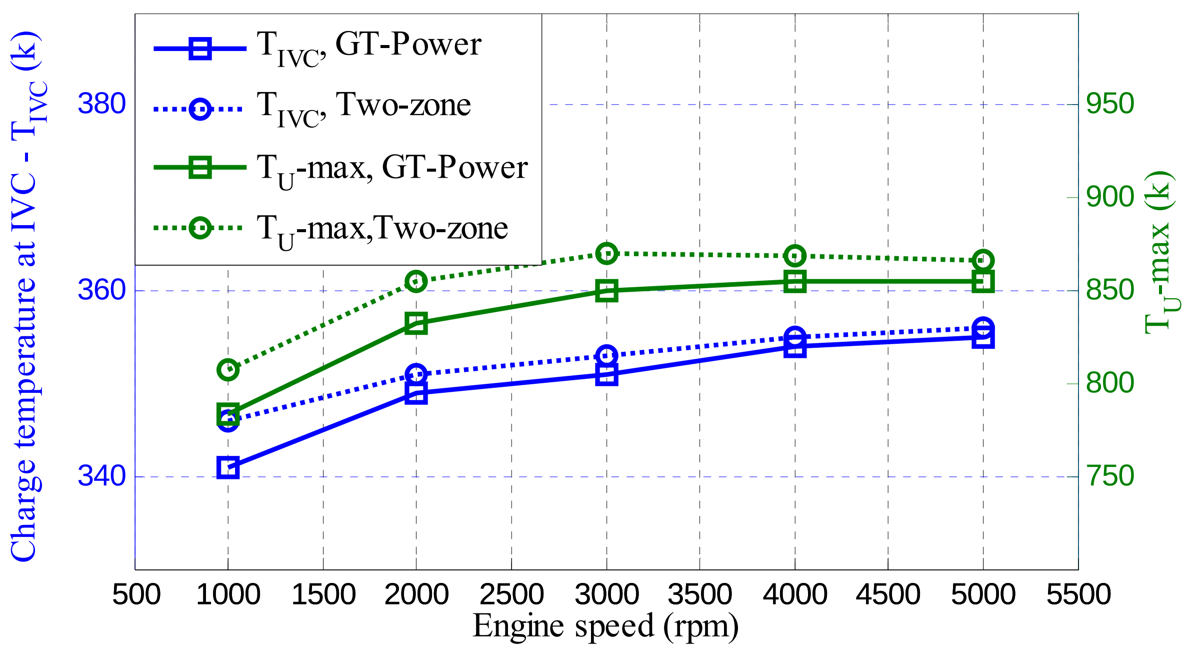

Figure 3.15: Correlations between the peak unburned zone temperature T_U-*max* and in-cylinder gas temperature at IVC T_{IVC} for PVO at different engine speed

3.7.3 One-zone HCCI combustion model validation

Figure 3.16 shows that the one-zone model can simulate the HCCI combustion process as well as the GT-Power model. For this simulation, 16 mg of fuel was injected into each cylinder every engine cycle to generate 5.02 bar IMEP at 2000 rpm, which is close to the upper load limitation of the HCCI combustion. Note that for the HCCI combustion the engine load is not decided by MAP but by the injected fuel quantity due to the un-throttled operation. The valve lift profiles of both intake and exhaust were switched to the low stage ones since the decrease in exhaust valve lift makes it possible to trap more internal residual gas with NVO and the decrease in intake valve lift enables un-throttled engine operation.

The HCCI combustion timing is also sensitive to the intake and exhaust valve timings. Proper valve timing selections lead to improved combustion quality. For instance, in the simulation results presented in Figure 3.16, intake valve timing was advanced to make the effective compression ratio smaller to avoid engine knock at the upper load limitation of the HCCI combustion. The simulations were extended for different valve timings, and these results were compared with the GT-Power simulation results shown in Figure 3.17 with good correlation.

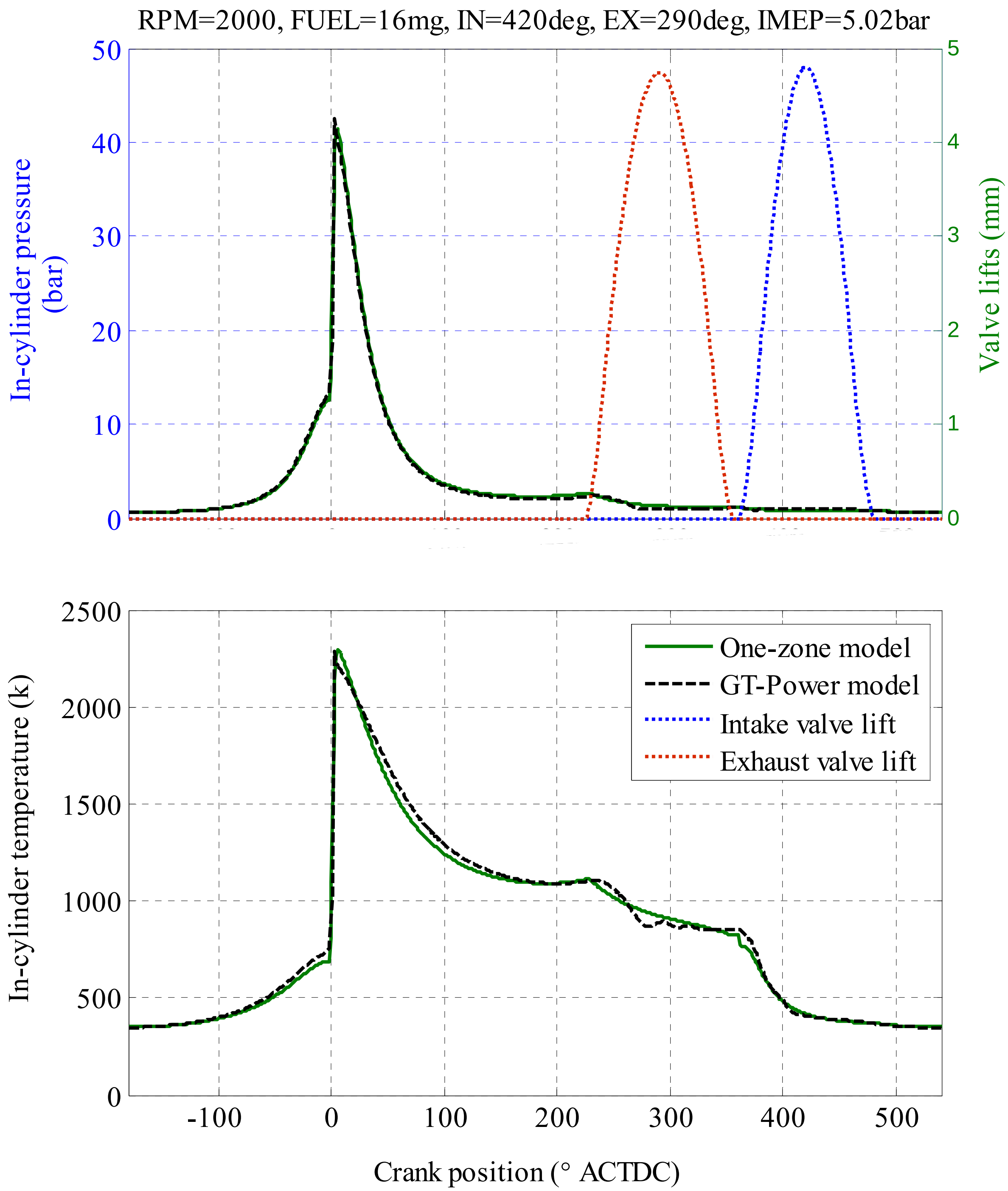

Figure 3.16: In-cylinder pressure and temperature traces: correlations between the one-zone HCCI combustion model and GT-Power model

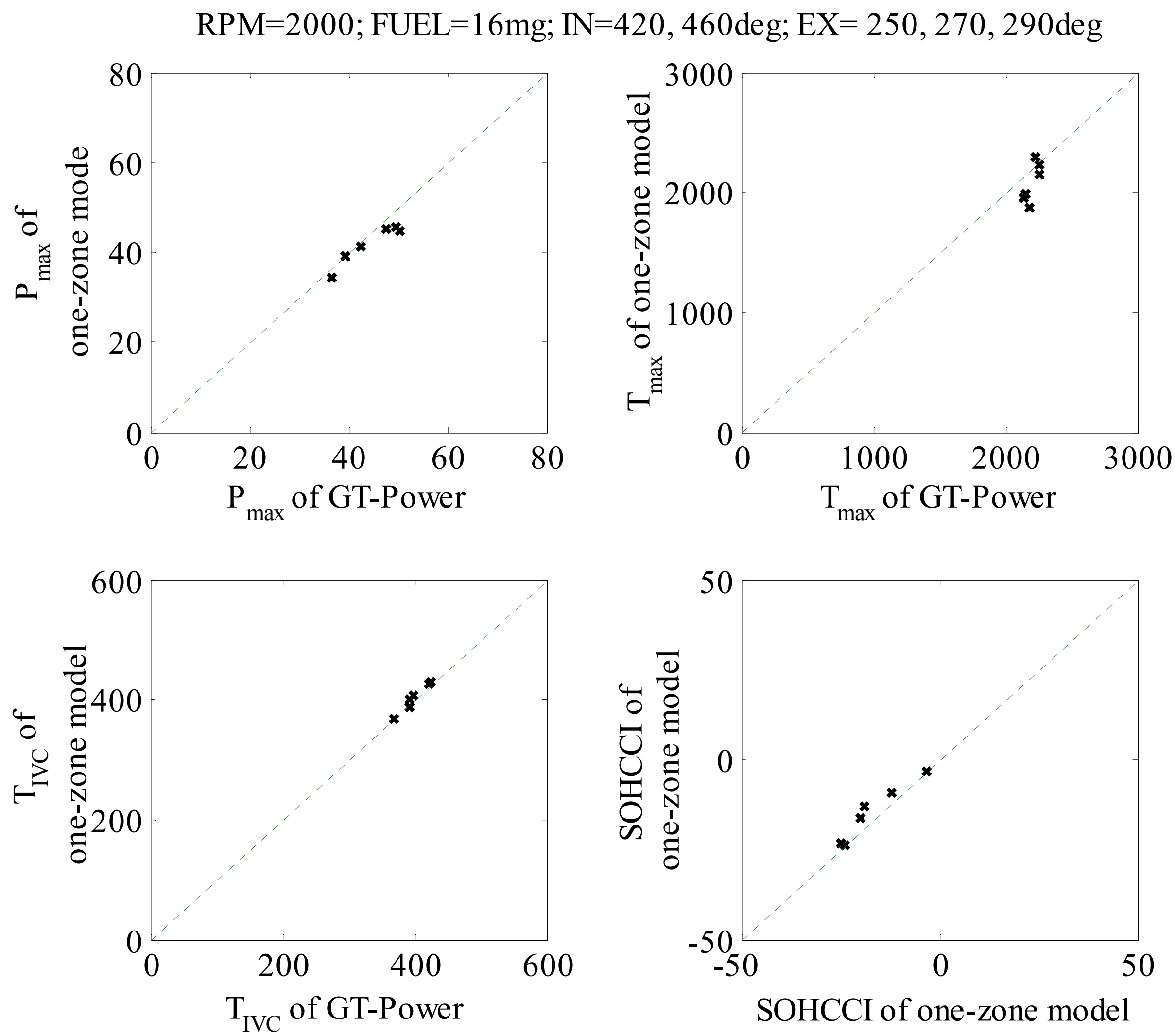

Figure 3.17: One-zone HCCI combustion model correlations: peak in-cylinder pressure P_{max}, peak in-cylinder gas temperature T_{max}, in-cylinder gas temperature at IVC T_{IVC} and crank position of SOHCCI

3.7.4 The impact of external EGR

The impact of the EGR percentage to the hybrid combustion modes was also investigated through steady-state simulations. HCCI combustions have much shorter burn duration than that of SI combustions. This leads to high peak in-cylinder pressure and temperature, as shown in Figure

3.16. High peak in-cylinder pressure leads to high engine efficiency if it occurs at a proper timing (5 to 10 crank degree after TDC), whereas high in-cylinder temperature is an adverse condition for NOx emissions. However, the HCCI combustion is capable of operating with higher EGR rate than that of the SI combustion. Figure 3.18 demonstrates how the cooled EGR rate affects the in-cylinder gas temperature. The simulation results in Figure 3.18 were completed with 3.7 bar IMEP, where the exhaust valve timing, spark timing and fuel quantity were adjusted to maintain a constant IMEP (3.7 bar) and SOHCCI (0° ACTDC) for each simulation. Simulation results show that the higher EGR rate the lower the peak in-cylinder gas temperature.

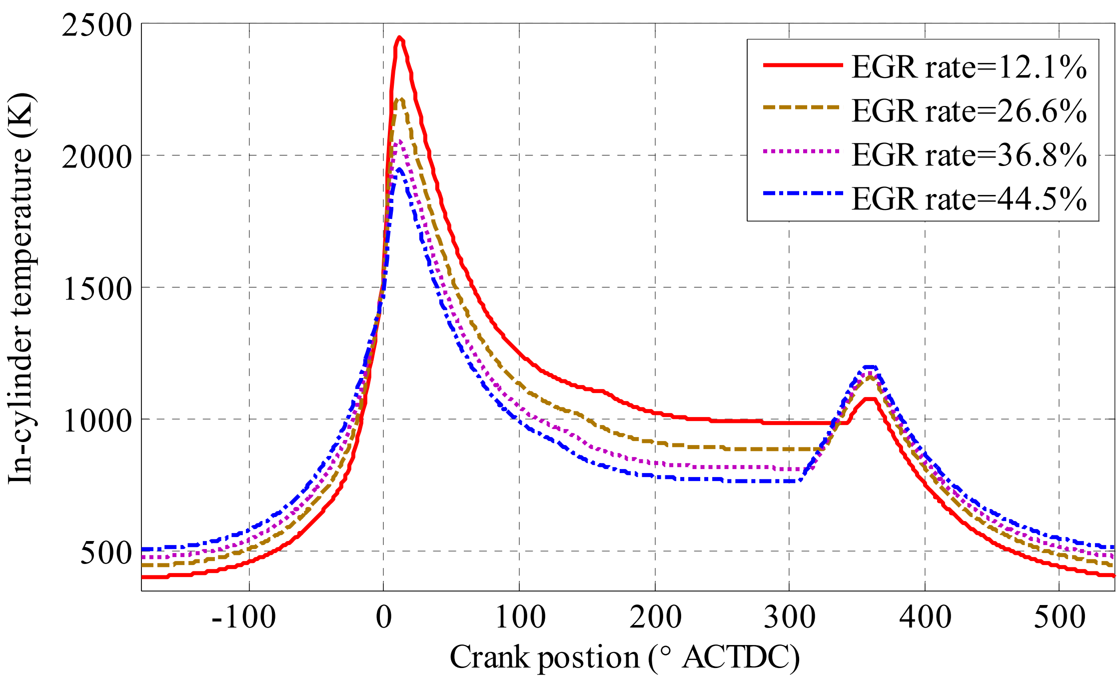

Figure 3.18: In-cylinder gas temperature traces for different external EGR rate

3.8 Conclusions

In this chapter, the SI-HCCI hybrid combustion model was developed based on the two-zone SI combustion model and the one-zone HCCI combustion model. The gas exchange model was also updated for improved accuracy. As two special operational modes of the SI-HCCI hybrid combustion, the SI combustion and the HCCI combustion modes were simulated in HIL simulation system respectively. Simulation results were also compared with the corresponding GT-Power ones. The following are the conclusions:

- Both one-zone and two-zone SI combustion models provide accurate simulations of the in-cylinder gas pressure and average temperature of both burned and unburned zones at different engine operational conditions.
- The two-zone SI combustion model is more accurate than the one-zone model for simulating in cylinder temperatures of both burned and unburned zones. Note that the unburned zone gas temperature of the SI combustion is related to T_{IVC} (in-cylinder gas temperature at IVC) and is the key factor of simulating the start of the HCCI combustion (SOHCCI) that can be controlled by adjusting the intake and exhaust valve timings.
- The gas exchange model has higher accuracy for negative valve overlap (NVO) than positive valve overlap (PVO). It is proper to be used for the SI-HCCI hybrid combustion.
- The one-zone HCCI combustion model is proper for the HCCI combustion modeling as part of the SI-HCCI hybrid combustion
- Cooled external EGR gas can be used to reduce in-cylinder gas temperature during the HCCI combustion process.

CHAPTER 4

IMPLEMENTATION OF ENGINE MODEL IN THE HIL SIMULATION ENVIROMENT

4.1 Introduction

The engine sub-models introduced in Chapters 2 and 3 can be used to conduct offline simulations individually for validation purpose. To simulate the entire engine model, the model needs to be implemented into a HIL simulation environment for real-time simulation.

As mentioned in Chapter 1, real-time HIL simulation is a powerful tool for engine control strategy development and validation. With the HIL simulations, the initial engine control strategy calibration can be generated and control implementation issues can be resolved. This chapter explores how the mathematic engine sub-models presented from the last chapters are integrated into an engine model, and implemented into the dSPACE based HIL simulation environment.

This chapter is organized as follows. Section 4.2 discusses the integration of the entire Simulink engine model module-by-module in the Matlab/Simulink environment; the methods of model solutions are presented in this section, too. In Section 4.3 the integrated Simulink engine model will be implemented into the dSPACE HIL simulation environment. In Section 4.4 results of two transient simulations are presented based upon the HIL simulations to validate the transient performance of the developed engine model. At last, conclusions are drawn in Section 4.4.

4.2 From Mathematic Equations to Simulink Model

This section discusses the integration of the mathematic equations in Chapters 2 and 3 into a entire engine model, used for the HIL simulations, in Simulink.

4.2.1 Build engine in Simulink

The engine model was assembled module-by-module. Figure 4.1 shows the layout of these sub-models used for assembling the Simulink engine model. Each block represents an engine subsystem. Signals transferred between these blocks are the state variables calculated by the governing equations embedded inside each block. The governing equations are presented in the last two chapters. These sub-models were also calibrated and validated separately. Simulink dialogue box is used to input the sub-model calibrations, see Figure 4.2 for an example. The functionality of each sub-model can be tested individually by applying signals to the input ports and observing the output signals.

Integrating the Simulink engine model in such a way makes it easy to change the engine model configurations. The engine model shown in Figure 4.1 is for the dual-stage turbocharger 3 cylinder SI engine in Chapter 2. It takes only hours to convert this engine model into an HCCI capable 4 cylinder engine model in Chapter 3 due to the module architecture.

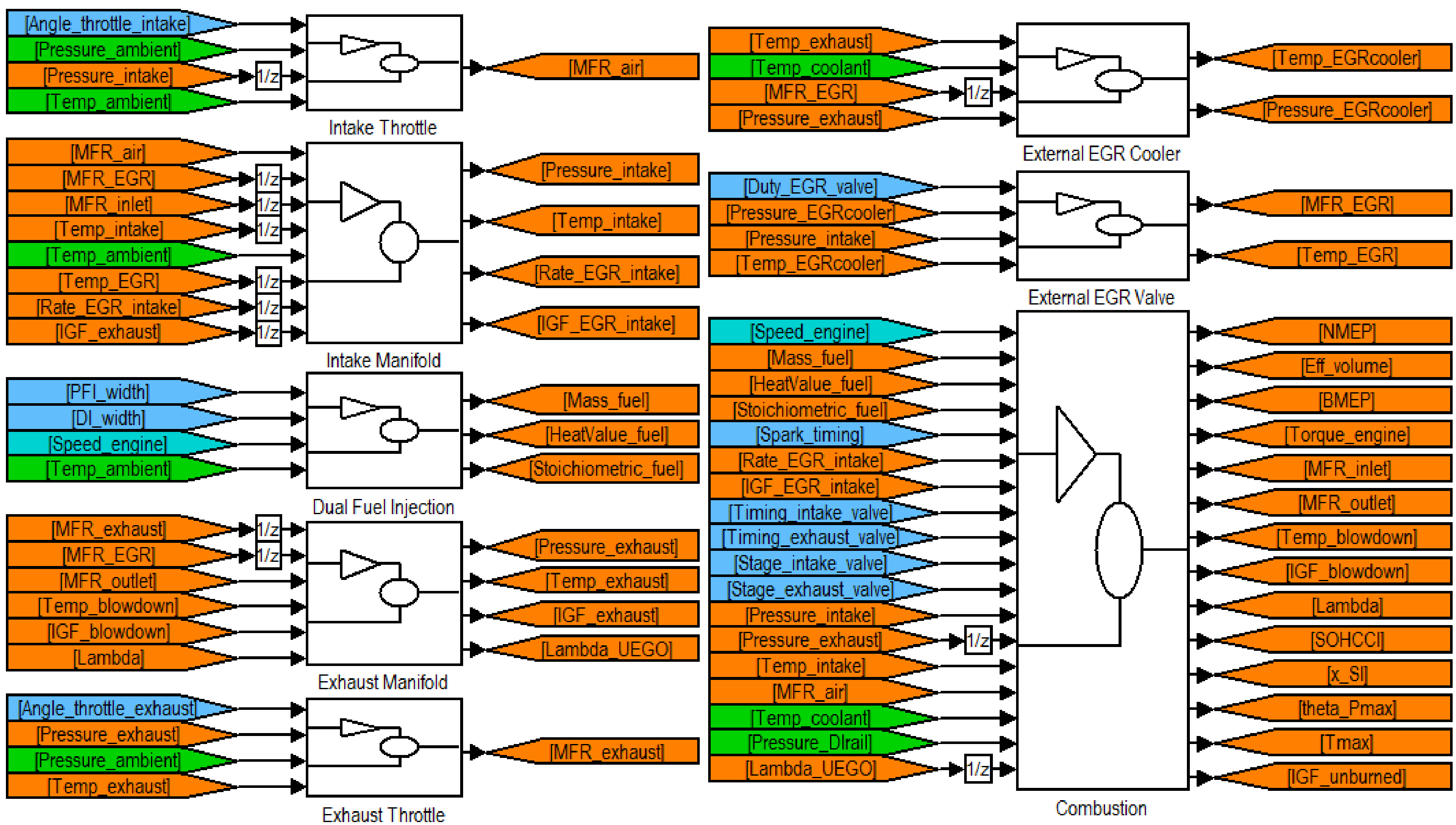

Figure 4.1: Simulink engine model - layout of each subsystem

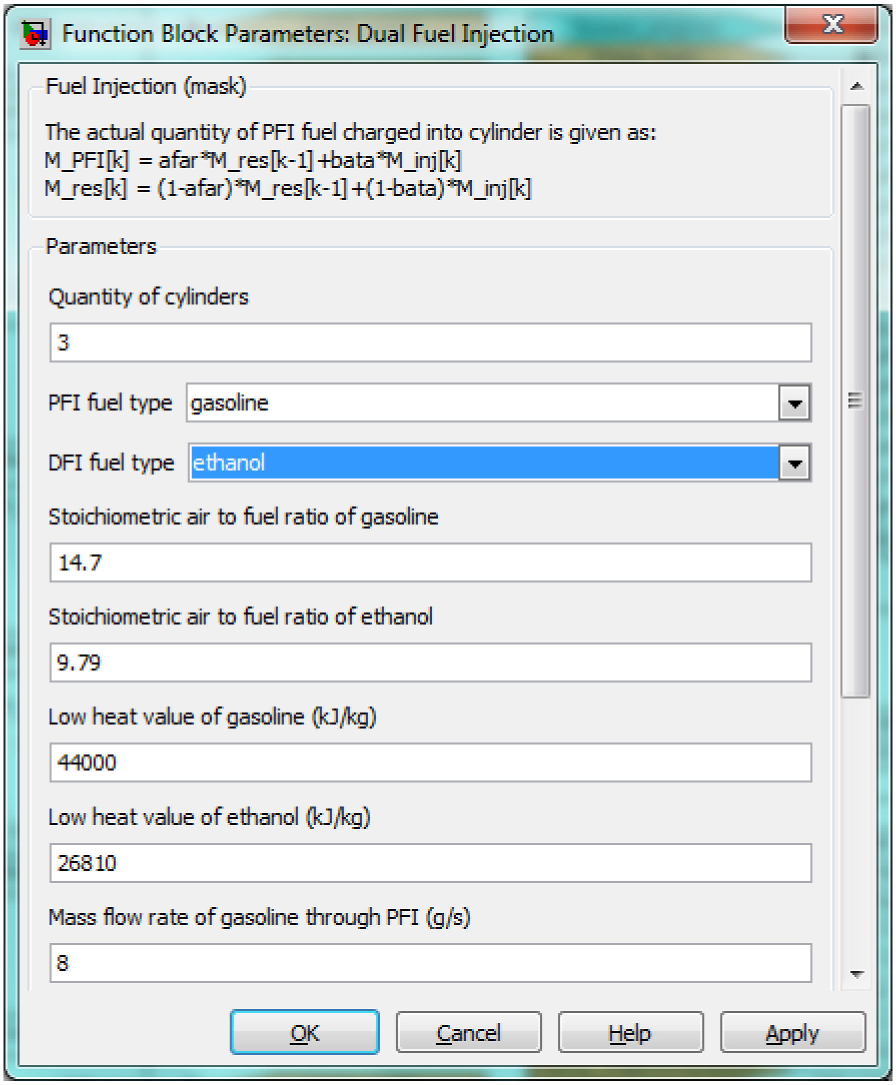

Figure 4.2: Dialogue box for fuel injection system

4.2.2 Model solution in Simulink

The entire engine model consists of more than hundred mathematic equations. Some of them are nonlinear differential equations. To solve these equations analytically is almost impossible. In Simulink these equations are solved by numeric method. Typically, the differential equations in the engine model can be written in a simple form as

$$\dot{x} = f(x) \tag{4.1}$$

where x is the state space of the engine model and $\dot{x}$ represents the time derivative of x. One way to solve the above differential equation is to use the iterative method with first order approximation, where the above equation can be approximated by the following

$$\frac{x(t+\Delta t)-x(t)}{\Delta t} \approx f\left(x(t)\right) \tag{4.2}$$

where Δt is the time step for the numeric solution. $x(t+\Delta t)$ is the updated state and $x(t)$ is the known current state. Accordingly $f(x(t))$ is known since $x(t)$ is known. Therefore, the solution can be approximated by

$$x(t+\Delta t) \approx x(t) + f\left(x(t)\right)\Delta t \tag{4.3}$$

The solution can also be represented in discrete time domain (z domain) as

$$x(z) \doteq x(z)\frac{1}{z} + f\left(x(z)\frac{1}{z}\right)\Delta t \tag{4.4}$$

where z is a delay operator. In fact, majority of the nonlinear differential equations are solved in such way with either variable step or fixed step. Our Simulink engine model is numerically solved by this approach and that is why there are many unit delay blocks ($1/z$) in the Simulink engine model; see Figure 4.1. The crank based combustion model was solved based on the same concept as discussed above but the time step Δt is replaced by crank angle step $\Delta\theta$. For this engine model, the crank step $\Delta\theta$ equals to one crank degree.

Note that in equation (4.3), as time step Δt approaches 0 $x(t+\Delta t)$ approaches $x(t)$. Accordingly small Δt leads to high accuracy. However Δt cannot be too small due to the computational throughput limitation. Currently in the Simulink engine model Δt is fixed at 1.0 ms, and for most subsystems this time step is acceptable, but for system like turbocharger smaller time step could be required. To reduce the step size for a specific subsystem, multiple iterations within single time step is used.

To implement multiple iterations in single time step, equation (4.3) is rewritten as

$$x^{i+1}(t+\Delta t) = x^{i}(t) + f\left(x^{i}(t)\right)\frac{\Delta t}{m} \qquad i = 0,1,\cdots\cdots(m-1) \tag{4.5}$$

and

$$\begin{aligned} x^{0}(t) &= x(t) \\ x(t+\Delta t) &= x^{m}(t+\Delta t) \end{aligned} \tag{4.6}$$

where m is the specified iteration number in one time step. Figure 4.3 illustrates how m affects the transient performance of the Simulink engine model. The simulation in Figure 4.3 was conducted with Δt = 5ms, and m = 10 and shows proper accuracy without adding a lot of computational throughput. Note that it is difficult to implement multiple iterations in single step directly in Simulink. In the Simulink engine model, the sub-model of the dual-stage turbocharger was programmed in C language, and compiled as an *S*-function and called by Simulink block, because it is easy to execute a particular piece of code for multiple times in C language.

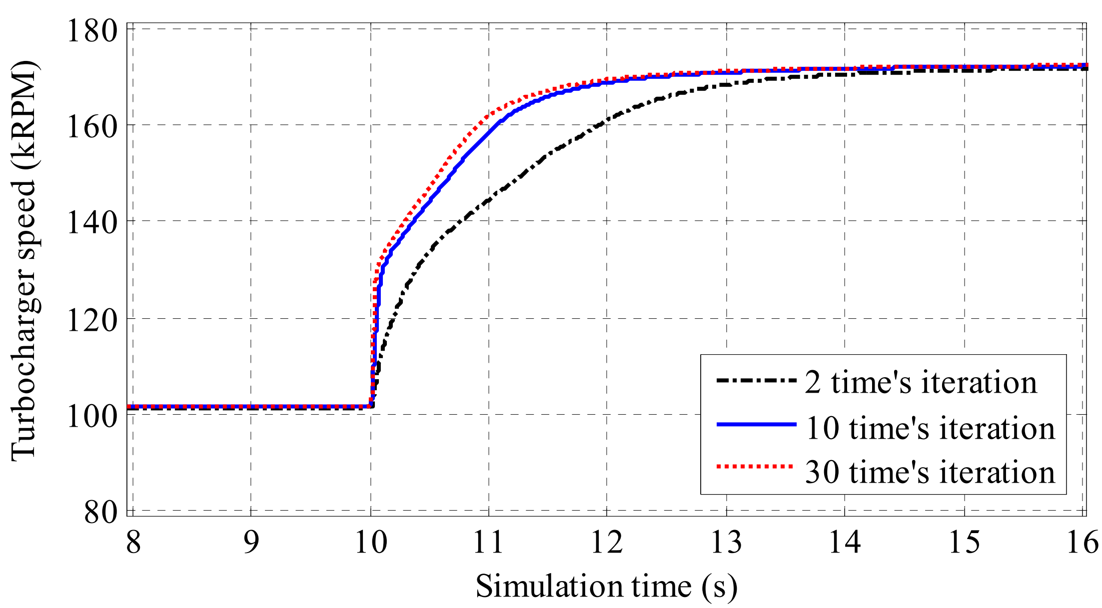

Figure 4.3: Transient performance of the turbocharger shaft rotational speed: comparison between different times of iteration using single step multiple iteration approach

4.3 Model Implementation in HIL Simulator

The Simulink engine model developed has three tasks: the 1.0 ms time step task for the mean value sub-models (such as the engine air handling subsystem), the crank based task for the combustion model, and the cycle based task for sub-models like the fuel wall wetting dynamics. The crank based and the cycle based tasks are independent of simulation time step. To simulate these three tasks in a parallel way, crank and cycle based interrupts need to be generated. A dSPACE HIL simulator was selected for the engine simulations. This section introduces the functionality of the dSPACE HIL system and discusses the implementation of the Simulink engine model in the dSPACE HIL simulation environment for engine real-time simulations.

4.3.1 The engine simulator hardware

A dSPACE PX20 was selected for the real-time simulation, see Figure 4.4. A DS-1006 microprocessor board was used as the simulation engine, and a DS-2211 automotive application board along with other I/O boards was used to form the HIL simulator.

The most important feature of dSPACE systems is that the Simulink block diagram can be auto-coded into C and compiled to be executed in the dSPACE system. Also, there are many Simulink block libraries that make the programming fairly easy.

Figure 4.4: The dSPACE hardware

4.3.2 HIL simulation system architecture

Figure 4.5 shows the system architecture of the HIL simulation system. For simplicity, not all the signals and subsystems are included in the diagram. It is only used to explain how the Simulink engine model was implemented in the HIL simulation environment. In Figure 4.5, the ECU (engine control unit) in the upper area of the diagram is the engine control target of the HIL simulation, and it is not the focus of this chapter. All blocks below the ECU block are from the HIL simulator. In the center it is the engine model, the main sub-models were displayed. On the output side of the engine model, signal conditioning block converts all computed parameters to real engine signals that the ECU can recognize. On the input side of the engine model, signal preprocessing block translate all ECU control signals back to the parameters that engine model can recognize.

During the HIL simulations, the time based mean value sub-models are executed in real-time at a fixed time step (1.0 ms). Among these sub-models, the engine crankshaft dynamic model as described by equation (2.4) provides the engine speed. Based on the modeled engine speed, engine crank signal (720 pulses per cycle), TDC signal (2 pulses per cycle) and cam signal (1 pulse per cycle) are generated using the dSPACE hardware, as shown in Figure 4.6. The signals are sent to synchronize the HIL simulator with the ECU. At the same time, crank and CAM signals are looped back to the HIL simulator as input signals to generate interruptions for crank and cycle based simulations. During the interruptions, crank based and cycle based interruption sub-model routines are executed. The interruption triggered by crank signal has the top priority in the interruption queue, since the crank based routine needs to be executed within a specific crank angle.

Figure 4.6 presents a snapshot of the oscilloscope signals during the HIL simulation, in-cylinder pressure and temperature signals are the output from this HIL simulation. A picture of the entire HIL engine simulation platform is shown in Figure 4.7. One can find that some auxiliary instruments like the oscilloscope and host PC are required to facilitate the real-time HIL simulations.

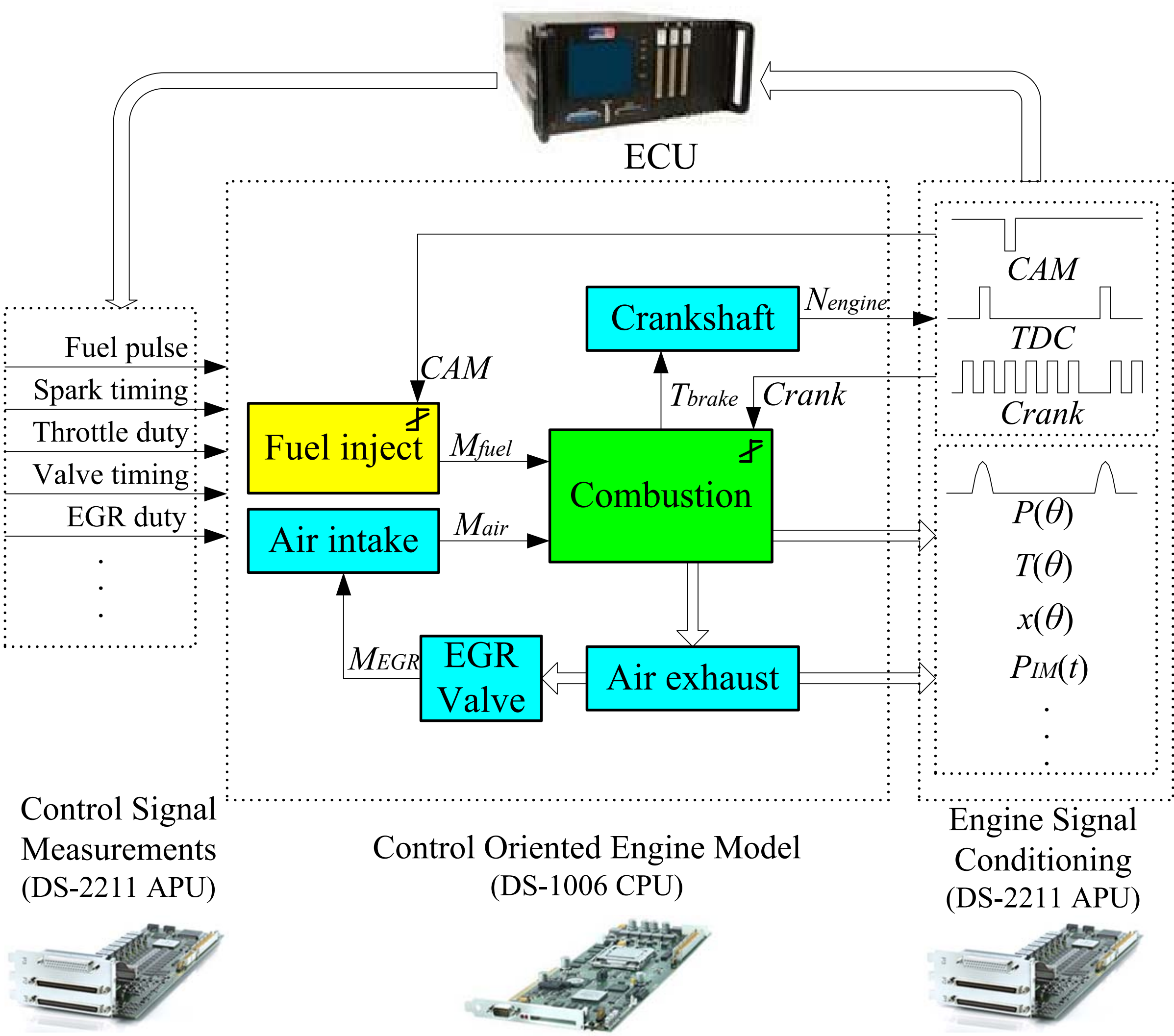

Figure 4.5: System architecture of the integrated HIL simulation environment

Figure 4.6: Simulated engine signals displayed on oscilloscope

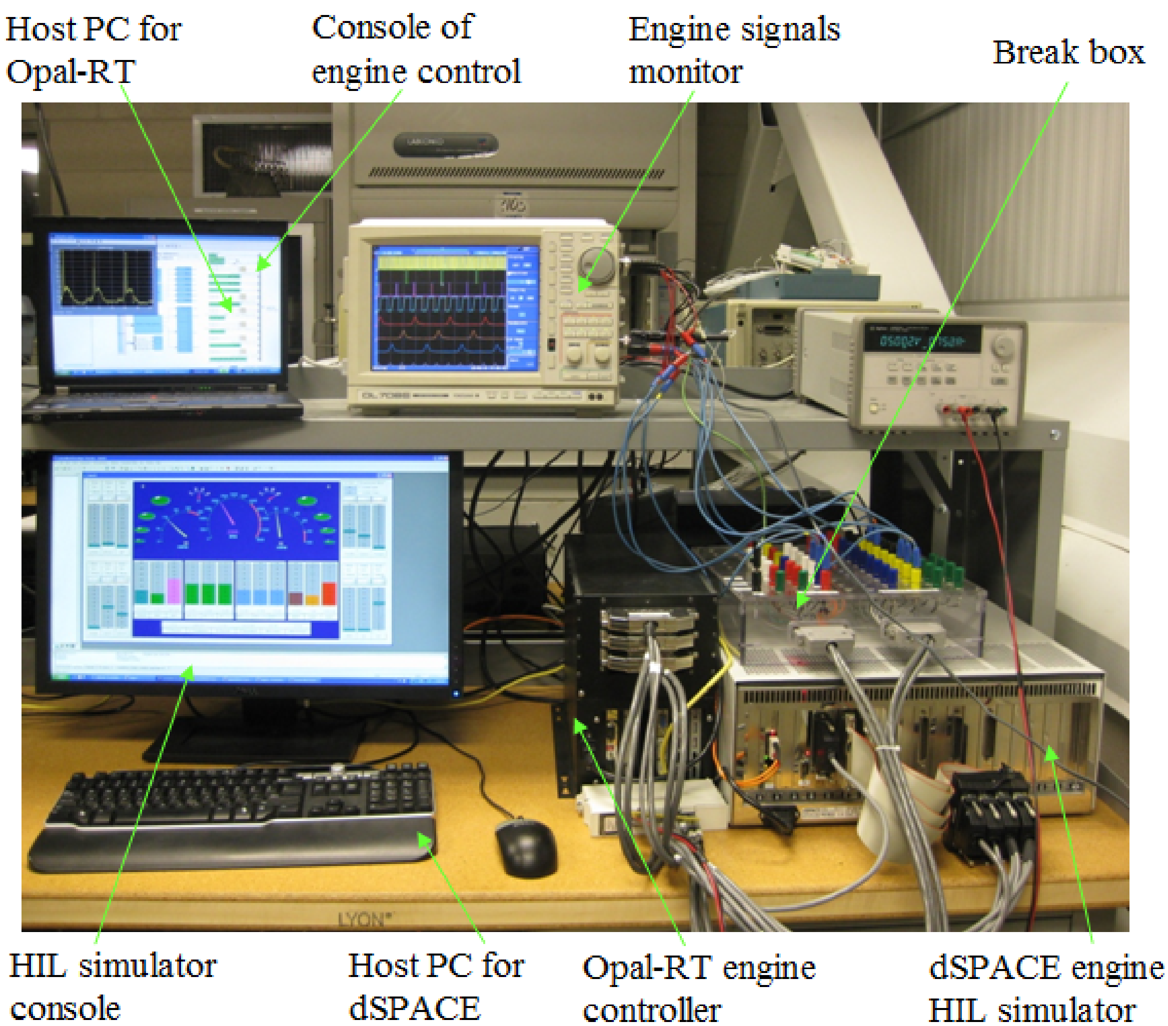

Figure 4.7: Snapshot of HIL simulation platform

4.4 Engine HIL Simulations

In order to demonstrate the transient performance of the developed engine model, turbocharger lag simulation and the SI-HCCI combustion mode transition simulation were performed. The simulation results motivated the control study in the next phase of the research.

4.4.1 Transient performance of engine with dual-stage turbocharger

Two transient simulation responses were performed using the developed HIL simulation environment, one with feedforward fuel control and the other without. Both simulations utilize closed-loop fuel control with a PID control strategy. The transfer function of the feedforward controller is:

$$\frac{M_{FF}(s)}{P_{IM}(s)} = \frac{g(N_e)\cdot s}{\tau \cdot s + 1} \tag{4.7}$$

where g is a function of engine speed, N_e, implemented as a lookup table; τ is the time constant of feedforward fuel control. The control system block diagram is shown in Figure 4.8.

Note that except for the fuel control, all the other engine control parameters remained unchanged for both simulations. Engine speed was at 2500 rpm with 10% throttle and the MBT spark timing. The control reference of the air-to-fuel ratio was set at stoichiometric ratio when a step throttle of 90% was applied, which sets the throttle to WOT (wide open throttle). The waste-gates of both stages are closed when the throttle was opened. As a result, the engine started switching from the partial load to the full load condition.

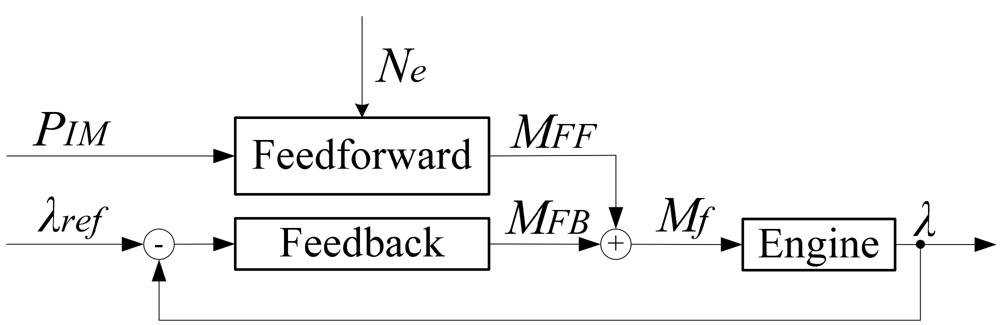

Figure 4.8: Control architecture for transient response simulation of the SI engine with dual-stage turbocharger

The corresponding engine dynamic responses, plotted in Figure 4.9, show that the feedforward fuel control provides additional fuel output to improve transient response. With the feedforward fuel control, the engine air-to-fuel ratio response settles within 1 second, while without the feedforward fuel control it takes about 4 seconds. The corresponding engine torque settling time decreases from 2.11 seconds without feedforward control to 1.29 seconds with the feedforward control, which is significant. One can see this improvement of transient response in Figure 4.10.

From Figure 4.9 it can be observed that even with feedforward control, during the transition operation there exists an impulsive overshoot of the relative air-to-fuel ratio, which indicates that lean combustion occurs right after the step throttle and last for a few engine cycles. This is mainly due to the special engine architecture. As mentioned in Chapter 2, the engine throttle locates between the intake manifold and engine head. The lack of volume between the engine throttle and the intake valve leads to a rapid increment of engine volumetric efficiency when the throttle is suddenly opened. From Figure 4.10, one can see that the corresponding MAP also drops at the same time due to the rapid increment of air flow to engine cylinders, which reduces the air mass in the intake manifold. This makes it difficult to control the air-to-fuel ratio precisely.

As shown in Figure 4.11, during the transient operation, both stages of turbochargers accelerate. Obviously, the HP-stage turbocharger has faster transient response since it has a smaller size with small shaft rotational momentum. This is an advantage of the dual-stage turbocharger system, which can used to reduce turbo lag. One can also find both engine torque and boost pressure increase rapidly at beginning due to the quick response of the HP-stage turbocharger and then the response slows down when the LP-stage turbocharger plays the main role.

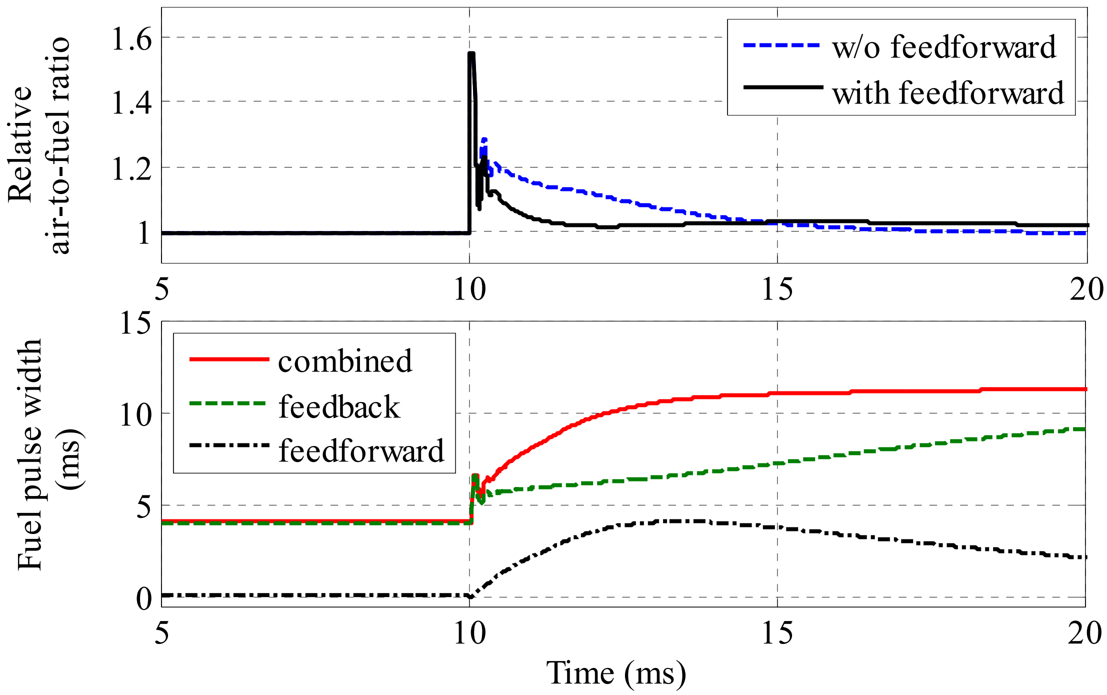

Figure 4.9: Transient response of relative air-to-fuel ratio and fuel pulse width

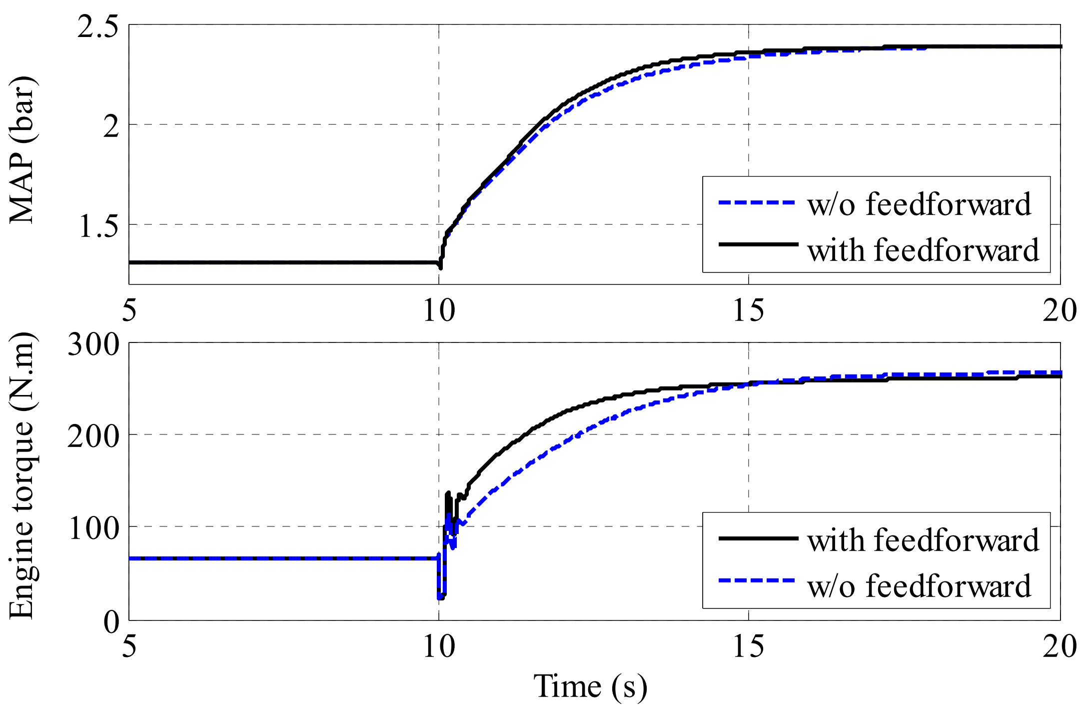

Figure 4.10: Responses of engine torque and intake manifold pressure

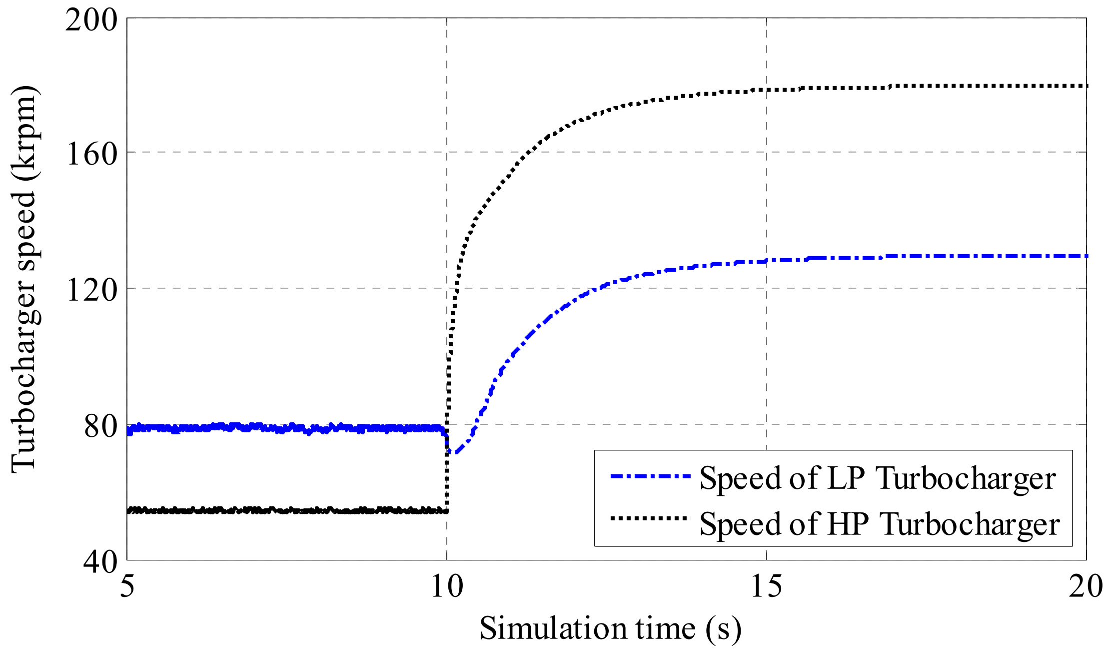

Figure 4.11: Responses of the turbocharger shafts' rotational speed of each stage

4.4.2 SI to HCCI combustion mode transition

To demonstrate the effectiveness of the SI-HCCI hybrid combustion mode for mode transition, an SI-HCCI mode transition process was simulated by two different strategies. One uses the hybrid combustion mode and the other switches from the SI to HCCI combustion mode in one step. Figure 4.12 shows the in-cylinder pressure traces generated in simulations using the two strategies. The pressure profiles vary significantly from cycle to cycle during the mode transition for both strategies. The engine control parameters used for the simulations are spark timing, fuel quantity, intake and exhaust valve timings and lifts. For the simulation results presented in Figure 4.12, these control parameters were adjusted manually to have the best (smooth) transition. To obtain smooth combustion mode transition for the entire engine operating range, advanced control strategy will be developed in the next stage of the research.

In the mode transition simulations, 26 engine cycles of combustions were simulated and recorded for both control strategies. Engine speed was set to 2000 rpm throughout the entire process. In the first 15 cycles, engine was operated in the SI mode and 12 mg (per cycle) of gasoline was injected to each cylinder; spark timing was set to be -23° ACTDC; intake and exhaust valve timings (at peak lift position) were set to 440° ACTDC and 270° ACTDC, respectively; and the lifts of both valves were in the high stage. Starting at engine cycle 16, the combustion mode transition from the SI to HCCI combustion modes was initiated. At cycle 16 both intake and exhaust valves switched to low stage mode, but the valve timing change was limited to 10 crank degrees per cycle due to the continuing operation of the electric variable valve timing actuating system. Note that10 crank degrees per cycle were for the engine operated at 2000 rpm. The valve speed limitation varies as a function of engine speed. Also at cycle 16, spark was eliminated for the control strategy without hybrid combustion mode and the control parameters were adjusted to make the HCCI combustion possible with minimal IMEP variation. On the other hand, for the hybrid combustion mode transition, spark was kept on in cycles 16, 17 and 18 and advanced. After cycle 19 the spark was cut. At cycle 19, the intake and exhaust valves also reached their target cam phase positions and stopped moving. Throughout the entire mode transition process, fuel mass was adjusted to minimize the IMEP fluctuation. All selected control parameters can be found in Figure 4.13.

In Figure 4.14, some key combustion performance parameters are shown. Engine IMEP is the most important performance parameter for the mode transition since the less IMEP variation is, the less the engine brake torque variation or the smoother the combustion mode transition. For the one step transition, the IMEP drop is significant right after spark ignition was eliminated, see cycles 16 and 17. Note that during mode transition, the in-cylinder gas mixture can’t reach appropriate temperature for the HCCI combustion at IVC with or without hybrid mode of combustions, see T_{IVC} trace in Figure 4.14. If spark were cut at this engine cycle, the SOHCCI timing would be retarded significantly. It can be observed from Figure 4.12 and Figure 4.14. The retarded SOHCCI timing leads to large IMEP reductions, or even misfires under certain extreme conditions. Therefore, the spark assistant HCCI combustion, or the hybrid HCCI combustion, is a necessary tool for smooth mode transition. Based upon Figure 4.12 the hybrid combustion mode exists in cycles 16, 17 and 18 and the IMEP variation is significantly reduced, comparing to the one-step mode transition. Figure 4.15 shows the MFB profiles of the SI-HCCI hybrid combustions during the mode transition and illustrate how the combustion timing changes during the process.

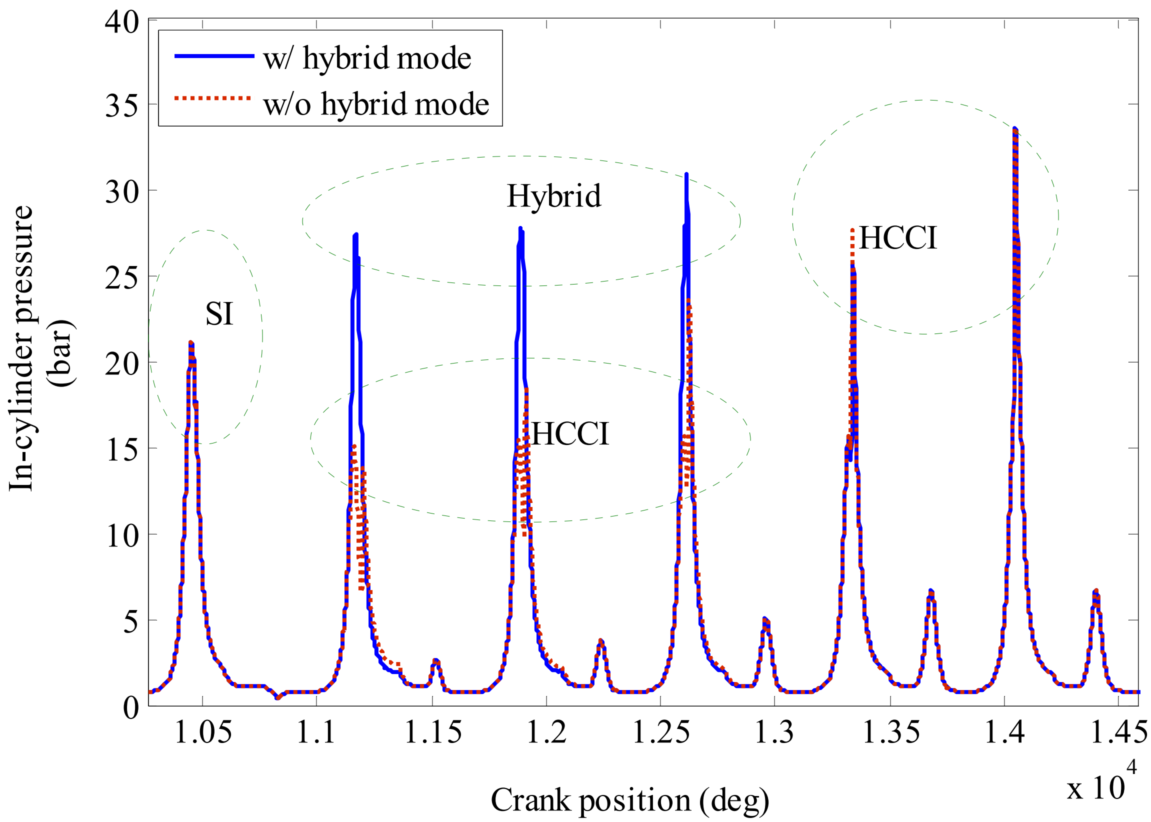

Figure 4.12: In-cylinder pressure traces in SI-HCCI transition

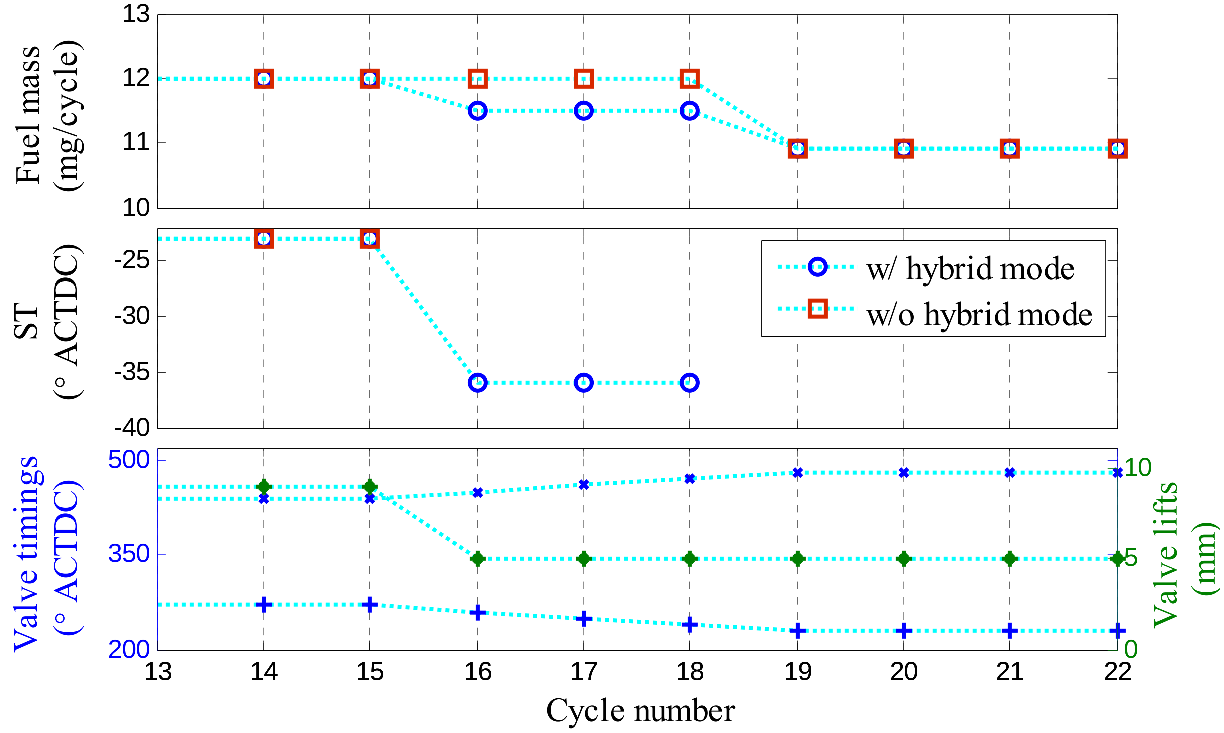

Figure 4.13: Combustion parameter settings in SI-HCCI transition

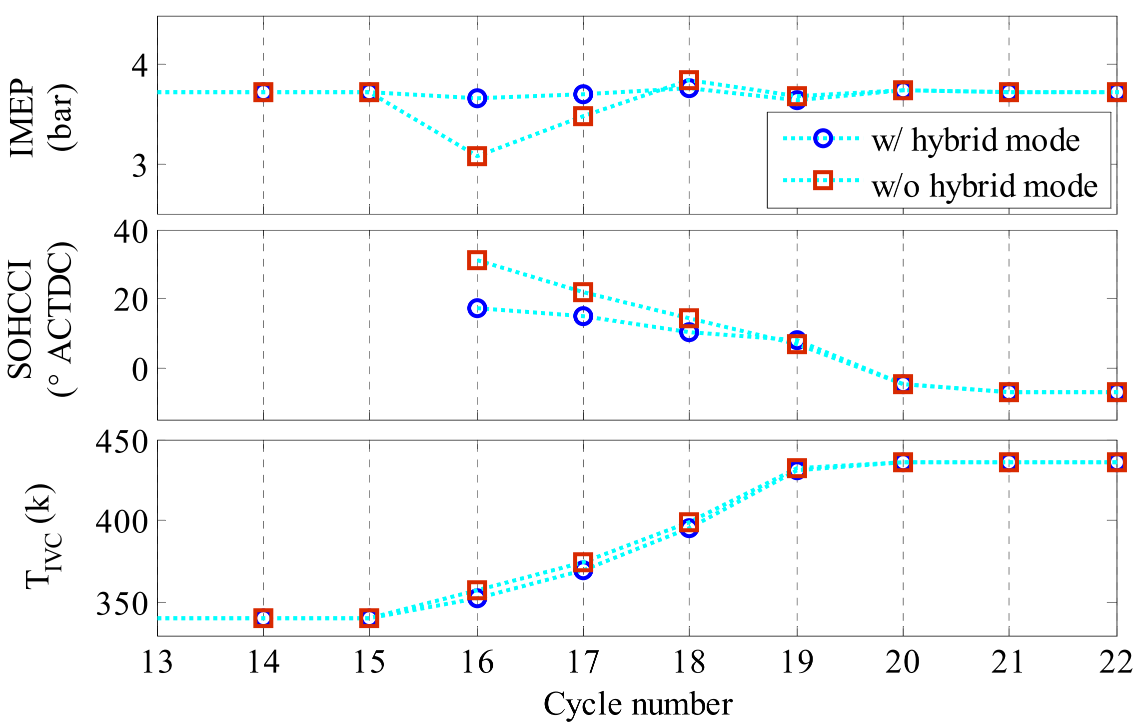

Figure 4.14: Combustion performance in SI-HCCI transition

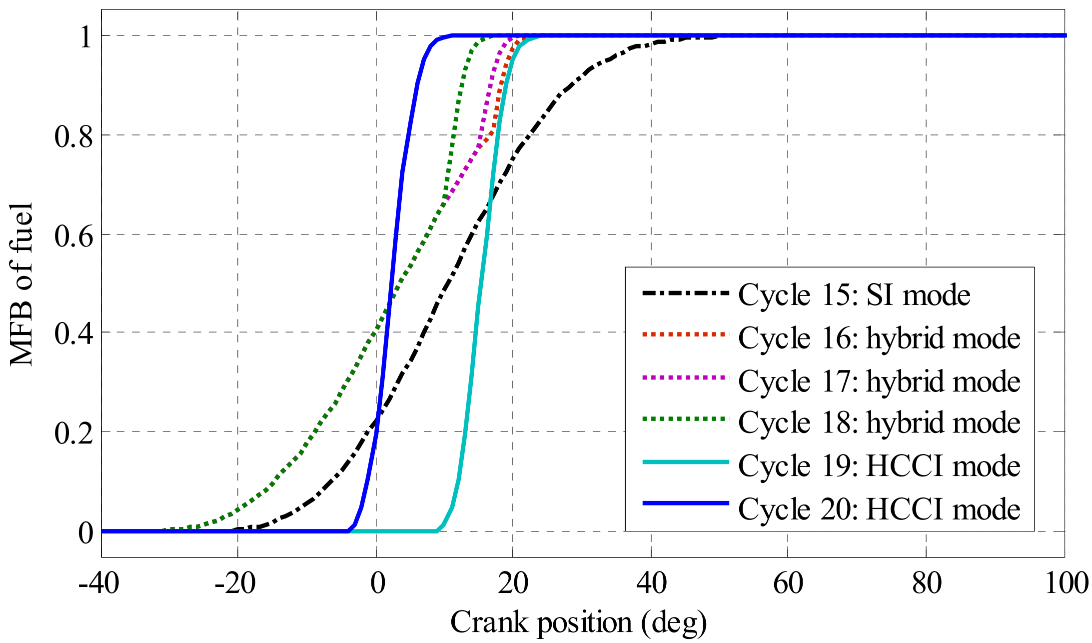

Figure 4.15: MFB profiles in SI-HCCI transition with hybrid mode

4.5 Conclusions

This chapter describes the implementation of the developed engine model into the MSU dSPACE HIL simulation system. HIL simulations were conducted for both steady state and transient engine operations. The following is a list of conclusions:

- The mixed mean value and crank based engine model is feasible for the dSPACE based real-time HIL simulation.
- The dual-stage turbocharger configuration is capable of reducing turbo lag.
- The feedforward fuel control improves the transient performance of the closed loop control of the dual-stage turbocharged engine.
- The SI-HCCI hybrid combustion mode can be realized during the combustion mode transition, and it is capable of reducing the engine torque variations during the mode transition.

CHAPTER 5

SI AND HCCI COMBUSTION MODE TRANSITION CONTROL

5.1 Introduction

In order to take advantage of the HCCI combustion mode, a traditional SI engine needs to operate in both SI and HCCI modes, and the mode transition between the SI and HCCI combustions is necessary. It is fairly challenging to operate the engine in the two distinct combustion modes, and it is more difficult to have smooth combustion mode transition between the two modes due to the distinct engine operational parameters over the two combustion modes and the cycle-to-cycle residual gas dynamics ([86] and [87]). The control problem becomes even more complicated for a multi-cylinder engine studied in this project.

In recent years, more and more attentions have been paid to the mode transition control between the SI and HCCI combustions. In [39] and [40], smooth mode transitions between the SI and HCCI combustions are realized for a single cylinder engine equipped with the camless VVA system. However, high cost and package issues prevent the implementation of the camless VVA system in production engines [88]. In [42] a VVT (variable valve timing) system with dual-stage lifts was used on a multi-cylinder engine for studying the mode transition. Experimental results showed the potential of achieving smooth mode transition by controlling the throttle opening timing and the DI (direct injection) fuel quantity. However, satisfactory mode transition was accomplished due to the lack of the robust mode transition control strategy.

In this chapter a multistep SI to HCCI combustion mode transition control strategy was developed using the HIL simulation environment developed in the last chapters. It takes several engine cycles to complete the combustion mode transition. During the combustion mode transition, a model based linear quadratic (LQ) tracking control ([89] and [90]) of engine MAP was used to maintain the air-to-fuel ratio in the desired range by regulating the engine throttle; the DI fuel quantity of individual cylinder was controlled via iterative learning control ([91] and [92]); and spark ignitions were maintained to enable the SI-HCCI hybrid combustion mode during the mode transition; the other engine parameters, such as the intake/exhaust valve timing and lift, external EGR (exhaust gas recirculation) valve opening are controlled in an open loop. The entire control strategy is also validated in the HIL simulation environment. The simulation results demonstrated the effectiveness of the proposed control strategy under both constant and transient engine operating conditions.

This chapter is organized as follows. Section 5.2 discusses the control problem of the combustion mode transition. In Section 5.3, the development of the multistep combustion mode transition strategy is described, along with the control architecture. The details of the DI fuel quantity control are given in Section 5.4, and the following section introduces the air-to-fuel ratio control. In section 5.6, HIL engine simulation results are presented, compared, and discussed for the validation of the proposed control strategies. Conclusions are finally drawn in Section 5.7.

5.2 The Control Problem Formulation

This section discusses the control target of the mode transition between the SI and HCCI combustion modes. The challenges of achieving the control target were found during the study of the simple one-step mode transition strategy. Based on the finding, a more complex control strategy is developed in the next section.

5.2.1 Control target of the combustion mode transition

In this chapter, the combustion mode transition is studied for the engine operated at 2000 rpm with 4.5 bar IMEP. Table 5.1 lists the engine parameters associated with the SI and HCCI combustions. These parameters are optimized for the steady state engine performance with the best fuel economy that satisfies the engine knock limit. That is, the maximum pressure rise rate ($dP/d\theta$) is less than or equal to 3 bar per crank degree. It can be seen in Table 5.1 that the optimized engine control parameters are quite different between the SI and HCCI combustion modes. Due to actuator dynamics, some of these parameters can be adjusted within one engine cycle, such as θ_{ST}, F_{DI} and Π_{lift}; and some of them cannot.

Table 5.1: Engine control parameters for SI and HCCI combustion modes

Parameter \ Mode	SI	HCCI
θ_{ST} (deg ACTDC)	-36	none
ϕ_{EGR} (%)	3	26
I_{ETC} (A)	0.84	5
F_{DI} (ms/cycle)	2.06	1.6
θ_{INTM} (deg AGTDC)	70	95
θ_{EXTM} (deg BGTDC)	100	132
Π_{lift} (mm)	9	5

The combustion characteristics are also quite different between these two combustion modes as illustrated in Figure 5.1. For example, the HCCI combustion has higher peak in-cylinder pressure comparing with that of the SI combustion, due to the fast fuel burn rate. Most likely, it also has a recompression phase due to negative valve overlap (NVO), while the SI combustion does not. The goal of the combustion mode transition is to transfer the combustion mode without detectable engine torque fluctuation by regulating the engine control parameters, or in other words to maintain the engine IMEP during the combustion mode transition.

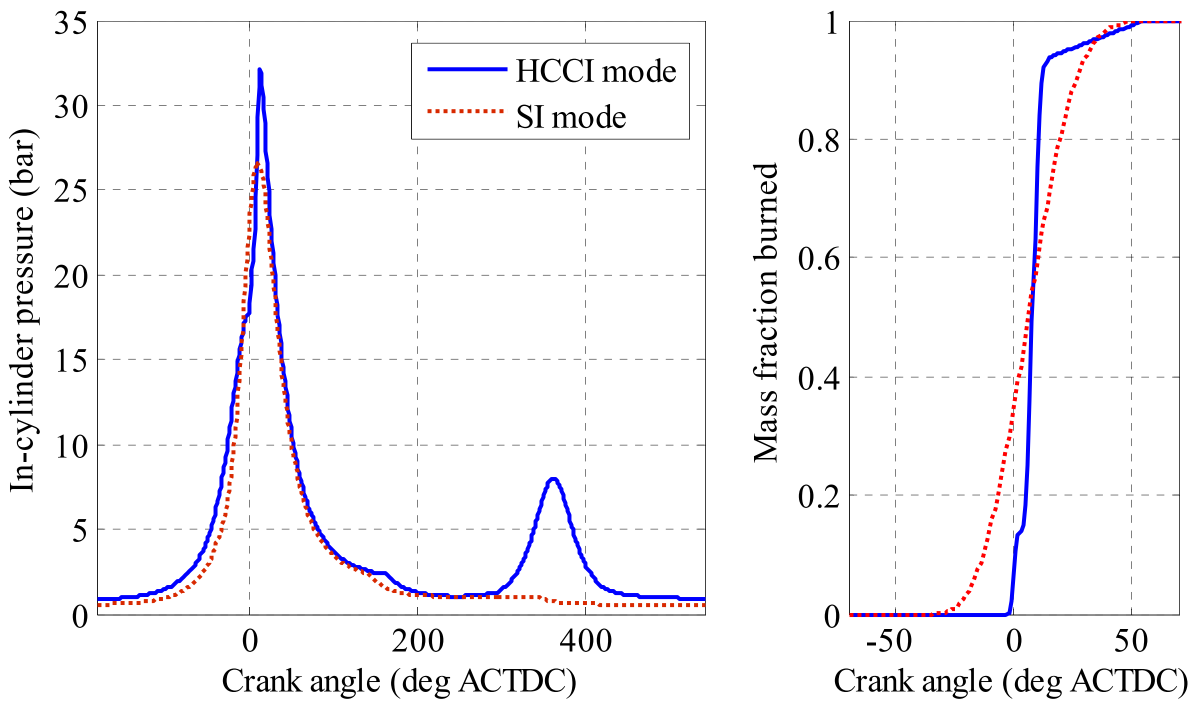

Figure 5.1: Steady state combustion characteristics of SI and HCCI modes

5.2.2 Existing one-step combustion mode transition

In order to investigate the control problem of the combustion mode transition, the control strategies development starts with one-step transition strategy. That is to directly change the control references of all engine control parameters from the SI mode to the HCCI mode, in one engine cycle. HIL simulations of the one-step transition strategy were conducted and key engine variables are plotted in Figure 5.2 and Figure 5.3.

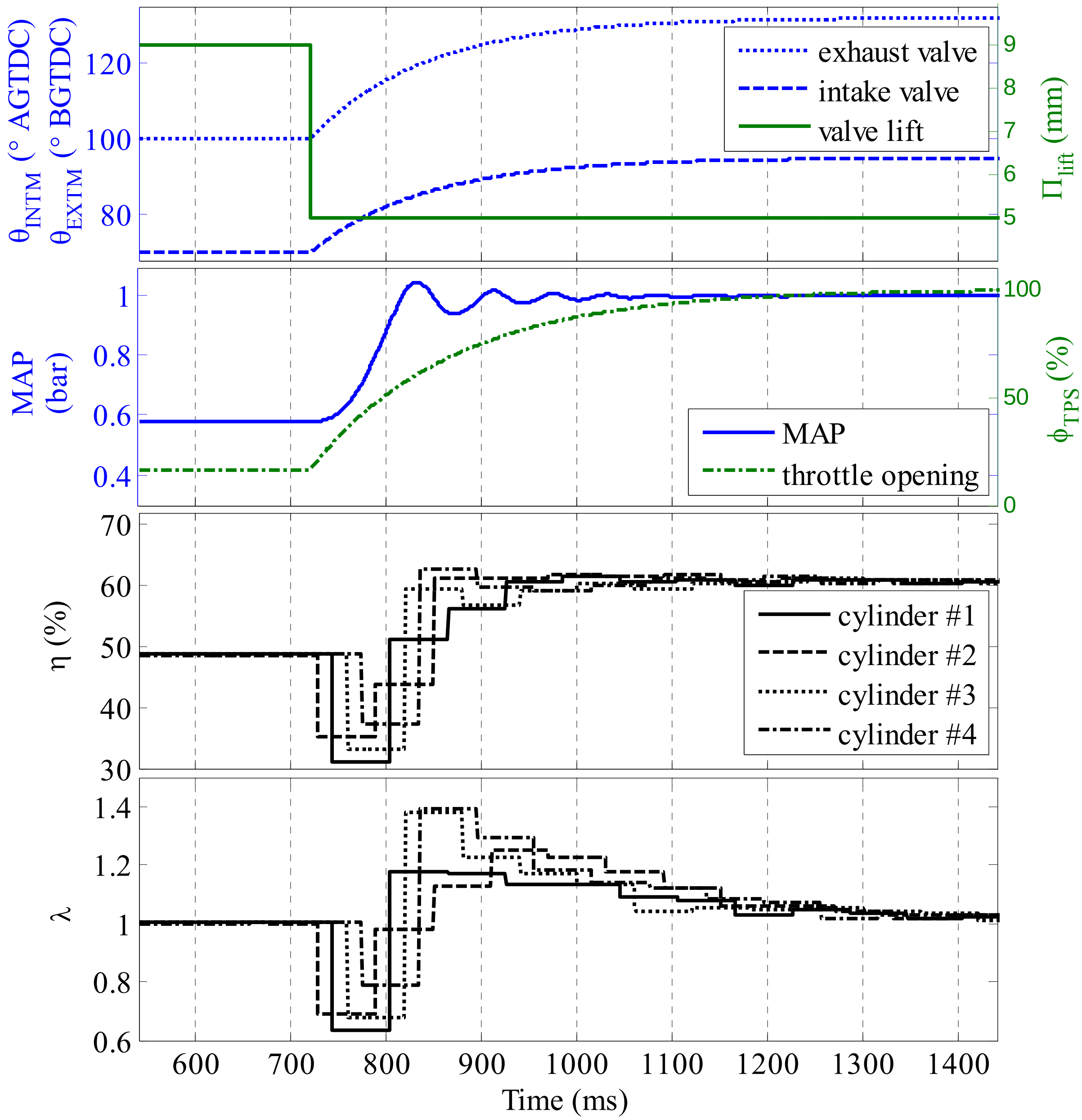

Figure 5.2: Engine responses of one-step combustion mode transition strategy

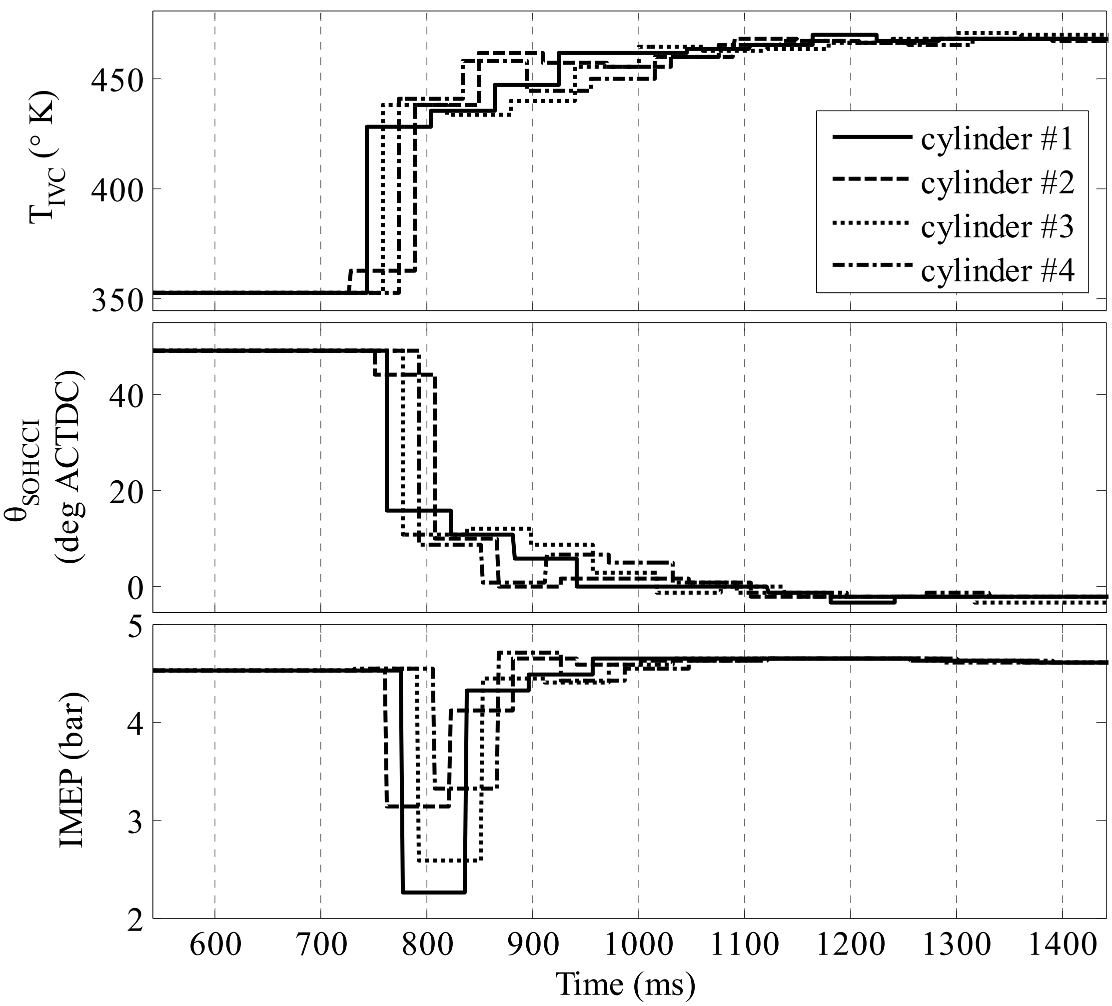

Figure 5.3: Combustion performance of one-step combustion mode transition strategy

By analyzing the simulation results in Figure 5.2 and Figure 5.3, the control problems of the combustion mode transition are summarized as following.

- Extreme rich conditions of gas-fuel mixture (see the response of λ) are found for all cylinders at the first engine cycle after the valve lift switch of Π_{lift}. This indicates the lack of fresh air charge in the engine cylinders.
- Fairly lean conditions of the gas-fuel mixture are observed at the cycles following the first

one after the switch of Π_{lift} due to the fast increment of the engine MAP.

- The thermodynamic condition (T_{IVC}) of the first few engine cycles after the combustion mode switch is below the required condition for HCCI combustions due to the response delay of the valvetrain actuators (see θ_{INTM} and θ_{EXTM}).
- The combustion timings (θ_{SOHCCI}) of the first few engine cycles after the combustion mode switch are retarded corresponding to the thermodynamic condition (T_{IVC}). It could lead to unstable HCCI combustions, and even misfire in the worst case.
- Cylinder-to-cylinder variations were observed at combustion related variables during the mode transition since the adjustments of Π_{lift}, θ_{INTM} and θ_{EXTM} affect all engine cylinders globally while each cylinder is undergoing different stroke.
- Slight oscillations were found to combine with the first order response delays of T_{IVC} and θ_{SOHCCI}. This is a strong indication of the cycle-to-cycle residual gas dynamics of the HCCI combustions.

Engine IMEP cannot be maintained as illustrated in Figure 5.3. Thereby it is very difficult to achieve smooth combustion mode transition in one step, due to all the issues described above. To solve the problems and reduce the fluctuation of the engine IMEP response during the mode transition, a multistep mode transition scheme with some control strategies was proposed. The corresponding control architecture will be presented in the next section.

5.3 Control Architecture of Multistep Combustion Mode Transition

The multistep combustion mode transition strategy was proposed by inserting a few SI-HCCI hybrid combustion cycles between the SI and HCCI combustions. As illustrated in Figure 5.4, five engine cycles are reserved for bridging the SI and HCCI combustions.

During the transitional cycles some engine parameters are adjusted in an open loop according to the schedule shown in Figure 5.4. At the end of cycle 2, the intake/exhaust valve lift Π_{lift} switches from high lift to low, and the control references of ϕ_{EGR}, θ_{INTM} and θ_{EXTM} are set to those of the steady state HCCI combustion mode as listed in Table 5.1. Cycles 1 and 2 are used for engine throttle control. They provide enough time for the engine MAP to be adjusted due to the impacts of Π_{lift} switching from high to low. Spark timing θ_{ST} of each cylinder was kept constantly during the transitional cycles and was eliminated at the end of cycle 5.

Throughout the transitional cycles, the engine control parameters I_{ETC} and F_{DI} were regulated in time-based control with 1 ms sampling rate and cycle-based control logics, respectively. The corresponding control algorithm will be described in the next two sections.

Under the regulations of the engine parameters, the combustion characteristics during the transitional engine cycles are different from those of the typical SI and HCCI combustion modes. The combustions at cycles 1 and 2 are still in SI combustion mode, but the air-to-fuel ratio might not be stoichiometric and most likely is lean due to the throttle (I_{ETC}) control. During cycles 3 to 5, engine charge temperature T_{IVC} is higher than that of the SI mode and lower than the desired temperature of the HCCI mode. Under such condition, during cycles 3 to 5 the engine is operated in the SI-HCCI hybrid combustion mode with the help of the maintained spark ignitions.

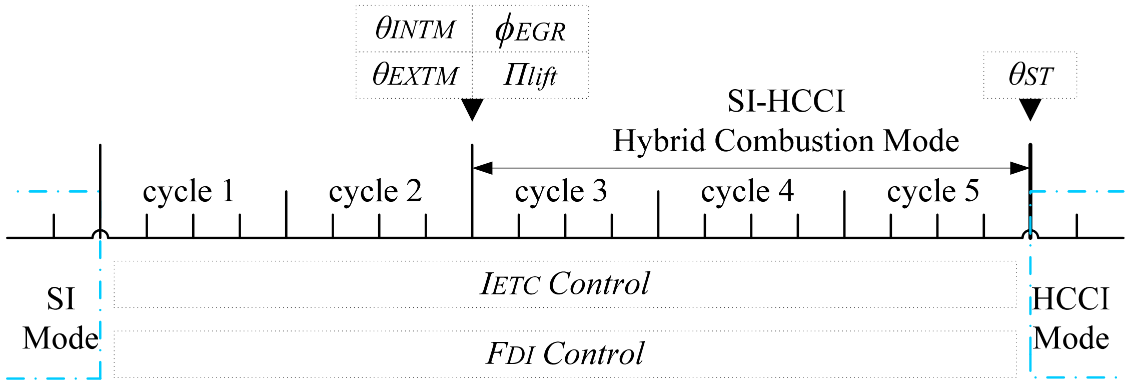

Figure 5.4: SI to HCCI combustion mode transition control events and schedules

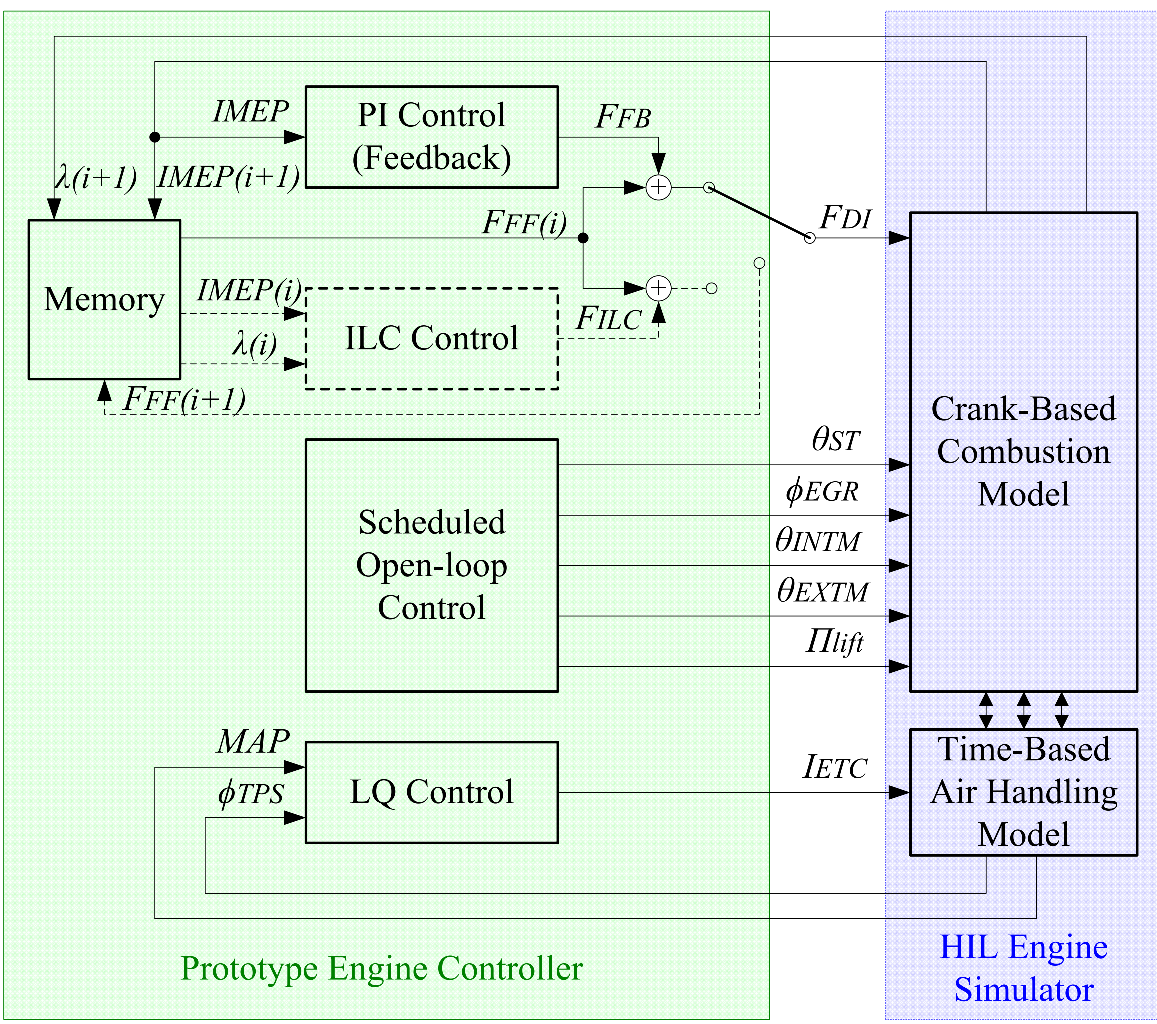

Figure 5.5: SI to HCCI combustion mode transition control diagram

Figure 5.5 shows the control diagram of the multistep combustion mode transition controller and its interface with the HIL engine simulator. The multistep combustion mode transition is activated as engine IMEP switches from above $IMEP_{ref}$ ($IMEP_{ref}$=4.5 bar in the case) to below $IMEP_{ref}$. Once the transition is initiated, the engine parameters are controlled in different ways. I_{ETC} is controlled by the LQ tracking control; F_{DI} is controlled in different modes, the learning and transient modes, according to the different engine operating conditions; all other parameters are controlled by the pre-scheduled open loop control.

In Figure 5.5, the learning mode of the F_{DI} control is represented by the dashed lines and the solid lines represent the transient mode. For both control modes, F_{DI} is adjusted every engine cycle for each cylinder. The transient mode is used for engine operations with fast load variations, such as the engine tip-out and tip-in operations. In this mode, the learned feedforward term F_{FF} reduces the cylinder-to-cylinder IMEP variance, and the feedback term F_{FB} helps with the drive load tracking. To run the learning mode, the engine load is required to be relatively stable and fairly close to the specified reference. Accordingly, this mode can only be operated during the vehicle cruise operational condition or during the engine calibration process. Note that in the learning mode, F_{DI} is not only used as control output but also stored to the nonvolatile memory of the controller as the feedforward term F_{FF} for next learning iteration or the transient mode control.

5.4 IMEP Regulation for DI Fuel Quantity Control

In this section the DI fuel quantity is used as a direct control arm to regulate the IMEP of each engine cylinder.

5.4.1 Sensitivity analysis of engine IMEP

As discussed in Section 5.2.2, the engine control variables T_{IVC} and θ_{SOHCCI} have response delays due to actuator dynamics, and after the engine reference parameters Π_{lift}, θ_{INTM} and θ_{EXTM} are adjusted at the end of cycle 2. It takes a few engine cycles for them to reach the desired levels corresponding to the HCCI combustion mode, see Figure 5.3. Under such transient conditions, if the engine were forced to switch to the HCCI combustion mode the engine IMEP could not be maintained with cycle-by-cycle fuel control F_{DI}. Also the increased cooling effect caused by the increment of F_{DI} reduces the charge temperature and leads to degraded HCCI combustions.

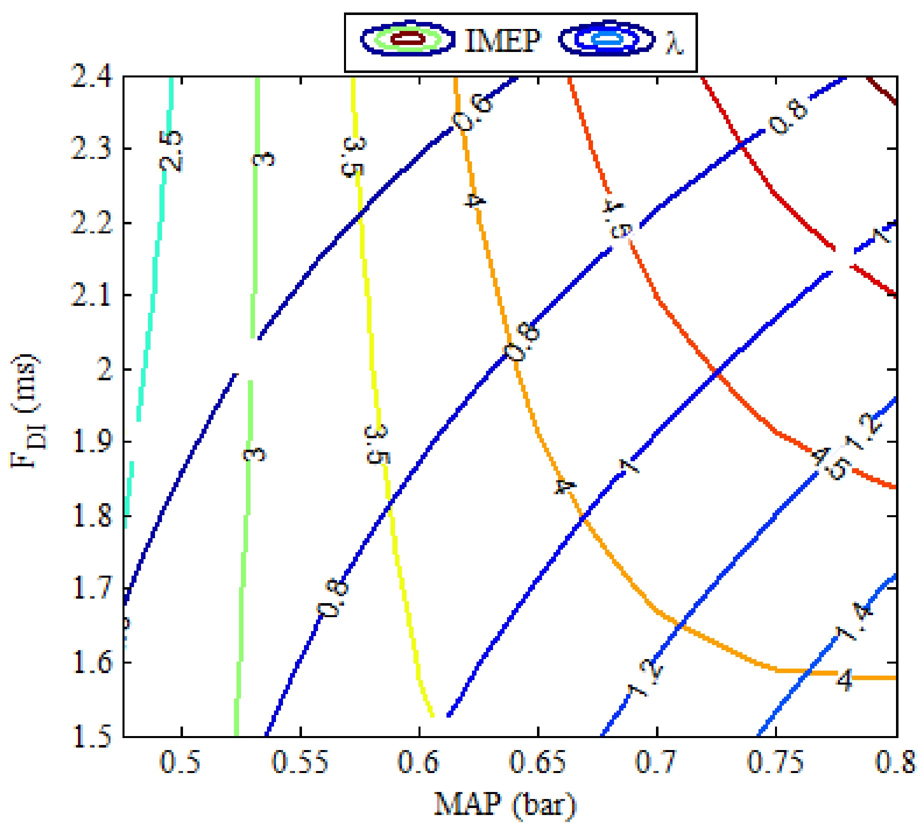

Figure 5.6: IMEP sensitivity with F_{DI} input for the SI-HCCI hybrid combustion mode

To solve this issue, the engine sparks are maintained during cycles 3 to 5, and the engine operates in the SI-HCCI hybrid combustion mode during these cycles as shown in Figure 5.4. For the hybrid combustion mode the engine IMEP is highly correlated to F_{DI} with the lean gas-fuel mixture, as illustrated in Figure 5.6. Accordingly it is possible to control the engine IMEP of each cylinder by regulating F_{DI} of the corresponding cylinder.

5.4.2 DI fuel quantity control for learning mode

When the DI fuel control F_{DI} switches to the learning mode, F_{DI} is regulated through the following equation,

$$\begin{aligned} F_{DI}(i+1) &= F_{FF}(i) + F_{ILC}(i) \\ &= F_{FF}(i) + K_{ILC}\left[IMEP_{ref} - IMEP(i) \right] \end{aligned} \tag{5.1}$$

where the iterative learning control parameter F_{ILC} is calculated by a P-type (proportional) self learning algorithm as described in [93] and [94], and the iterative learning gain K_{ILC} is derived from the IMEP sensitivity (shown in Figure 5.6) satisfying

$$K_{ILC} < \frac{\Delta F_{DI}}{\Delta IMEP} \tag{5.2}$$

Note that in this case the stability of the iterative learning is guaranteed. The feedforward term F_{FF} is the learned control variable from the last step that is stored in the memory of the controller. After each learning F_{FF} is updated as

$$F_{FF}(i+1) = F_{DI}(i+1) \tag{5.3}$$

5.4.3 DI fuel quantity control for transient mode

When F_{DI} control switches to the transient mode, the iterative learning control is deactivated and the feedback control is activated, as illustrated in Figure 5.5; F_{DI} is controlled by the combination of the feedforward and feedback controls. It is represented by

$$F_{DI} = F_{FF} + F_{FB} \tag{5.4}$$

where the feedforward term F_{FF} is the same learned control variable as in (5.1); The feedback term F_{FB} is the output of a PI (proportional and integral) controller.

5.5 Air-to-Fuel Ratio Control

In the last section, the F_{DI} controller is used to control the individual cylinder IMEP. To maintain the controllability of the fuel control, lean gas-fuel mixture is required during the mode transition. However, the combustion could become unstable if the mixture becomes extreme lean since the engine spark might not be able to ignite the extremely lean gas mixture during the transitional cycles. For this study the desired normalize air-to-fuel ratio is set between λ_{min} (0.97) and λ_{max} (1.3). In the earlier work presented in [25], a throttle pre-opening approach was proposed to prevent rich combustions at cycle 3, but it leads to very lean combustions at the following engine cycles. In this section, an LQ optimal control strategy is developed to achieve the air-to-fuel ratio target.

5.5.1 Tracking reference of engine MAP

As discussed above, the normalized air-to-fuel ratio needs to be maintained within the optimal range ($\lambda_{min} < \lambda < \lambda_{max}$) during the SI to HCCI combustion mode transition. This control target is difficult to be achieved through the air-to-fuel ratio feedback control due to transportation delay and short mode transition period. It is proposed to use the LQ tracking approach to regulate the air-to-fuel mixture to the desired level. To implement this control strategy, the optimal operational range of λ is translated into the operational range of MAP shown in Figure 5.7, where the upper boundary is corresponding to λ_{max} and lower boundary is corresponding to λ_{min}. an engine MAP tracking reference shown in Figure 5.7 was generated for the engine Map to stay within the target range. The reference signal is represented by

$$z(k) = \begin{cases} Z_{SI} & \text{if} \quad k_S < k \le k_1 \\ Z_{SI} + (Z - Z_{SI})\dfrac{k - k_1}{k_2 - k_1} & \text{if} \quad k_1 < k \le k_2 \\ Z + (Z_{HCCI} - Z)\dfrac{k - k_1}{k_2 - k_1} & \text{if} \quad k_2 < k \le k_E \end{cases} \tag{5.5}$$

where k is the sampling index; k_S and k_E indicate the beginning and ending indices of the mode transition and they were set to 600 and 900, respectively as shown in Figure 5.7; k_1 and k_2 are switch timings and they equal 670 and 720, respectively.

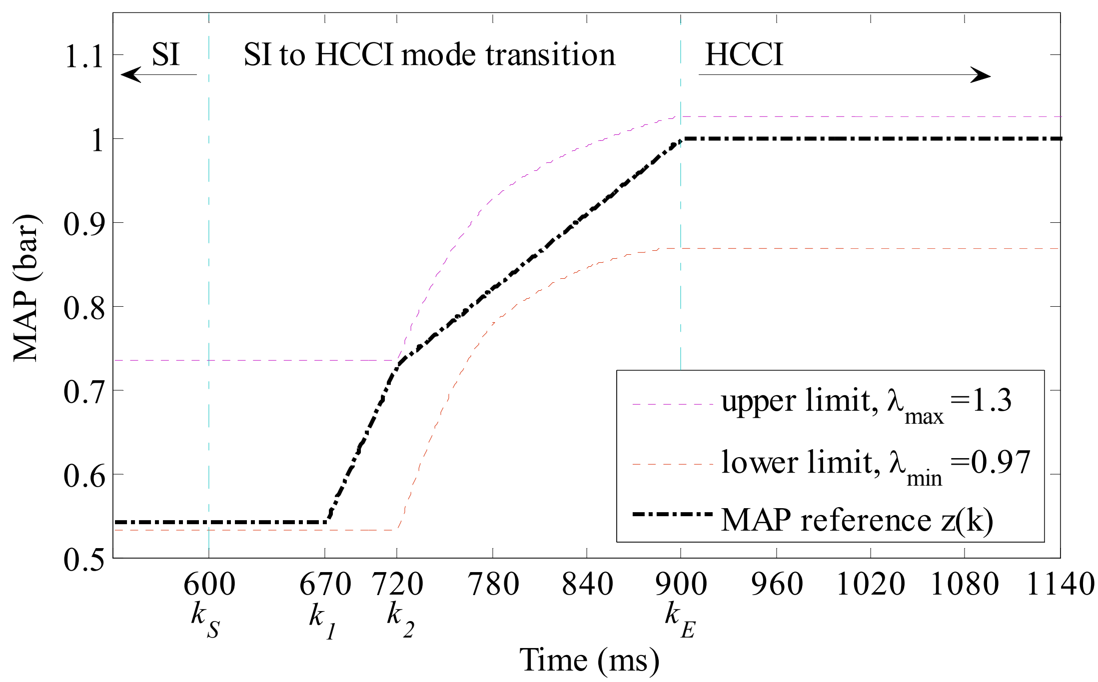

Figure 5.7: The target MAP operational range and MAP tracking reference

5.5.2 Control oriented MAP model

To develop the proposed LQ tracking control strategy, a control oriented engine MAP model is required to represent the relationship between the control input (I_{ETC}) and the system output (MAP). The simplified dynamics is represented by a second order dynamics due to the gas filling dynamics (first order) of the engine intake manifold and the first order response delay of the engine throttle, assuming that the rotational momentum of the throttle plate is small enough to be ignored. The governing equation of gas filling dynamics is represented by

$$\frac{dMAP}{dt} = -\eta \frac{V_d N_e}{120 V_m} MAP + \varphi \frac{RT_{amb} C_D \pi r^2 P_{amb}}{V_m \sqrt{2RT_{amb}}} \phi_{TPS} \tag{5.6}$$

The dynamics of the throttle response is approximated by

$$\frac{d\phi_{TPS}}{dt} = -\frac{k_{ETC}}{b_{ETC}} \phi_{TPS} + \frac{c_{ETC}}{b_{ETC}} I_{ETC} \tag{5.7}$$

Equations (5.6) and (5.7) can be combined, discretized and represented by the following discrete state space model

$$\begin{aligned} x(k+1) &= Ax(k) + Bu(k) \\ y(k) &= Cx(k) + Du(k) \end{aligned} \tag{5.8}$$

where

$$u = I_{ETC}; \quad x = \begin{bmatrix} x_1 \\ x_2 \end{bmatrix} = \begin{bmatrix} MAP \\ \phi_{TPS} \end{bmatrix}; \quad y = MAP \tag{5.9}$$

are the system input, state and output, respectively. The system matrices are

$$\begin{aligned} A &= \begin{bmatrix} 1 - \dfrac{\eta(k) V_d N_e}{120 V_m} \Delta T & \dfrac{\varphi(k) RT_{amb} C_D \pi r^2 P_{amb}}{V_m \sqrt{2RT_{amb}}} \Delta T \\ 0 & 1 - \dfrac{k_{ETC}}{b_{ETC}} \Delta T \end{bmatrix}; \quad B = \begin{bmatrix} 0 \\ \dfrac{k_{ETC}}{b_{ETC}} \Delta T \end{bmatrix} \\ C &= \begin{bmatrix} 1 & 0 \end{bmatrix}; \quad D = 0 \end{aligned} \tag{5.10}$$

where ΔT is the sample period. State space model (5.8) is linear time-variant since the volumetric efficiency η and multiplier φ in equations (5.6) and (5.10) are functions of the tracking reference $z(k)$. Moreover, the sampling time ΔT in (5.10) equals 1 millisecond, and sample time index k is the same as that from equation (5.5).

5.5.3 LQ optimal controller synthesis

Based on the control oriented engine MAP model, a finite horizon LQ optimal tracking controller was designed to follow the reference $z(k)$. More specifically, the control objective is to minimize the tracking error $e(k)$ defined in (5.11) with the feasible control effort I_{ETC} or the feasible throttle control current. The tracking error $e(k)$ is defined as

$$e(k) = y(k) - z(k) = Cx(k) - z(k) \tag{5.11}$$

and the restriction on I_{ETC} is -5A < I_{ETC} < 5A. To satisfy the objective, the cost function of the LQ optimal tracking control is defined as

$$\begin{aligned} J \; = \; & \frac{1}{2}[Cx(k_f) - z(k_f)]^T F[Cx(k_f) - z(k_f)] \\ & + \frac{1}{2}\sum_{k=k_0}^{k=k_f-1} \left\{[Cx(k) - z(k)]^T Q[Cx(k) - z(k)] + u^T(k)Ru(k)\right\} \end{aligned} \tag{5.12}$$

where F and Q are positive semi-definite and R is positive definite. For the control design, F and Q were selected as constant matrices and R is a function of sample step k (see Figure 5.10) used to tradeoff between the tracking performance and the control effort.

$$F = \begin{bmatrix} 1 & 0 \\ 0 & 0 \end{bmatrix} 10^{-8}, \quad Q = \begin{bmatrix} 4 & 0 \\ 0 & 0 \end{bmatrix} 10^{-7}, \quad R = R(k) \tag{5.13}$$

Based on the cost function the corresponding Hamiltonian is as follows

$$H = \frac{1}{2}[Cx(k) - z(k)]^T Q[Cx(k) - z(k)] + \frac{1}{2}u^T(k)Ru(k) + p^T(k+1)\left[Ax(k) + Bu(k)\right] \tag{5.14}$$

According to [89], the required conditions for the extremum in terms of the Hamiltonian are represented as

$$\frac{\partial H}{\partial p^*(k+1)} = x^*(k+1) \quad \Rightarrow \quad x^*(k+1) = Ax^*(k) + Bu^*(k) \tag{5.15}$$

$$\frac{\partial H}{\partial x^*(k)} = p^*(k) \quad \Rightarrow \quad p^*(k) = A^T p^*(k+1) + C^T QCx^*(k) - C^T Qz(k) \tag{5.16}$$

$$\frac{\partial H}{\partial u^*(k)} = 0 \quad \Rightarrow \quad 0 = B^T p^*(k+1) + Ru^*(k) \tag{5.17}$$

Note that the superscript "*" denotes the optimal trajectories of the corresponding vectors. The augmented system of (5.15) and (5.16) becomes

$$\begin{bmatrix} x^*(k+1) \\ p^*(k) \end{bmatrix} = \begin{bmatrix} A & -BR^{-1}B^T \\ C^T QC & A' \end{bmatrix} \begin{bmatrix} x^*(k) \\ p^*(k+1) \end{bmatrix} + \begin{bmatrix} 0 \\ -C^T Q \end{bmatrix} z(k) \tag{5.18}$$

Based upon (5.17) the optimal control is in the form of

$$u^*(k) = -R^{-1}B^T \left[P(k)x^*(k) - g(k) \right] \tag{5.19}$$

Note that matrix $P(k)$ can be computed by solving the difference Riccati equation backwards

$$P(k) = A^T P(k+1)[I + EP(k+1)]^{-1} A + C^T QC \tag{5.20}$$

with the terminal condition

$$P(k_f) = C^T FC \tag{5.21}$$

and vector $g(k)$ can be computed by solving the vector difference equation

$$g(k) = A^T \left\{ I - [P^{-1}(k+1) + E]^{-1} E \right\} g(k+1) + C^T Qz(k) \tag{5.22}$$

with the terminal condition

$$g(k_f) = C^T Fz(k_f) \tag{5.23}$$

The optimal control in (5.19) can be written into the following form

$$u^*(k) = -L_{FB}(k)x^*(k) + L_{FF}(k)g(k+1) \tag{5.24}$$

where the feedforward gain L_{FF} is computed by

$$L_{FF}(k) = [R + B^T P(k+1)B]^{-1} B^T \tag{5.25}$$

and the feedback gain L_{FB} is computed by

$$L_{FB}(k) = [R + B^T P(k+1)B]^{-1} B^T P(k+1)A \tag{5.26}$$

Note that equation (5.24) is the offline representation of the LQ optimal tracking control since the state x^* used in the feedback control is computed exactly from the closed-loop system (5.8) as

$$x^*(k+1) = [A - BL_{FB}(k)]x^*(k) + BL_{FF}(k)g(k+1) \tag{5.27}$$

However, when the control is implemented in the HIL simulation environment or the actual engine control system, the feedback signals are replaced by the physical signals measured by the on-board engine sensors. In these cases the LQ controller is represented by the online form as

$$u(k) = -L_{FB}(k)x(k) + L_{FF}(k)g(k+1) \tag{5.28}$$

where x represents the sampled states. Note that both of the states, MAP and ϕ_{TPS} can be measured in the HIL simulator or in the engine system.

5.6 HIL Simulation Results and Analysis

The multistep combustion mode transition control strategy is composed of the DI fuel quantity control and LQ optimal MAP tracking control with the SI-HCCI hybrid combustions during the mode transition. In this section, HIL simulation results are presented.

5.6.1 SI-HCCI hybrid combustion mode

As mentioned in Section 5.3, the engine is operated in the SI-HCCI hybrid combustion mode at cycles 3 to 5 (see Figure 5.4) in the multistep mode transition strategy. To disclose the significance of using this hybrid combustion mode, the key engine variables, such as T_{IVC}, x_{HCCI}, and IMEP, are analyzed and plotted in Figure 5.8, for the cases with and without the SI-HCCI hybrid combustion mode.

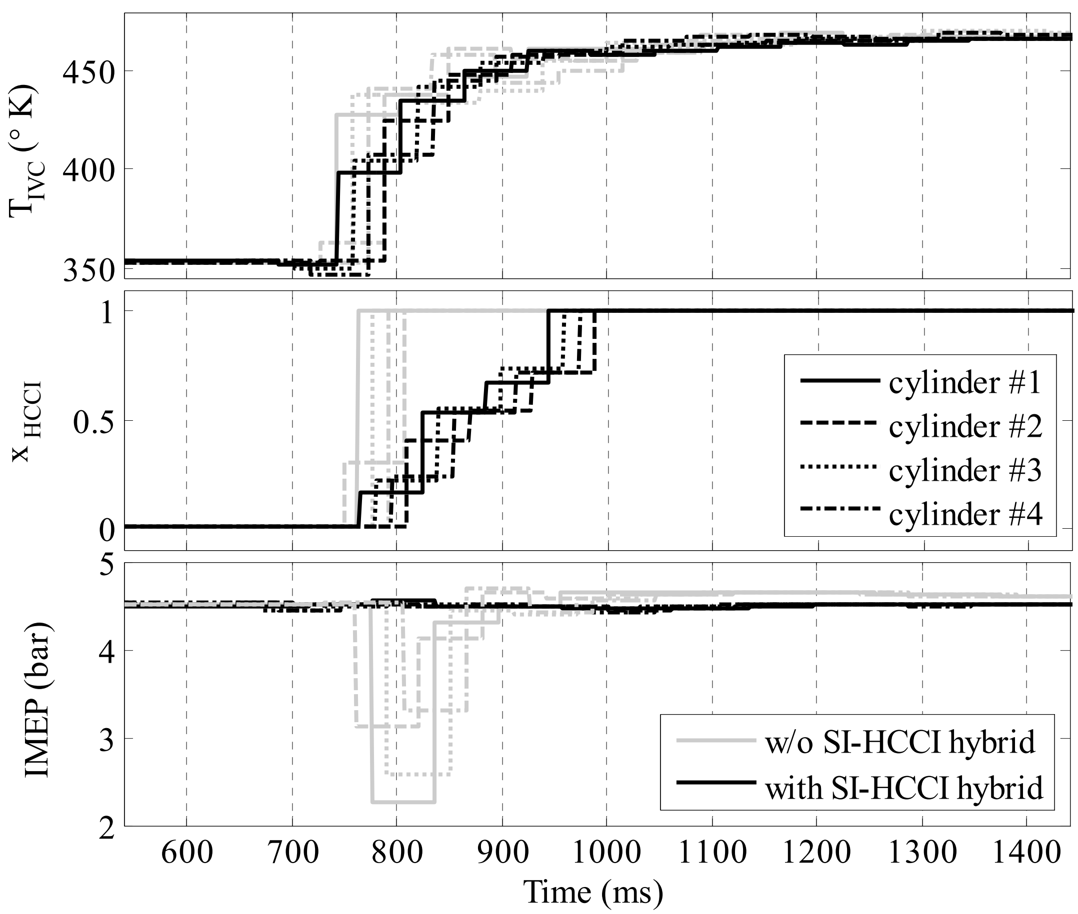

Figure 5.8: Combustion performances with and without SI-HCCI hybrid combustions

As shown in Figure 5.8, temperature at intake valve closing T_{IVC} has response delay with or without the hybrid combustion mode due to the dynamics of the valvetrain system and the NVO operation. Under such thermodynamic condition, if the engine was forced into the HCCI combustion mode, start of combustion timing would be greatly retarded, causing large IMEP fluctuations. The large fluctuation of IMEP cannot be improved through combustion control due to the lack of available control variables in HCCI mode as discussed in Section 5.4.1. However by using the hybrid combustion mode, percentage of HCCI combustion x_{HCCI} is gradually increased as T_{IVC} approaches the desired temperature. Also note that due to the LQ optimal tracking of the desired air-to-fuel ratio, the engine IMEP can be regulated by controlling F_{DI}. As a result, smooth IMEP can be achieved during the mode transition. Note that for the simulation results in Figure 5.8, the proposed air-to-fuel ratio and DI fuel quantity controls are used during the mode transition with the hybrid combustions.

Therefore, using the SI-HCCI hybrid combustions during the mode transition is a key control technique for the smooth combustion mode transition.

5.6.2 Air-to-fuel ratio control

The developed LQ optimal MAP tracking control was implemented in the prototype engine controller and validated through the HIL engine simulations. The simulated control input I_{ETC}, the system states MAP and ϕ_{TPS}, and λ are plotted in Figure 5.9. For comparison purpose, the simulated responses of these variables with open loop control are also shown in Figure 5.9, in which I_{ETC} is set to the target level before the adjustment of Π_{lift} (happens at 720 ms), as a result, the engine throttle is gradually opened to the wide open throttle (WOT) position and the MAP is increased before the valve lift switch. The increased MAP ensures enough fresh charge to each cylinder when the valve lift switches the low position. However the step I_{ETC} control leads to a rapid increment of the engine MAP or excessive fresh air charge, leading to extreme air-to-fuel ratio λ in the following engine cycles.

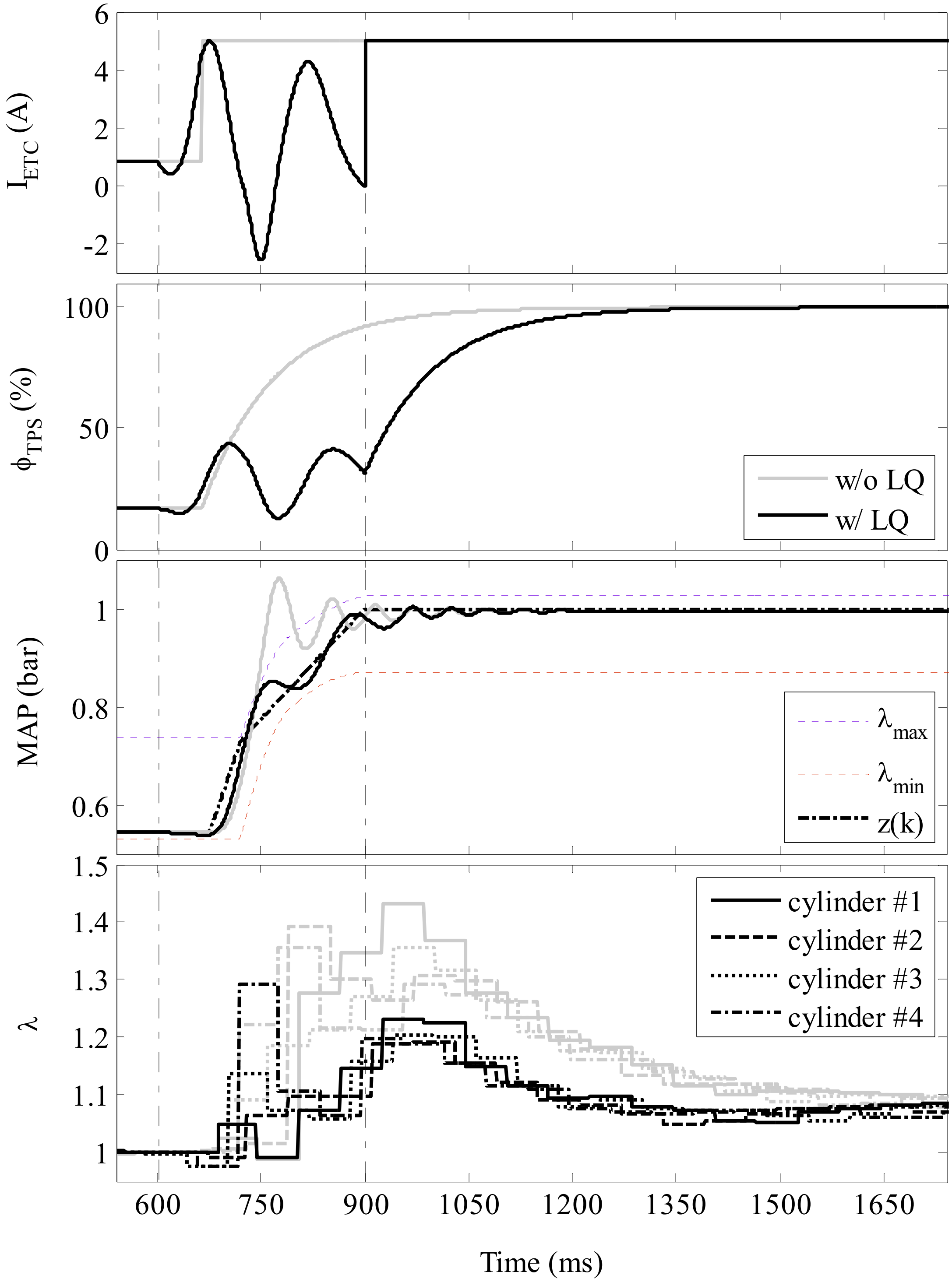

Figure 5.9: Engine performances with and without MAP tracking control

Using the proposed LQ MAP tracking control strategy, throttle current I_{ETC} is regulated in a non-monotonic increasing pattern. Note that to maintain I_{ETC} in the feasible range (-5A < I_{ETC} < 5A) the weighting matrix R in the cost function (5.12) is adjusted as illustrated in Figure 5.10. The same pattern can also be found for ϕ_{TPS} with a small phase lag. As a result, the engine MAP tracks the reference trace $z(k)$ after the intake valve lift Π_{lift} switches to the low lift, and λ of each cylinder is successfully maintained within the desired range. Therefore, with the help of the LQ optimal control, the in-cylinder air-to-fuel ratio is maintained within the desired range, leading to stable combustions.

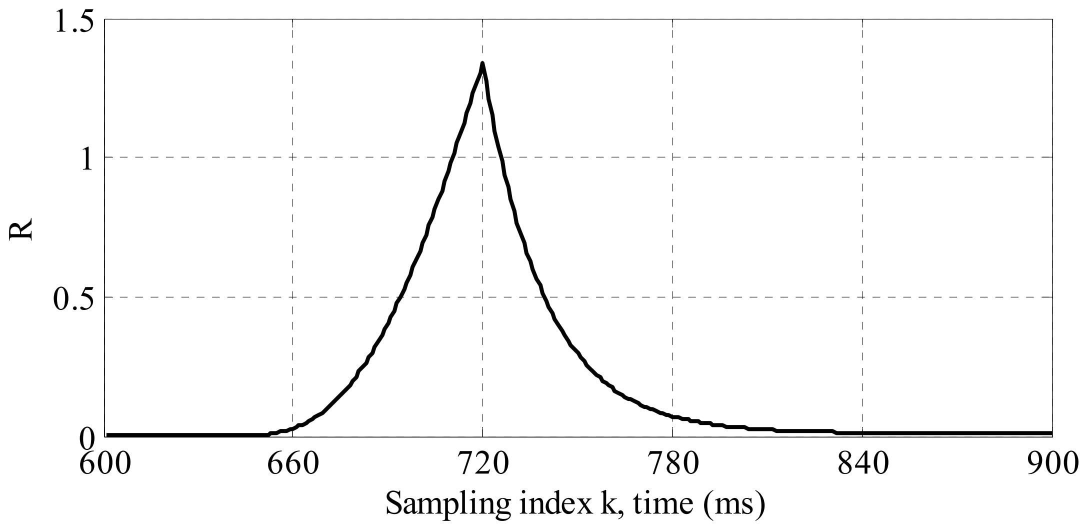

Figure 5.10: Adjustment of weighting matrix R in cost function (5.12)

Slight oscillations in the MAP responses are found with both control approaches, which are due to the flow dynamics of the engine air-handling system. It is almost impossible to eliminate them due to the slow throttle actuator dynamics. However, the MAP oscillation associated with the LQ optimal control is within the desired MAP range.

5.6.3 DI fuel quantity control with iterative learning mode

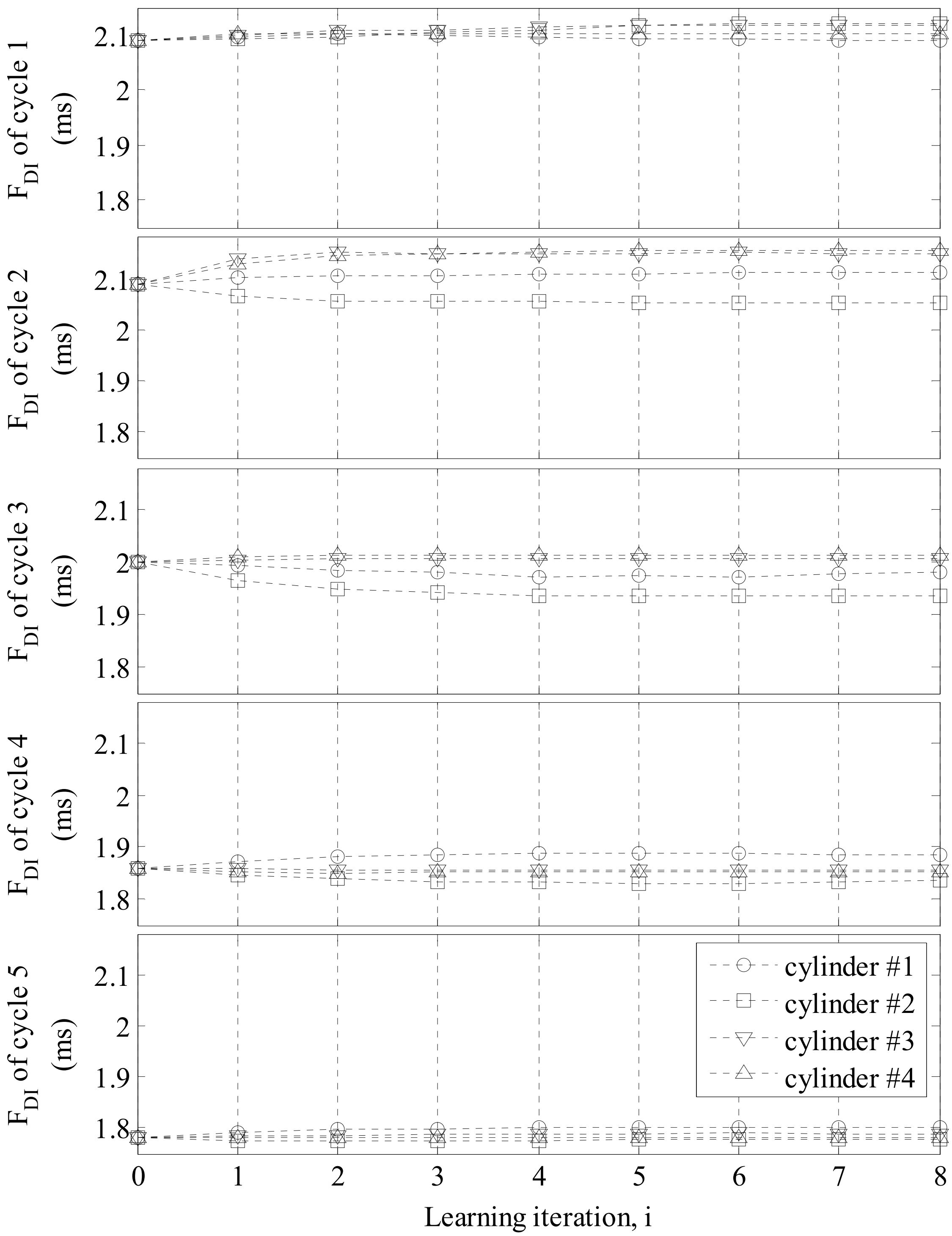

Figure 5.11: Correction of DI fuel quantity after iterative learning

When the air-to-fuel ratio is maintained within the desired range, the iterative learning of F_{DI} was conducted in the learning mode. Figure 5.11 shows that F_{DI} of each cylinder converges after a few iterations of learning. F_{DI} in cycle 2 was adjusted most significantly due to the large variation of the engine MAP. The first engine cycle (cycle 3) after the intake/exhaust valve lift switch demonstrated the largest improvement, leading to significant correction of F_{DI}. The cylinder-to-cylinder adjustment of F_{DI} after iterative learning compensates for the intake charge variations, and leads to smooth IMEP of individual cylinder as shown in Figure 5.12. Therefore, it can be concluded that smooth SI to HCCI combustion mode transition is achievable through the iterative learning control of the DI fuel quantity.

In Figure 5.12, without ILC the slight IMEP oscillations as discussed in Section 5.2 can be observed for T_{IVC} and θ_{SOHCCI}, however, the oscillations disappears after the ILC was applied. These oscillations indicate unstable combustions and are due to the cycle-to-cycle residual gas dynamics of HCCI combustions (including the SI-HCCI hybrid combustions), which has been discussed in great details in [34] and [36]. Due to the residual gas dynamics, retarded (or advanced) θ_{SOHCCI} of current engine cycle leads to advanced (or retarded) θ_{SOHCCI} for the next engine cycle. As a result, combustion oscillations occur. During the combustion mode transition, the impact of adjusting Π_{lift} to the individual in-cylinder combustion is quite different. Cylinder 1 experiences the most significant impact since it is during the exhaust stroke when it happens. Both residual gas quantity and fresh charge quantity were affected. Therefore the IMEP fluctuations of cylinder 1 are dominated as shown in Figure 5.12. By using the ILC of DI fuel quantity, θ_{SOHCCI} was regulated to the appropriate timing as well as the IMEP was regulated to the control reference.

Accordingly the oscillations of T_{IVC} and θ_{SOHCCI} were suppressed, and combustion stability during the mode transition was improved by the iterative learning control.

As a result of suppressing the oscillations of T_{IVC} and θ_{SOHCCI}, engine knock index was also reduced during the combustion mode transition, see Figure 5.13. Note that $dP/d\theta$ is a good indicator of engine knock [62].

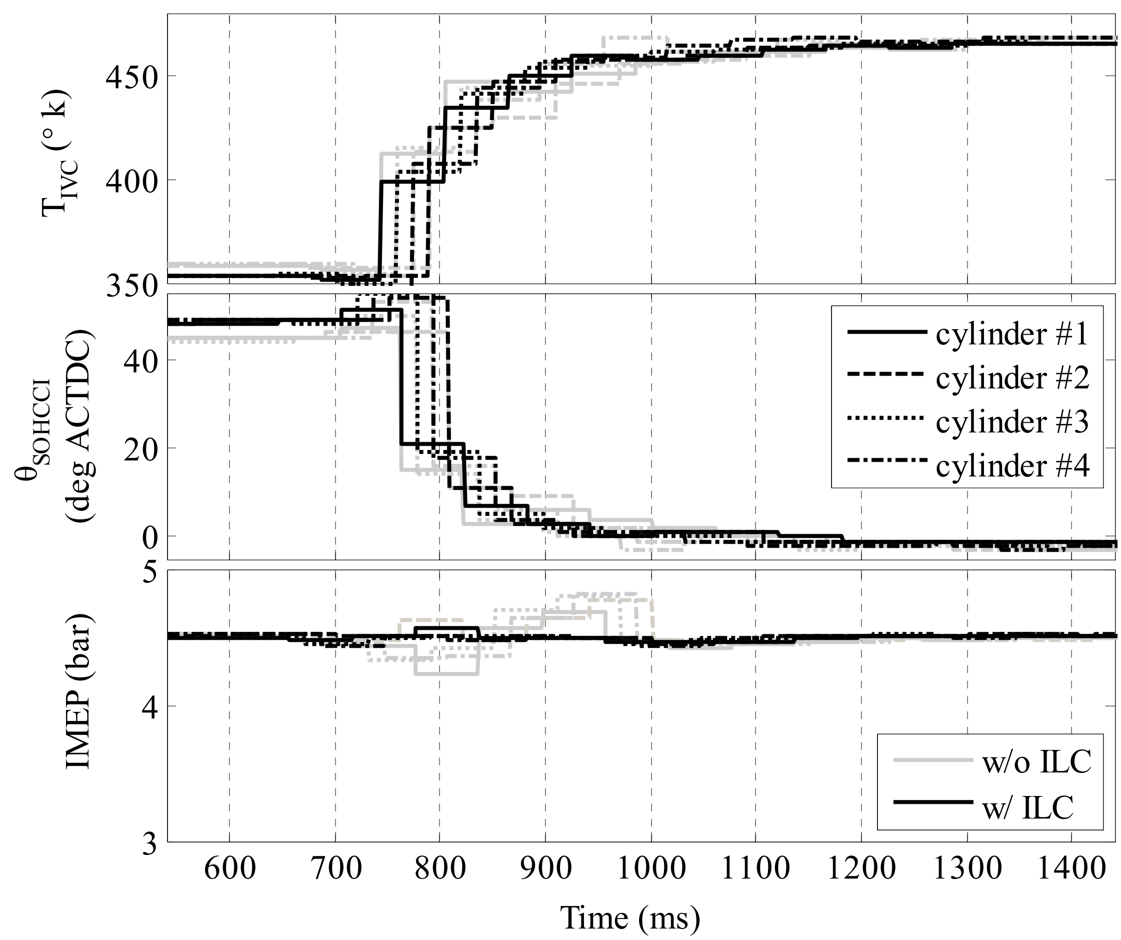

Figure 5.12: Combustion performances with and without ILC

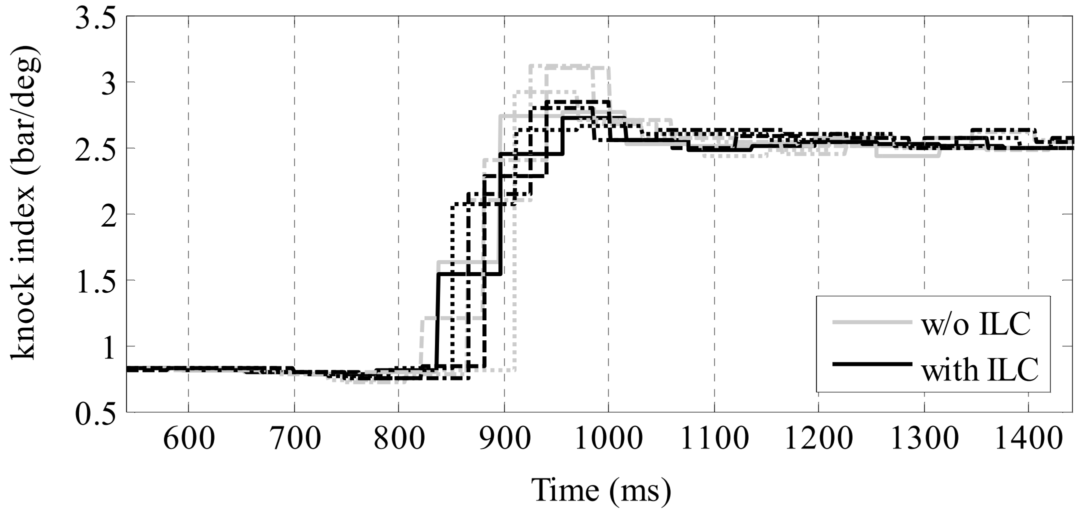

Figure 5.13: Engine knock index (*dP/dθ*) with and without ILC

5.6.4 Engine torque performance comparison

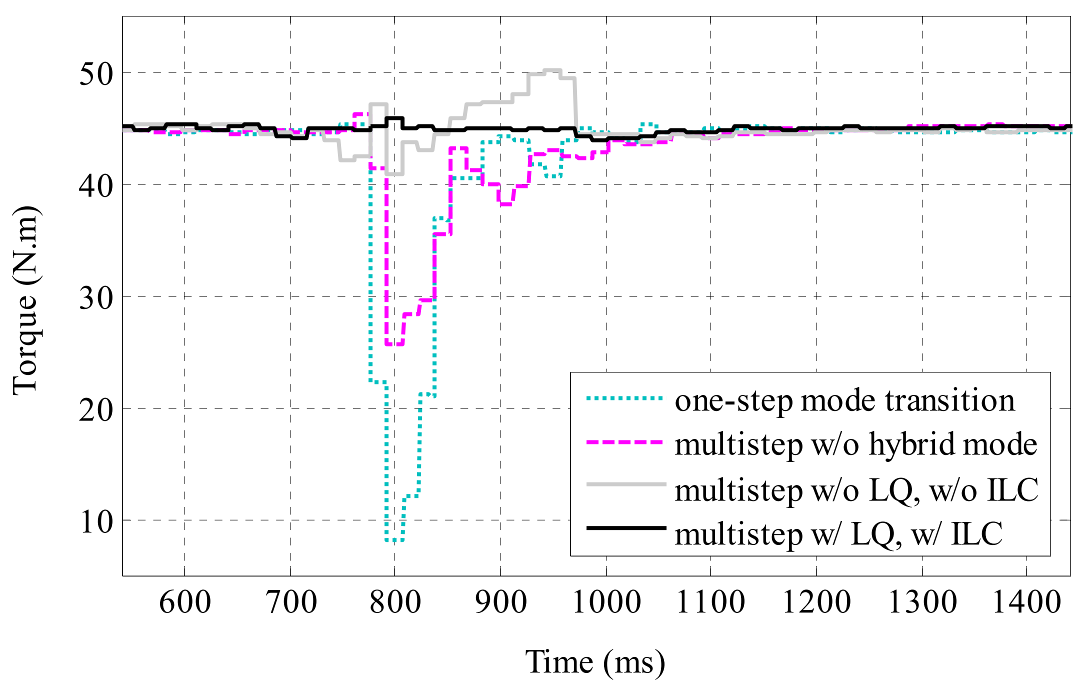

Figure 5.14: Engine torque performances of different control strategies

Table 5.2: Engine performance comparisons for different control strategies

	IMEP error (%)	**Max $dP/d\theta$ (bar/deg)**	**Torque error (%)**
One-step mode transition	51.6	N/A	81.8
Multistep w/o hybrid mode	26.9	N/A	43.1
Multistep w/o LQ, w/o ILC	7.1	3.13	11.2
Multistep w/ LQ, w/ ILC	1.6	2.82	2.2

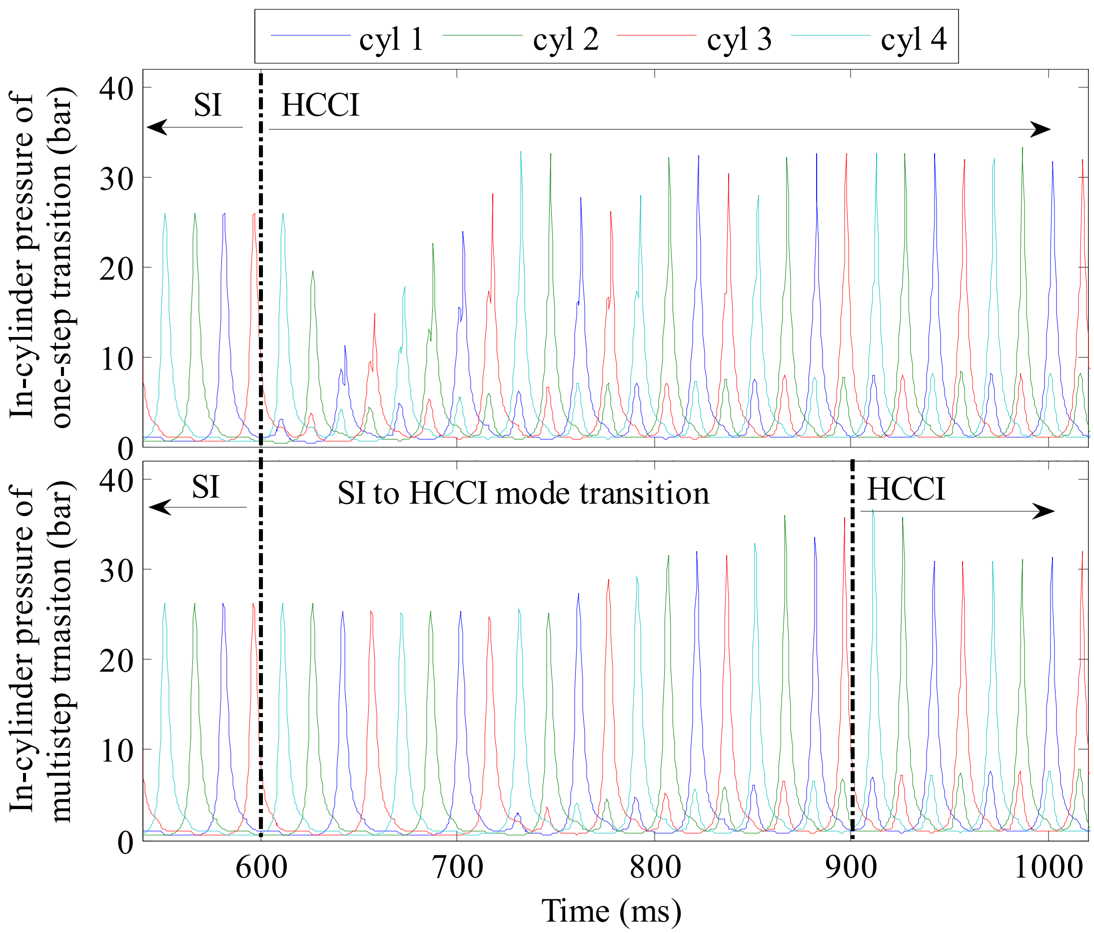

Figure 5.15: In-cylinder gas pressure profiles during SI to HCCI combustion mode transition

Engine torque responses during the combustion mode transitions using the different control strategies are plotted in Figure 5.14. Their statistics are listed in Table 5.2 for comparison. The largest engine torque fluctuation is produced by the one-step approach. The fluctuation of engine torque is reduced when multistep strategy is used. It is further improved as the SI-HCCI hybrid combustion mode is implemented. At last, smooth combustion mode transition is realized in multi-steps when both the air-to-fuel ratio (LQ control) and the DI fuel quantity (ILC) controls are used. The combined control of the LQ tracking and ILC DI fueling with SI-HCCI hybrid combustions leads to the lowest torque fluctuations (2.2%) when the engine operational conditions transit from the steady state SI mode to the HCCI mode. The in-cylinder gas pressure profiles are plotted in Figure 5.15. One can see significant improvement of combustion quality during the transitional cycles.

5.6.5 Engine performance during the throttle tip out operation

In order to study the mode transition under the transient operation, an HIL simulation was conducted to simulate the engine throttle tip out operation, where the engine was initially operated in the SI mode. As a step input was applied to the acceleration pedal, the pedal position decreased from 40% to 15%. As a result, the engine IMEP reduced from 8.1 to 4 bar, which crosses the combustion mode transition threshold of 4.5 bar. Accordingly the combustion mode transition was triggered. Two mode transition strategies were simulated. Both of them were multistep strategies with the hybrid combustions. One was with the air-to-fuel ratio control (LQ) and the DI fuel quantity control, the other was not. Note that the DI fuel quantity control was switched to the transient mode during the engine tip out operation, and the feedforward term F_{FF} used in the transient mode control was learned by the ILC. The transient responses of engine variables are plotted in Figure 5.16.

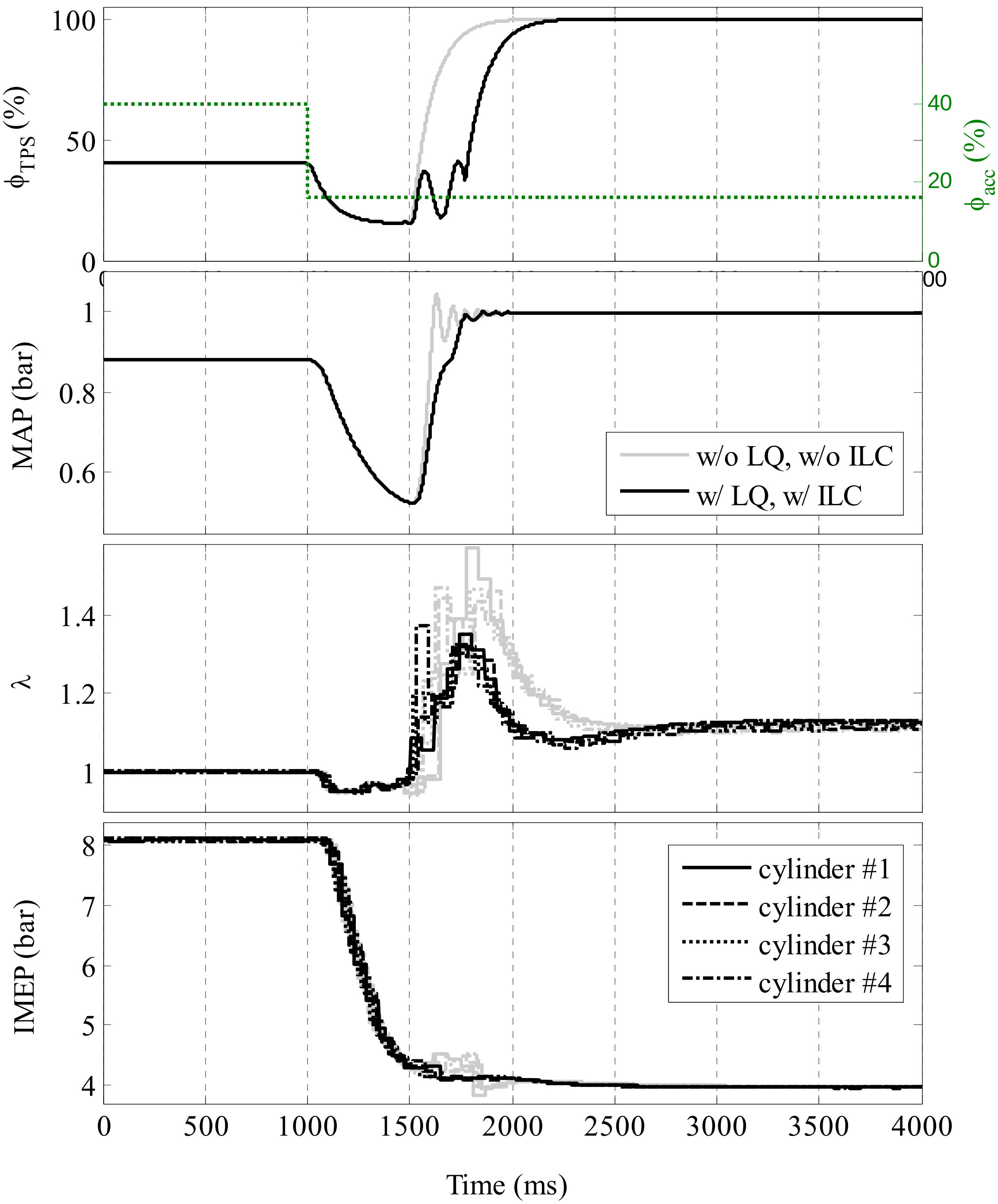

Figure 5.16: Engine responses during Tip out operation

In Figure 5.16 after the step input to the acceleration pedal, both ϕ_{TPS} and MAP are decreased at first, and then increased due to the combustion mode transition. Slightly rich combustions can be observed during the early stage of the tip out operation since the throttle opening is decreased in the SI mode. Once the mode transition is started, the in-cylinder gas-fuel mixture becomes lean for both strategies. However, with air-to-fuel ratio LQ MAP tracking control λ is maintained within the desired range throughout the engine tip out operation. Furthermore, with the proposed DI fuel quantity control smooth IMEP responses were achieved for all cylinders comparing with those without the iterative fuel control. Similar improvement in engine torque output can also be found in Figure 5.17.

Based on the simulation results shown in Figure 5.16 and Figure 5.17, it can be concluded that the proposed LQ optimal MAP tracking control is capable of maintaining the air-to-fuel ratio during engine transient operations, and the iterative DI fuel quantity control is also effective in transient mode.

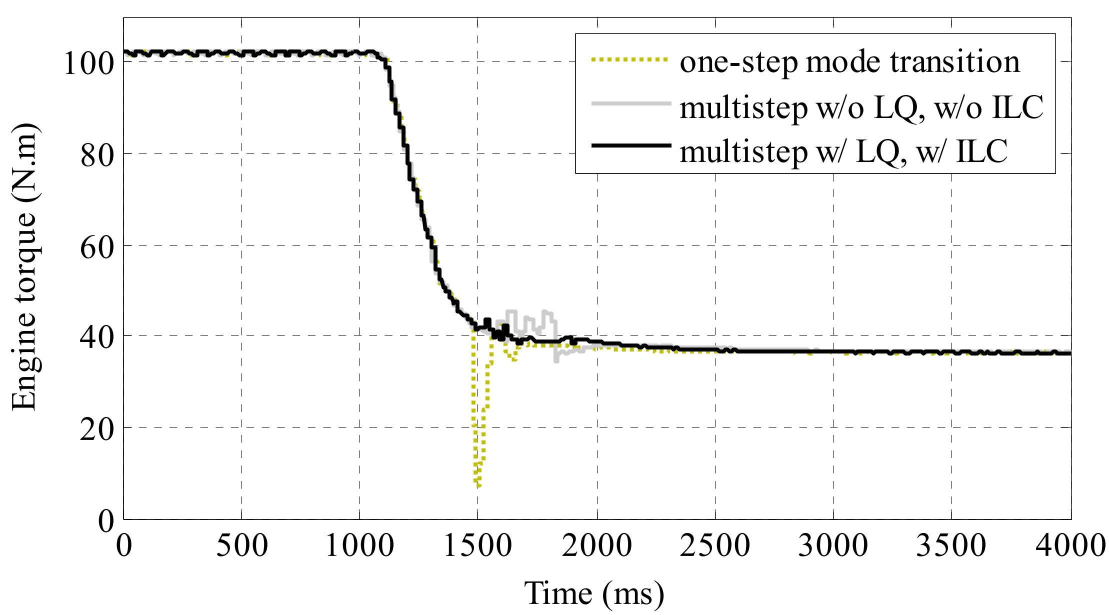

Figure 5.17: Engine torque response during tip out operation

5.7 Conclusions

The combustion mode transition between the SI and HCCI combustions is challenging but necessary to implement the promising HCCI combustion technology to production SI engines. As demonstrated in this chapter, smooth combustion mode transition can be realized in a multi-cylinder gasoline engine equipped with the dual-lift VVT valvetrain system. The mode transition was accomplished within multiple engine cycles with the help of the LQ MAP tracking control and the ILC of DI fuel quantity. Based on the HIL simulation results presented in this chapter, the LQ control tracks the engine MAP to the desired target with small oscillations; and the normalized air-to-fuel ratio is maintained within the desired range. As a result, the individual cylinder IMEP can be regulated through adjusting the corresponding DI fuel quantity. With the help of the ILC DI fuel control, the cylinder-to-cylinder variations of the engine IMEP can be reduced significantly and tracks the control reference. Furthermore, the ILC is able to compensate the influence of the cycle-to-cycle residual gas dynamics, and accordingly reduces the fluctuations of the engine knock index during the mode transition. In addition, combining the learned feedforward control with the PI feedback control, smooth SI to HCCI combustion mode transition can also be realized during transient engine operations.

CHAPTER 6

CONCLUSIONS AND FUTURE WORK

6.1 Conclusions

To model IC engine behaviors for the purpose of real time control strategy development and validation, this dissertation investigates an engine modeling approach that combines time-based and crank-based modeling methods. The engine air-handling system is modeled in time-based by “so-called” mean-value models, and engine combustion process is modeled as functions of the engine crank angle. This modeling approach was first applied to a dual-stage turbocharged SI engine and satisfactory HIL simulation results were obtained. As a result, this approach was used to model the HCCI capable SI engine. The developed SI-HCCI hybrid combustion model of the HCCI capable SI engine is capable of simulating the SI, HCCI and SI-HCCI hybrid combustion modes. The entire HCCI capable SI engine model was calibrated and validated with the corresponding one-dimensional GT-Power model. Afterward, it was implemented into the HIL simulation environment. Based on the HIL simulation results the following conclusions are drawn.

- The mixed time-based and crank-based engine models are capable of real-time HIL simulation
- The developed engine models are effective in simulating both continuous and discrete engine dynamics in the HIL simulation environment
- The SI-HCCI hybrid combustion model is appropriate for the control strategy development of the combustion mode transition, since it models the SI, HCCI and SI-HCCI hybrid

combustion modes seamlessly.

The control strategy development for the SI to HCCI combustion mode transition is the other research concentration of this dissertation. It was developed based upon the developed HCCI capable SI engine model. The developed control strategy was a multistep mode transition control strategy. The SI-HCCI hybrid combustion mode was implemented in the combustion mode transition to bridge the gap between the SI and HCCI combustion modes. The LQ optimal MAP tracking control was applied in the multistep control strategy to optimize the engine air-to-fuel ratio. DI fuel quantity of each cylinder was optimized by the iterative learning control. The entire control strategy was validated in the HIL simulation environment. The following are the conclusions:

- Smooth SI to HCCI combustion mode transitions are realized for both steady state and transient operating conditions using the proposed multistep control strategy
- The SI-HCCI hybrid combustion mode plays an important role in the multistep combustion mode transition control strategy
- Smooth SI to HCCI combustion mode transition is achievable for an HCCI capable SI engine equipped with dual-stage valve lift and electrical VVT systems

6.2 Recommendations for Future Work

The engine models presented in this dissertation are in the quasi-steady state. The calculations of in-cylinder gas mass, mass flow rate across intake/exhaust valve, heat exchange, etc., are mainly based on governing equations of mass and energy conservations, whereas the gas flow dynamics (momentum conservation) is ignored. However, the intake gas flow dynamics affects the homogeneity of the in-cylinder gas-fuel mixture seriously, hence, it affects the HCCI combustion. Combining the gas flow dynamics model with the existing combustion model described in Chapter 3 could improve the modeling accuracy for the HCCI combustion and combustion mode transition.

In addition, the SI-HCCI hybrid combustion mode has one additional control variable, spark timing that affects the start of the HCCI (SOHCCI) combustion time and the HCCI combustion percentage (x_{HCCI}) in the hybrid combustion mode as demonstrated in HIL simulations. It is recommended to use this control variable to extend the HCCI combustion to higher engine load.

With the successful demonstration of smooth combustion mode transition from the SI to HCCI modes using the multistep control strategy developed in Chapter 5, the logical next step is to extend the control strategy to the mode transition from the HCCI to SI combustion. Note that this is not a simple reversed process since the mode transition from the HCCI to SI combustion has quite different dynamics, comparing to the transition from SI to HCCI.

Finally, the most important future work is to use engine test data to validate the developed engine models and demonstrate the proposed control strategy in the engine dynamometer tests.

BIBLIOGRAPHY

BIBLIOGRAPHY

[1] X. Yang and G. G. Zhu, "A Mixed Mean Value and Crank-based Model of a Dual-Stage Turbocharged SI Engine for Hardware-In-the-Loop Simulation", Proceedings of 2010 American Control Conference, Baltimore, MD, 2010.

[2] G. Colin, Y. Chamaillard, and B. Bellicaud, "Robust Control for the Air Path of a Downsized Engine," Proceedings of the Institution of Mechanical Engineers, Part D: *Journal of Automobile Engineering July*, 2011 vol. 225 no. 7 930-943.

[3] A. Lefebvre and S. Guilain, "Modeling and Measurement of the Transient Response of a Turbocharged SI Engine," *SAE Technical Paper*, 2005-01-0691.

[4] Byungchan Lee, *Dual-Stage Boosting Systems: Modeling of Configurations, Matching and Boost Control Options*, PhD thesis, University of Michigan, 2009.

[5] A. Chasse, "Double Stage Turbocharger Control Strategies Development," *SAE Technical Paper*, 2008-01-0988, 2008.

[6] S. Saulnier and S. Guiliain, "Computational Study of Diesel Engine Downsizing Using Two-stage Turbocharging," *SAE Technical Paper*, 2004-01-0929, 2004.

[7] S. Kim, T. Wakisaka, and Y. Aoyagi, "A Numerical Study of the Effects of Boost Pressure and Exhaust Gas Recirculation Ratio on the Combustion Process and Exhaust Emissions in a Diesel Engine," *International Journal of Engine Research*, 2007 8: 147.

[8] Y. Duchaussoy, A. Lefebvre and R. Bonetto, "Dilution Interest on Turbocharged SI Engine Combustion," *SAE Technical Paper*, 2003-01-0629.

[9] W. Chatlatanagulchai, K. Yaovaja, S. Rhienprayoon, and K. Wannatong, "Fuzzy Knock Control of Diesel-Dual-Fuel Engine," *SAE International*, 2011-01-0690.

[10] I. Haskara, G. Zhu, C. Daniels, and J. Winkelman, "Closed Loop Maximum Dilution Limit Control using In-Cylinder Ionization Signal," *SAE Technical Paper*, 2005-01-3751, SAE Powertrain and Fluid Systems Conference & Exhibition, San Antonio, Texas, USA.

[11] G. G. Zhu, I. Haskara, and J. Winkelman, "MBT Timing Detection and its Closed-Loop Control Using In-Cylinder Ionization Signal," *SAE Technical Paper*, 2004-01-2976, SAE Powertrain and Fluid Systems Conference, Tampa, Florida, USA.

[12] G. G. Zhu, C. Daniels, and J. Winkelman, "MBT Timing Detection and Its Closed-Loop Control Using In-Cylinder Pressure Signal," *SAE Technical Paper*, 2003-01-3266, SAE Powertrain and Fluid Systems Conference & Exhibition, Pittsburgh, Pennsylvania, USA.

[13] C. F. Daniels, G. G. Zhu, and J. Winkelman, (2003) "Inaudible Knock and Partial Burn Detection Using In-Cylinder Ionization Signal," *SAE Technical Paper*, 2003-01-3149.

[14] F. Zhao, T. Asmus, D. Assanis, J.E. Dec, J.A. Eng, and P.M. Najt, *Homogeneous Charge Compression Ignition (HCCI) Engines Key Research and Development Issues*. 2003, Warrendale, Pennsylvania: Society of Automotive Engineers.

[15] R. M. Wagner, K. D. Edwards, et al, "Hybrid SI-HCCI Combustion Modes for Low Emissions in Stationary Power Applications," 3rd Annual Advanced Stationary Reciprocating Engines Meeting Argonne National Laboratory, Argonne, IL June 28-30, 2006.

[16] H. Zhao, J. Li, T. Ma, and N. Ladommatos, "Performance and Analysis of a 4-Stroke Multi-Cylinder Gasoline Engine with CAI Combustion," *SAE International*, 2002-01-0420, 2002.

[17] C. J. Chiang and A. G. Stefanopoulou, "Stability Analysis in Homogeneous Charge Compression Ignition (HCCI) Engines With High Dilution," IEEE Transactions on Control System Technology, Vol. 15, No. 2, March 2007.

[18] J. S. Souder, J. H. Mack, J. K. Hedrick, and R. W. Dibble, "Microphones and Knock Sensors for Feedback Control of HCCI Engines," Proceedings of ICEF'04 2004 ASME Internal Combustion Engine Division Long Beach, California, USA, October 24-27, 2004.

[19] M. Hillion, J. Chauvin, O. Grondin, and N. Petit, "Active Combustion Control of Diesel HCCI Engine: Combustion Timing," *SAE Technical Paper*, 2008-01-0984.

[20] U.S. Department of Energy Energy, Efficiency and Renewable Energy Office of Transportation Technologies, *Homogeneous Charge Compression Ignition (HCCI) Technology*, A Report to the U.S. Congress, April 2001.

[21] X. Lu, Y. Hou, L. Zu, and Z. Huang, "Experimental Study on the Auto-Ignition and Combustion Characteristics in the Homogeneous Charge Compression Ignition (HCCI) Combustion Operation with Ethanol/*n*-Heptane Blend Fuels by Port Injection," *Fuel*, 85 (2006) 2622 – 2631.

[22] S. C. Kong, R. D. Reitz, "Application of Detailed Chemistry and CFD for Predicting Direct Injection HCCI Engine Combustion and Emission," Proceedings of the Combustion Institute, Volume 29, 2002/pp. 663–669.

[23] Sloane, Thompson Milton, Tsai, Ping-ho, *Method of operating HCCI engines at low speed and low load*, United States Patent 6662785.

[24] Halim G. Santoso, *Managing Transient Behaviors of a Dual Mode Spark Ignition / Controlled Auto Ignition Engine with a Variable Valve Timing System*, PhD thesis, Massachusetts Institute of Technology, 2000.

[25] X. Yang and G. Zhu, "SI and HCCI Combustion Mode Transition Control of A Multi-Cylinder HCCI Capable SI Engine Via Iterative Learning," Proceedings of the 4th Annual Dynamic Systems and Control Conference, Westin Arlington Gateway, Arlington, VA, USA. Oct 31 - Nov 2, 2011.

[26] S. S. Nathan, J. M. Mallikarjuna, A. Ramesh, “Effects of charge temperature and exhaust gas re-circulation on combustion and emission characteristics of an acetylene fuelled HCCI engine,” *Fuel*, 89 (2010) 515–521

[27] Z. Ren, G. Zhu, “Modeling and Control of an Electric Variable Valve Timing System for SI and HCCI Combustion Mode Transition,” Proceedings of 2011 American Control Conference, San Francisco, California, USA, 2011.

[28] N Kalian1, H Zhao1, and J Qiao, “Investigation of transition between spark ignition and controlled auto-ignition combustion in a V6 direct-injection engine with cam profile switching,” Proc. IMechE Vol. 222 Part D: J. Automobile Engineering, IMechE 2008.

[29] G. Haraldsson, P. Tunestal, B. Johansson, and J. Hyvönen, “HCCI Closed-Loop Combustion Control Using Fast Thermal Management,” *SAE Technical Paper*, 2004-01-0943.

[30] G. M, Shaver, M. J. Roelle1, P. A. Caton1, N. B. Kaahaaina1, et al, “A Physics-Based Approach to the Control of Homogeneous Charge Compression Ignition Engines with Variable Valve Actuation,” *International Journal of Engine Research*, 2005 6: 361.

[31] G. M. Shaver, *Physics-Based Modeling and Control of Residual-Affected HCCI Engines Using Variable Valve Actuation*, PhD thesis, Stanford University, September, 2005.

[32] G. M. Shaver, J. C. Gerdes and M. J. Roelle, “Physics-Based Modeling and Control of Residual-Affected HCCI Engines,” *Journal of Dynamic Systems, Measurement, and Control*, Volume 131, Issue 2, 021002, February 2009.

[33] N. Ravi, H. H. Liao, A. F. Jungkunz, and J. C. Gerdes, “Modeling and Control of Exhaust Recompression HCCI Using Split Injection,” Proceedings of 2010 American Control Conference, Baltimore, MD, 2010.

[34] N. Ravi, M. J. Roelle, A. F. Jungkunz, J. C. Gerdes, “Model-Based Control of HCCI Engines Using Exhaust Recompression,” *IEEE Transactions on Control Systems Technology*, Published by: IEEE Control Systems Society, Volume 18, Issue 6, pp 1289 - 1302, Nov. 2010.

[35] N. J. Killingsworth, S. M. Aceves, et al, “HCCI Engine Combustion-Timing Control: Optimizing Gains and Fuel Consumption Via Extremum Seeking,” IEEE Transactions on Control Systems Technology, Vol. 17, No. 6, November 2009, pp. 1350-1361.

[36] J. Kang, C. Chang, and T. Kuo, “Sufficient Condition on Valve Timing for Robust Load Transients in HCCI Engines,” *SAE International*, 2010-01-1243

[37] Jason Scott Souder, *Closed-Loop Control of a Multi-Cylinder HCCI Engine*, PhD thesis, University of California, Berkeley, 2004.

[38] G. M. Shaver, M. J. Roelle and J. C. Gerdes, "Modeling cycle-to-cycle dynamics and mode transition in HCCI engines with variable valve actuation," *Control Engineering Practice*, Volume14 (2006) 213–222.

[39] Y. Zhang, H. Xie, et al, "Study of SI-HCCI-SI Transition on a Port Fuel Injection Engine Equipped with 4VVAS", SAE Paper 2007-01-0199.

[40] M. J. Roelle, G. M. Shaver, and J. C. Gerdes, "Tackling the Transition: A Multi-Mode Combustion Model of SI and HCCI for Mode Transition Control," Proceedings of IMECE 2004 International Mechanical Engineering Conference and Exposition, Anaheim, California, USA, November 13-19, 2004.

[41] G. Tian, Z. Wang, Q. Ge, J. Wang, and S. Shuai, "Mode Switch of SI-HCCI Combustion on a GDI Engine," *SAE International*, 2007-01-0195.

[42] H. Wu, M. Kraft, et al, "Experimental Investigation of a Control Method for SI-HCCI-SI Transition in a Multi-Cylinder Gasoline Engine," *SAE International*, 2010-01-1245.

[43] Zhang, Y., H. Xie, N. Zhou, T. Chen, and H. Zhao, "Study of SI-HCCI-SI Transition on a Port Fuel Injection Engine Equipped with 4VVAS," *SAE International*, 2007-01-0199.

[44] A. Cairns and H. Blaxhill, "The Effects of Two-Stage Cam Profile Switching and External EGR on SI-CAI Combustion Transitions," *SAE International*, 2007-01-0187.

[45] X. Yang, G. G. Zhu and Z. X. Sun, "A Control Oriented SI and HCCI Hybrid Combustion Model for Internal Combustion Engines", Proceedings of 2010 ASME Dynamic Systems and Control Conference, Cambridge, MA, 2010.

[46] J. H. Park, S. Han, and W. H. Kwon, "LQ Tracking Controls with Fixed Terminal States and Their Application to Receding Horizon Controls," *Systems & Control Letters*, Volume 57, Issue 9, Pages 772-777. September 2008.

[47] T. N. Trajkov, H. Koppe, and U. Gabbert, "Active Vibration Control Using Optimal LQ Tracking System with Additional Dynamics," *International Journal of Control*, Vol. 78, No. 15, October 2005, 1182-1197.

[48] M. S. Meridjet and N. Debbache, "Control Motor Using State Space Discrete Time Optimal Tracking Controller," *Journal of Theoretical and Applied Information Technology*.

[49] K. Kinosita, T. Sogo, and N. Adachi, "Iterative Learning Control Using Adjoin Systems and Stable Inversion," *Asian Journal of Control*, Vol. 4, No. 1, pp. 60-67, March 2002.

[50] Abdelhamid Tayebi, "Adaptive Iterative Learning Control for Robot Manipulators," *Automatica*, 40 (2004) 1195 – 1203. Available online at www.sciencedirect.com.

[51] M. Heertjes and T. Tsoc, "Nonlinear Iterative Learning Control with Applications to Lithographic Machinery," *Control Engineering Practice*, 15 (2007) 1545–1555. Available online at www.sciencedirect.com.

[52] K. Lamberg, P. Walterman, "Using HIL Simulation to Test Mechatronic Components in Automotive Engineering," 2nd Congress on Mechatronics in Automobile, Munich, Nov. 2000.

[53] Andy Beaumont, "Hardware in the Loop (HIL) for Engine Control Strategy Development," 3rd Biennial dSPACE USA User Conference, Plymouth, MI, 21-23 June 2004.

[54] M. Jung, R. G. Ford, "Parameterization and Transient Validation of a Variable Geometry Turbocharger for Mean value Modeling at Low and Medium Speed-Load Points," *SAE Technical Paper*, 2002-01-2729.

[55] D. J. Rausen, et al, "A mean value model for control of homogeneous charge compression ignition (HCCI) engines," *ASME Journal of Dynamics, Measurement, and Control*, Vol. 127, September, 2005, pp. 355-362.

[56] N. Killingsworth, S. Aceves, D. Flowers, and M. Krstic, "A Simple HCCI Engine Model for Control," IEEE International Conference on Control Applications, Munich, Germany, October 4, 2006 through October 6, 2006.

[57] M. Shahbakhti, C. R. Koch, "Control Oriented Modeling of Combustion Phasing for an HCCI Engine," American Control Conference, July 9-13, 2007, New York, NY, USA.

[58] M. Canova, R. Garcin, M. M. Shawn, Y. Guezennec, and G. Rizzoni, "A Control - Oriented Model of Combustion Process in a HCCI Diesel Engine," 2005 American Control Conference, June 8-10, 2005, Portland, OR, USA.

[59] G. G. Zhu, I. Haskara, and J. Winkelman, "Closed-Loop Ignition Timing Control for SI Engines Using Ionization Current Feedback," *IEEE Transaction on Control System Technology,* VOL. 15, NO. 3, MAY 2007.

[60] J. Bengtsson, P. Strandh, R. Johansson, P. Tunest, and B. Johansson, "Closed-Loop Combustion Control of Homogeneous Charge Compression Ignition (HCCI) Engine Dynamics," *International Journal of Adaptive Control and Signal Processing*, 18: 167–179 2004.

[61] F. Willems, E. Doosje, F. Engels, and X. Seykens, "Cylinder Pressure-Based Control in Heavy-Duty EGR Diesel Engines Using a Virtual Heat Release and Emission Sensor," *SAE International*, 2010-01-0564.

[62] M. M. Andreae, W. K. Cheng, T. Kenney, and J. Yang, "On HCCI engine Knock," *SAE International*, 2007-01-1858, 2007.

[63] Aceves, S.M., D.L. Flowers, R.W. Dibble, and A. Babajimopoulos, *Overview of Modeling Techniques and their Application to HCCI/CAI Engines, in HCCI and CAI Engines for the Automotive Industry*, H. Zhao, Editor. 2007, Woodhead Publishing: Cambridge.

[64] O. Colin, A. P. Cruz, and S. Jay, "Detailed Chemistry-Based Auto-Ignition Model Including Low Temperature Phenomena Applied to 3-D Engine Calculations," Proceedings of the Combustion Institute 30 (2005) 2649–2656.

[65] P.M. Diaz, D. Prasad, and S. M. Raman, "A CFD Investigation of Emissions Formation in HCCI Engines, Including Detailed NOx Chemistry," *IETECH Journal of Mechanical Design*, Vol: 1, No: 1, 056 – 061, 2007.

[66] Gamma Technology, "*Engine Performance Application Manual,*" GT-Suite version 7.0, Sep. 2009. Available: http://www.gtisoft.com/.

[67] W. Chatlatanagulchai, K. Yaovaja, S. Rhienprayoon, and K. Wannatong, "Fuzzy Knock Control of Diesel-Dual-Fuel Engine," SAE International, 2011-01-0690.

[68] G. G. Zhu, D. Hung and H. Schock, et al, "Combustion characteristics of a single-cylinder spark ignition gasoline and ethanol dual-fuelled engine," Proceedings of the Institution of Mechanical Engineers, Part D: *Journal of Automobile Engineering*, Volume 224, Number 3 / 2010, pp 387-403.

[69] L.Guzzella and C.H.Onder, *Introduction to Modeling and Control of Internal Combustion Engine Systems*, Springer, Inc., 2004.

[70] A. Y. Karnik, J. H. Buckland, J. S. Freudenberg, "Electronic Throttle and Wastegate Control for Turbocharged Gasoline Engines," American Control Conference, pp. 4434-4439, 2005.

[71] K. L. Hoag, R. J. Primus, *Fundamentals of Diesel Engine Performance*, Cummins Engine Company, Inc., 1992.

[72] M. Locatelli, C. H. Onder, and H. P. Geering, "An Easily Tunable Wall-Wetting Model for PFI Engines," SAE Technical Paper 2004-01-1461.

[73] J. B. Heywood, *Internal Combustion Engine Fundamentals*, McGraw-Hill, Inc., 1988.

[74] J. Chang, O. Guralp, "New Heat Transfer Correlation for an HCCI Engine Derived from Measurements of Instantaneous Surface Heat Flux," SAE 2004-01-2996.

[75] Lars Eriksson, "Spark Advance Modeling and Control," PhD Dissertation, Linkoping University, Linkoping, Sweden, 1999.

[76] J. Etheridge, S. Mosbach and M. Kraft, "A Fast Detailed-Chemistry Modeling Approach for Simulating the SI-HCCI Transition," *SAE International*, 2010-01-1241.

[77] Andreas Vressner, *Studies on the Load Range of an HCCI Engine using In-Cylinder Pressure, Ion Current and Optical Diagnostics*, PhD thesis, Lund University, Sweden. November, 2007.

[78] Zigler Bradley Thomas, *An experimental investigation of the ignition properties of low temperature combustion in an optical engine, PhD thesis*, University of Michigan, 2008.

[79] X. Yang and G. Zhu, "A Two-Zone Control Oriented SI-HCCI Hybrid Combustion Model for the HIL Engine Simulation," Proceedings of 2011 American Control Conference, San Francisco, California, USA, 2011.

[80] M. Canova and S. M. Mohler, Y. Guezennec, and G. Rizzoni, "Mean Value Modeling and Analysis of HCCI Diesel Engines with External Mixture Formation," *Journal of Dynamics, Measurement, and Control*, Vol. 131, January, 2009.

[81] M. Hillion, J. Chauvin, and N. Petit, "Controlling the Start of Combustion on an HCCI Diesel Engine," American Control Conference, June 11 – 13, 2008.

[82] M. McCuen, Z. Sun, and G. Zhu, "Control-oriented mixing model for homogeneous charge compression ignition engine," Proceedings of 2010 American Control Conference, Baltimore, MD, June 2010

[83] N. Ravi, H. H. Liao and A. F. Jungkunz, "Modeling and control of exhaust recompression HCCI using split injection," Proceedings of 2010 American Control Conference, Baltimore, MD, 2010

[84] Y. A. Cengel and M. A. Boles, *Thermodynamics: An Engineering Approach*, 5th edition, McGraw-Hill, 2006.

[85] A. Babajimopoulos and D. N. Assanis, "An Approach for Modeling the Effects of Gas Exchange Processes on HCCI Combustion and Its Application in Evaluating Variable Valve Timing Control Strategies," *SAE International*, 2002-01-2829.

[86] A. Ghazimirsaied, M. Shahbakhti, C. R. Koch, "HCCI Engine Combustion Phasing Prediction Using a Symbolic-Statistics Approach," *Journal of Engineering for Gas Turbines and Power*, Vol. 132 / 082805-1, August, 2010.

[87] A. Ghazimirsaied1, M. Shahbakhti, A. Audet, and C. R. Koch, "HCCI Engine Cyclic Variation Characterization Using Both Chaotic and Statistical Approach," Proceedings of Combustion Institute-Canadian Section, Spring Technical Meeting. University of Toronto, Ontario. May 12-14, 2008.

[88] J. Ma, G. G. Zhu, and H. Schock, "Adaptive Control of a Pneumatic Valve Actuator for an Internal Combustion Engine," *IEEE Transactions on Control Systems Technology*, Volume: 19 Issue: 4, pages: 730 - 743. July, 2011.

[89] D. Naidu, *Optimal Control Systems*, pp. 232-239. ISBN: 0849308925. Published by CRC Press. August 2002.

[90] K. Zhou, J. C. Doyle, and K. Glover, *Robust and Optimal Control*, ISBN-13: 978-0134565675, Published by Prentice Hall, August, 1995.

[91] Jian-Xin Xu and Ying Tan, *Linear and Nonlinear Iterative Learning Control*, ISBN 3540401733, published by Springer, 2003.

[92] Y. Chen, K. L. Moore, J. Yu, and T. Zhang, "Iterative learning control and repetitive control in hard disk drive industry—A tutorial," *International Journal of Adapt Control Signal Processing*, August, 2007.

[93] P. R. Ouyang, B. A. Petz and F. F. Xi, "Iterative Learning Control with Switching Gain Feedback for Nonlinear Systems," *Journal of Computational and Nonlinear Dynamics*, Vol. 6. January 2011.

[94] Adam James Heinzen, Iterative Learning Control of a Fully Flexible Valve Actuation System for Non-throttled Engine Load Control, MS Thesis, University OF Minnesota, May, 2011.